

---

---

# Thermal Conductivity of Polymer Materials

Reverse Nonequilibrium Molecular Dynamics Simulation



TECHNISCHE  
UNIVERSITÄT  
DARMSTADT

Vom Fachbereich Chemie  
der Technischen Universität

zur Erlangung des akademischen Grades  
eines Doktor rerum naturalium (Dr. rer. nat)

genehmigte Dissertation

vorgelegt von  
M.Sc. Elena Algaer  
aus Nowosibirsk (Russland)

Referent: Prof. Dr. Florian Müller-Plathe  
Korreferent: Prof. Dr. Nico van der Vegt

Eingereicht am: 26.01.2010  
Mündliche Prüfung am: 22.03.2010

Darmstadt, 2010

D 17

---

---

---

## I. Table of Contents

---

I. Table of Contents.....	i
II. Table of Pictures .....	ii
1. Zusammenfassung.....	1
2. Summary.....	3
3. Introduction: Calculation of the Thermal Conductivity of Molecular Liquids, Polymers and Carbon Nanotubes .....	5
3.1. Nonequilibrium Molecular Dynamics Methods.....	6
3.1.1. Reverse Nonequilibrium Molecular Dynamics .....	6
3.1.2. Dual-Thermostat Method.....	7
3.1.3. Thermal-Noise Method .....	9
3.1.4. Size Effects .....	10
3.2. Thermal Conductivity of Molecular Liquids.....	11
3.3. Thermal Conductivity of Polymers and its Anisotropy .....	16
3.3.1. Amorphous Polyamide-6,6.....	16
3.3.2. Crystalline Syndiotactic Polystyrene.....	19
3.3.3. Polyethylene.....	21
3.4. Thermal Conductivity and Thermal Rectification in Carbon Nanotubes.....	23
3.5. Force Field Considerations for the Calculation of Thermal Conductivities .....	28
4. Thermal Conductivity of Atactic Amorphous Polystyrene and its Mixture with Supercritical Carbon Dioxide .....	31
4.1. Computational Details .....	32
4.2. Thermal Conductivity of Neat Polystyrene .....	34
4.3. Thermal Conductivity of Neat Carbon Dioxide at Supercritical Conditions.....	38
4.4. Thermal Conductivity of Binary Mixtures of Polystyrene and Carbon Dioxide .....	40
4.5. Summary.....	45
5. Anisotropy of the Thermal Conductivity for Amorphous Polystyrene and its Mixture with Supercritical Carbon Dioxide .....	47
5.1. Computational Details .....	49
5.2. Anisotropy of the Thermal Conductivity of Neat Polystyrene.....	51
5.3. Anisotropy of the Thermal Conductivity of Binary Mixtures of Polystyrene and Carbon Dioxide.....	56
5.4. Dependence of the Thermal Conductivity on Number of Degrees of Freedom .....	58
6. Conclusions and Outlook.....	61
7. References.....	63
Acknowledgments .....	66
Curriculum Vitae.....	67
Publications.....	68
Eidesstattliche Erklärungen .....	69

---

---

## II. Table of Pictures

---

Figure 1-1. Reverse Nonequilibrium Molecular Dynamics Method. ....	6
Figure 1-2. Dual-Thermostat Method.....	8
Figure 1-3. Thermal-Noise method. ....	10
Figure 1-4. Simulated thermal conductivities versus corresponding experimental values for water, <sup>11</sup> <i>n</i> -hexane, <sup>11</sup> benzene, <sup>11,23</sup> methanol, <sup>22</sup> ethanol, <sup>22</sup> toluene, <sup>23</sup> <i>o</i> -xylene, <sup>23</sup> <i>m</i> -xylene, <sup>23</sup> and <i>p</i> -xylene. <sup>23</sup> .....	15
Figure 1-5. The calculated thermal conductivity of polyamide-6,6 as a function of degrees of freedom per repeat unit. The line is a linear fit to the data. Figure has been taken from the work of Lussetti <i>et al.</i> <sup>19</sup> .....	18
Figure 1-6. The $\delta$ modification of sPS viewed along the helix axis ( <i>z</i> direction). Backbone atoms are highlighted in yellow.....	19
Figure 1-7. Scheme of the different constraint patterns. Constrained bonds are marked by thick solid lines, flexible bonds by thin dashed lines. ....	20
Figure 1-8. Thermal conductivity versus tube length for (5, 5), (10, 0), (7, 7), (10, 10), (17, 0), (15, 15), and (20, 20) SWNTs at 300 K. ....	24
Figure 1-9. Thermal conductance $\sigma$ for different tubes at 300 K with a tube length between 50 and 350 nm.....	24
Figure 1-10. Thermal conductance $\sigma$ versus temperature for different SWNTs of 30 nm length after applying quantum correction.....	25
Figure 1-11. Atomic mass and temperature profiles in the (10, 10) single-walled nanotube with a mass gradient at an average temperature of 300 K. (a) Heat flows into the direction of lower atomic masses. (b) Heat flows into the direction of higher atomic masses. ....	26
Figure 1-12. Thermal conductivity versus nanotube length for various degrees of functionalization. ....	27
Figure 2-1. Schematic representation of atactic polystyrene which is characterized by a random distribution of the phenyl rings.....	31
Figure 2-2. Density of neat PS at 0.1 MPa as obtained in experiment <sup>90</sup> and by simulations....	34
Figure 2-3. Thermal conductivity of polystyrene versus temperature at 0.1MPa obtained in experiment <sup>2</sup> and by simulations.....	36
Figure 2-4. Thermal conductivity and density of polystyrene versus pressure at 400 K.....	36
Figure 2-5. Orientation of C-C bonds in the backbone.....	37
Figure 2-6. Simulated and experimental <sup>92</sup> densities of CO <sub>2</sub> under supercritical conditions. The uncertainties in the simulated densities are smaller than the size of the symbols. ...	38
Figure 2-7. Thermal conductivity of CO <sub>2</sub> at supercritical conditions versus pressure at different temperatures. The uncertainties of the simulated thermal conductivity are smaller than the size of the symbols. ....	39
Figure 2-8. Density of the binary mixture versus CO <sub>2</sub> concentration in mass % at 400 K and 16 MPa. ....	40
Figure 2-9. Thermal conductivity of the binary mixture versus mass concentration of CO <sub>2</sub> in % at 400 K and 16 MPa.....	41
Figure 2-10. Thermal conductivity of binary mixtures versus pressure for different mass concentrations of CO <sub>2</sub> in % at 400 K.....	41
Figure 2-11. Thermal conductivity of binary mixtures versus temperature for different mass concentrations of CO <sub>2</sub> in % at 16 MPa.....	42
Figure 2-12. Thermal conductivity of binary PS-CO <sub>2</sub> admixture as a function of the degrees of freedom per unit volume encountered in the system. ....	43
Figure 2-13. Thermal conductivity of the binary mixture as a function of CO <sub>2</sub> mass concentration derived by RNEMD simulations of the binary system and estimated via the interpolation. ....	45

Figure 3-1. Arrangement of stretched polystyrene in the simulation box as projected on the $xy$ and $xz$ plane. Stretching occurs in the $z$ direction. The carbon atoms in the backbone chain have been highlighted in red. ....	48
Figure 3-2. Pressure dependence of the thermal conductivity of anisotropic polystyrene at 400 K and a stretching ratio of 35 %. ....	52
Figure 3-3. Temperature dependence of the thermal conductivity of anisotropic polystyrene at 0.1 MPa and a stretching ratio of 21 %. ....	53
Figure 3-4. Thermal conductivity of anisotropic polystyrene as a function of the stretching ratio $r_s$ at 0.1 MPa and 400 K. The $\lambda_{\parallel}$ and $\lambda_{\perp}$ average has been labeled by a dashed curve. The straight line refers to the thermal conductivity of the isotropic sample. ....	53
Figure 3-5. Distribution of the direction cosines of the C-C bonds in the PS backbone and side chain in the direction of stretching. The simulations have been carried out at a temperature of 350 K and a pressure of 0.1 MPa. ....	54
Figure 3-6. Anisotropy of the thermal conductivity $\lambda_{\parallel}/\lambda_{\perp}$ of PS as a function of the averaged direction cosine of the C-C backbone bonds in the parallel direction $\langle \cos_{\parallel} \rangle$ . The RNEMD data have been derived for different temperatures and stretching ratios. ....	55
Figure 3-7. Pressure dependence of the thermal conductivity of a binary PS-CO <sub>2</sub> mixture with 10 mass % of CO <sub>2</sub> and a stretching ratio 22 %. The dashed curve is for the isotropic mixture. ....	56
Figure 3-8. Thermal conductivity of binary PS-CO <sub>2</sub> mixtures as a function of the CO <sub>2</sub> mass concentration at 400 K and 16 MPa for a stretching ratio of 23 %. The dashed curve is for the isotropic sample. ....	57
Figure 3-9. Thermal conductivity of a binary mixture with 10 mass % of CO <sub>2</sub> as a function of the stretching ratio at 400 K and 16 MPa. The mean thermal conductivity $(\lambda_{\parallel} + \lambda_{\perp})/2$ has been symbolized by a dashed curve. The straight line refers to the thermal conductivity of the isotropic sample. ....	57
Figure 3-10. Thermal conductivity ratio $\lambda_{\parallel}/\lambda_{\perp}$ a function of the average cosine between the C-C bonds of the backbone and the direction of heat transfer $\langle \cos_{\parallel} \rangle$ . for binary mixtures at different pressures, temperatures and concentrations of CO <sub>2</sub> ; see the same correlation for neat PS in figure 3-6. ....	58
Figure 3-11. Calculated thermal conductivity as a function of the degrees of freedom per volume for amorphous polyethylene, <sup>104</sup> amorphous polyamide-6,6, <sup>19</sup> crystalline syndiotactic polystyrene, <sup>10</sup> liquid benzene <sup>11</sup> , liquid n-hexane <sup>11</sup> , liquid cyclohexane <sup>11</sup> , supercritical CO <sub>2</sub> (present work), amorphous atactic polystyrene (present work) , amorphous atactic polystyrene +CO <sub>2</sub> (present work). ....	59

---

## 1. Zusammenfassung

---

In der vorliegenden Arbeit wurde die Wärmeleitfähigkeit von reinem Polystyrol sowie von einer Mischung aus Polystyrol und CO<sub>2</sub> untersucht. Des Weiteren wurde die Anisotropie der Wärmeleitfähigkeit in gestrecktem Polystyrol berechnet. Ein zentraler Bestandteil der Arbeit war es, die thermischen Transportprozesse auf Basis der Wärmeleitfähigkeit in verschiedenen molekularen Flüssigkeiten, amorphem Polyamid-6,6 und kristallinem Polystyrol zu untersuchen.

In **Kapitel 1** werden kurz bekannte Nichtgleichgewichts Molekular Dynamik Methoden zur Berechnung der Wärmeleitfähigkeiten vorgestellt. Außerdem werden aktuelle Entwicklungen in den Bereichen der molekularen Flüssigkeiten, Polymeren und Kohlenstoffnanoröhren diskutiert. Betrachtet wurde der Einfluss von Simulationsparametern, wie Thermostat, Austauschperiode, Größe der Simulationszelle und Kraftfeld, auf die berechneten Wärmeleitfähigkeiten. Die Aussagekraft molekular-dynamischer Methoden zur Berechnung thermischer Eigenschaften hängt in erster Linie vom Potenzial zur Beschreibung inter- und intramolekularer Wechselwirkungen ab. Wie in **Kapitel 1** demonstriert wurde, haben die Kraftfeldparameter einen großen Einfluss auf die berechneten Wärmeleitfähigkeiten.

In **Kapitel 2** wurde die Wärmeleitfähigkeit von ataktischem Polystyrol in superkritischem CO<sub>2</sub> mithilfe von Invertierten Nichtgleichgewichts Molekular Dynamik (Reverse Nonequilibrium Molecular Dynamics, kurz RNEMD)<sup>1</sup> Simulationen diskutiert. Da für die binären Systeme keine experimentellen Messungen vorliegen, wurden die Computersimulationen auf die reinen Komponenten Polystyrol und CO<sub>2</sub> ausgedehnt, denn für diese Komponenten standen Messdaten zur Verfügung.<sup>2,3</sup> Der Vergleich berechneter und gemessener Wärmeleitfähigkeiten ist Voraussetzung um die Leistungsfähigkeit der bestehenden theoretischen Methoden zu quantifizieren. Die Analyse hat den weiteren Vorteil, dass die Interpolationsformel es erlaubt die Wärmeleitfähigkeit der Komponenten Polystyrol und CO<sub>2</sub> mit der Leitfähigkeit des binären Systems zu korrelieren. Im Detail wurde die Wärmeleitfähigkeit der Mischung aus Polystyrol und CO<sub>2</sub> mit der RNEMD Methode als Funktion der Temperatur, des Druckes und der CO<sub>2</sub> Konzentration untersucht.

Viele Polymere sind sehr anisotrop, beispielsweise kristalline Polymere. Die Wärmeleitfähigkeit ist eine der Größen, bei der Anisotropien beobachtet wurden.<sup>4,8</sup> Die Anisotropie der Wärmeleitfähigkeit wurde bereits in einigen Experimenten und theoretischen Studien zu Polyamid-6,6 und Polyethylen untersucht.<sup>2,4,8</sup> In **Kapitel 3** wurde die Anisotropie der Wärmeleitfähigkeit von gestrecktem ataktischem Polystyrol in superkritischem CO<sub>2</sub> mithilfe von RNEMD Simulationen diskutiert.

---

In **Kapitel 4** wurden die wichtigsten Ergebnisse und Fortschritte dieser Arbeit zusammengefasst. Das Fazit gibt einen Ausblick auf künftig vielversprechende weitere Untersuchungsmöglichkeiten. Am Ende der Arbeit befindet sich die Liste der Publikationen, die im Rahmen der vorliegenden Dissertation, veröffentlicht wurden.

---

## 2. Summary

---

The purpose of the work presented in this thesis has been to investigate thermal transport in pure polystyrene as well as in a mixture of polystyrene and carbon dioxide. Another part of the work has been to calculate the anisotropy of the thermal conductivity in stretched polystyrene. To finally tie everything together, the most important part has been to understand thermal transport mechanisms on the basis of the thermal conductivity of polystyrene and thermal conductivity of several molecular liquids, amorphous polyamide-6,6 and crystalline polystyrene.

In **chapter 1** the nonequilibrium molecular dynamic methods for calculation of the thermal conductivity have been discussed. The methods have been well-known and described in literature in much detail. Additionally, recent improvements in the calculation of the thermal conductivity of molecular liquids, polymers and carbon nanotubes have been discussed. An analysis has been made of the influence of simulation parameters such as the use of thermostats, perturbation periods, the size of the system, and force field parameters on the calculated thermal conductivity. The ability of molecular dynamics simulations to predict thermodynamic properties is highly determined by the potential used to represent inter- and intramolecular interactions. As it has been discussed in **chapter 1**, the choice of the force field is of the great importance and has the greatest influence on the thermal conductivity calculated.

In **chapter 2** the thermal conductivity of atactic polystyrene (PS) swollen in supercritical CO<sub>2</sub> as evaluated by reverse nonequilibrium molecular dynamics simulations (RNEMD) has been discussed.<sup>1</sup> As experimental thermal conductivity values for the binary systems have not been reported, the computer simulations have been extended to the components PS and CO<sub>2</sub>, for which measured data is available.<sup>2,3</sup> The comparison of calculated and experimental thermal conductivities of the components is a prerequisite for quantifying the capability of the present theoretical tools. The analysis offers a second benefit, i.e. the presentation of an analytical interpolation formula to relate the thermal conductivity of the components PS and CO<sub>2</sub> to the thermal conductivity of the binary mixture. The thermal conductivity of PS-CO<sub>2</sub> mixtures as a function of temperature, pressure and CO<sub>2</sub> concentration by RNEMD simulations has been analyzed.

Many polymers are highly anisotropic, for example crystalline polymers. Thermal conductivity is one of the quantities for which anisotropic behavior has been observed.<sup>4-8</sup> The anisotropy of the thermal conductivity has been analyzed in several experimental and theoretical studies on polymers, such as amorphous polyamide-6,6 and polyethylene.<sup>2,4,8</sup> In **chapter 3** the anisotropy

---

of the thermal conductivity of stretched atactic polystyrene swollen in supercritical CO<sub>2</sub> by reverse nonequilibrium molecular dynamics simulations has been discussed.<sup>1,9-11</sup>

In **chapter 4** all important steps and achievements that have been done during this work have been summarized and an outlook on the work that can be done in the future has been given. In the end of the dissertation one can find a list of the papers that have been published during this PhD work.



---

### 3. Introduction: Calculation of the Thermal Conductivity of Molecular Liquids, Polymers and Carbon Nanotubes

---

In recent years, there have been significant improvements in the study and prediction of dynamic thermophysical properties of materials. Starting with the simulation of simple Lennard-Jones liquids,<sup>1,12,13</sup> theoretical calculations have progressed in the complexity of the materials<sup>10,14-21</sup> as well as in the accuracy of the prediction.<sup>22,23</sup> This significant development is important from two points of view. Firstly, property prediction is important for engineers who design new materials for a variety of applications. From one device to another, materials of different properties are required. One of the examples of simulation-based materials design is a secondary-hardening stainless steel for use in bearings in the fuel and oxidizer turbopumps of the space shuttle main engine.<sup>24</sup> In this case, during several simulation-design iterations, a prototype alloy has been evaluated, and it has demonstrated the desired doubling of fracture toughness at the required hardness level. If one knows the requirements, an iterative simulation-design process can help determine the material.<sup>25-27</sup> Secondly, simulations can give a better understanding of physical processes. Knowing, for example, the dependence between the chemical structure and its influence on the physics of the process, one can design a new material with properties designed for certain applications.<sup>28</sup> The thermal conductivity, for example, is required to be very low for polymers, which are employed both as on-chip dielectric materials and as active layer in plastic electronic devices.<sup>29,30</sup> In the encapsulation of electronic devices, however, a high thermal conductivity is desirable.

In this chapter we discuss recent improvements in the calculation of the thermal conductivity. There are two basic approaches. Equilibrium molecular dynamics (EMD) methods,<sup>31,32</sup> using either the Green-Kubo formalism or the Einstein relations, compute the time-dependent response of a fluid system to spontaneous fluctuations. Nonequilibrium methods (NEMD)<sup>1,33</sup> analyze the response of the system to externally applied perturbations. Both methods have their advantages and disadvantages, but they are comparable in efficiency.<sup>34,35</sup> In this work, we mainly concentrate on NEMD methods.

We summarize the thermal conductivity calculation for molecular liquids of different types and using different models, such as rigid, flexible, all-atom and united-atom. At this point we analyze an influence of simulation parameters, system size and force field on the predicted thermal conductivity. The ability of molecular dynamics to predict thermodynamic properties is highly determined by the potential used to represent inter- and intramolecular interactions. As we will discuss here, the choice of the force field is of great importance and has the largest influence on the calculated thermal conductivity. Calculations become more complicated when one moves from molecular liquids to polymers. The chosen force field plays a bigger

role, and small modifications in molecular structure and molecular orientation can lead to uncertainties in thermal conductivity.<sup>10,14,19</sup> In contrast, the calculation of thermal conductivities for single-walled carbon nanotubes seems to be robust against the force field and its potential form.<sup>36,37</sup> However, several aspects arise in connection with heat transport in carbon nanotubes. For example, thermal rectification has been observed experimentally<sup>38</sup> in carbon nanotubes which are externally loaded with heavy molecules in a conical deposit. This finding has greatly increased interest in the thermal transport in carbon nanotubes. Much theoretical work<sup>37,39,40</sup> has been done on this topic and some of it will be discussed in this paper.

### 3.1. Nonequilibrium Molecular Dynamics Methods

#### 3.1.1. Reverse Nonequilibrium Molecular Dynamics

The reverse nonequilibrium molecular dynamics method has been described in the literature several times.<sup>1,41</sup> It has been developing through the time<sup>11,19</sup> and has been successfully applied to the calculation of the thermal conductivity and shear viscosity of Lennard-Jones liquids,<sup>1</sup> molecular fluids,<sup>11</sup> polymers<sup>10,14,19</sup> and carbon nanotubes.<sup>37</sup> In this chapter we briefly review the original RNEMD method for the calculation of the thermal conductivity.

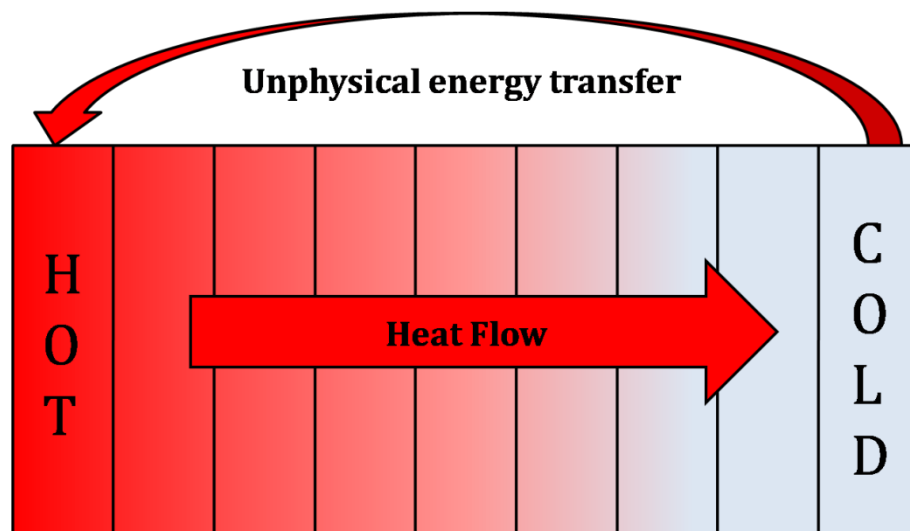


Figure 3-1. Reverse Nonequilibrium Molecular Dynamics Method.

Assume we have a periodic simulation box filled with particles, see figure 1-1. These particles have different velocities and box itself has a temperature corresponding to the velocity distribution. We divide the simulation box into several virtual slabs along, say, the  $z$  direction. One slab on the left side of the box is defined as the “hot” slab, and one slab on the right side of the simulation box is defined as the “cold” one. The RNEMD algorithm transfers energy, in artificial manner, from the “cold” to the “hot” slab. The coldest particle from the “hot” slab is chosen as well as the hottest particle from the “cold” slab. The algorithm exchanges the

---

velocities of these particles, thereby affecting an unphysical energy transfer. Only velocities of particles of identical mass are exchanged. Due to energy conservation and the developing temperature gradient, a physical energy transport is created in the opposite direction. It results in a heat flow  $j_z$  from the “hot” to the “cold” slab. When the steady state has been reached,  $j_z$  is equal in magnitude but opposite in direction to the known imposed artificial energy flow. Within linear-response theory, the thermal conductivity  $\lambda$  relates a heat flux  $j_z$  to the temperature gradient  $\frac{dT}{dz}$

$$j_z = -\lambda \left( \frac{dT}{dz} \right) \quad (1-1)$$

As we know the imposed heat flux  $j_z$ , the temperature gradient can be extracted from the simulation. Thus, thermal conductivity can be calculated using equation 1-1.

There are several simulation parameters, which influence the thermal conductivity calculated by the RNEMD: The perturbation period, in other words, frequency of velocity exchange in the RNEMD algorithm, use of atomic or molecular exchange, usage of thermostat and manostat. For the nonequilibrium methods, the system must be in the linear response regime, that is, the heat flux  $j_z$  and the temperature gradient  $\langle dT/dz \rangle$  must be proportional. It has been demonstrated in the simulations of molecular liquids as well as of polymers that, as long as system is in the linear response regime, the thermal conductivity deviates only within its error bars for different perturbation periods.<sup>11,14,19</sup> Thus, each particular system has to be tested for the linearity of the temperature gradient. If linearity holds, the thermal conductivity can be calculated. The thermal conductivity of molecular liquids has also been confirmed to be insensitive to the use of atomic or molecular (centre-of-mass) exchange in the RNEMD algorithm.<sup>11</sup> In order to impose a heat flux on the system, the RNEMD algorithm switches the velocities of two particles from “hot” and “cold” slabs. A particle can be an atom, a molecule or a part of the molecule, a so-called “semimolecule”. Only atomic or “semimolecular” exchange can be used for polymers.<sup>19</sup> Also the RNEMD method cannot be used for constrained molecules. In this case, the dual-thermostat method (chapter 1.1.2) should be used. The use of Berendsen thermostat has also been tested with RNEMD and no significant influence on the calculated thermal conductivity value has been observed, results agreeing to within their error bars.<sup>11</sup>

### 3.1.2. Dual-Thermostat Method

The setup of dual-thermostat method<sup>33</sup> is shown in figure 1-2. The hot and cold slabs in this method are coupled with Berendsen thermostat locally, and each slab is set to remain at a constant temperature  $T_H$  for the hot slab and  $T_C$  for the cold one ( $T_H > T_C$ ). When the system reaches the steady state, a linear temperature profile is established in the intervening slabs.

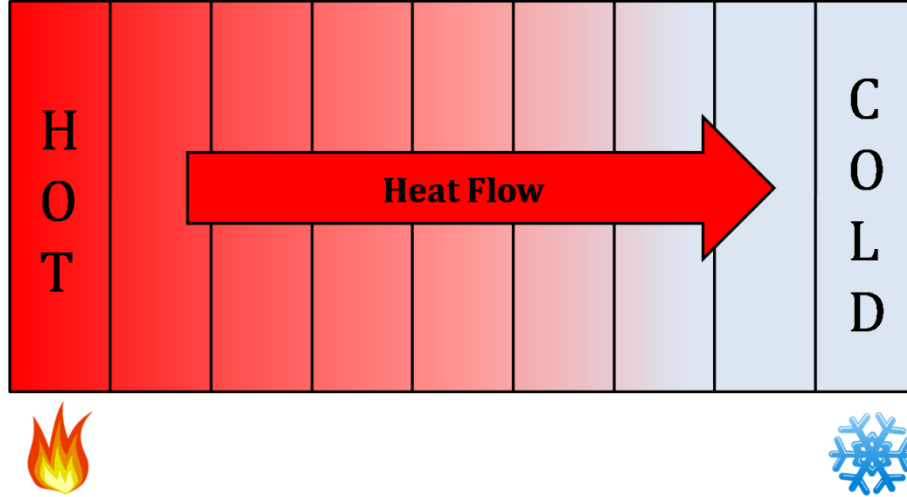


Figure 3-2. Dual-Thermostat Method.

The Berendsen thermostat creates energy in the hot slab, while heat is withdrawn from the cold slab. Since no temperature control is performed in the intervening region, the change in total energy per time step can be written as  $\langle \Delta E_{total} \rangle = \langle \Delta E_H \rangle + \langle \Delta E_C \rangle + \langle \Delta E_{err} \rangle$ , where  $\langle \Delta E_{err} \rangle$  is the change due to numerical errors per MD step and  $\langle \dots \rangle$  stands for time averaging. In each time step, the energy changes  $\Delta E_H$  and  $\Delta E_C$  due to the local Berendsen thermostats are evaluated in the hot and cold slabs. These energy changes are given by  $\Delta E_i \equiv (\eta_i^2 - 1)E_i^K$  ( $i = H, C$ ), where  $\eta_i$ ,  $\Delta E_i$ , and  $E_i^K$  are the velocity scaling factor in slab  $i$ , the energy change in the velocity scaling by the Berendsen thermostat, and the kinetic energy in the slab  $i$  given by  $E_i^K = \sum_{j \in i} m_j \mathbf{v}_j^2 / 2$ , respectively. The summation is carried out over atoms  $j$  contained in the slab  $i$ . Thus, the thermal conductivity  $\lambda$  can be obtained from the formula

$$\lambda = \frac{1}{2A} \frac{\langle \Delta E_i / \Delta t \rangle}{\langle |dT(z)/dz| \rangle}, \quad (1-2)$$

where  $A$  is the cross-sectional area of the simulation box perpendicular to the heat flow direction  $z$ , and the factor 2 arises from the periodicity.

In some of the previous computer simulations of the thermal conductivity, the magnitude of heat flux has been numerically obtained by the fluctuation-dissipation theorem. In these methods, the statistical error can become quite large. In the dual-thermostat method the error arises from the numerical integration only and can be neglected.

The Berendsen thermostat on the hot side may be replaced by a Langevin thermostat. In this case a similar analysis must be applied. Since the energy input of a Langevin thermostat is more difficult to obtain than that of the Berendsen thermostat, the heating rate of an uncooled system must be calculated in a separate equilibrium simulation. This method is commonly referred to as the heat-injection method.<sup>33</sup>

---

### 3.1.3. Thermal-Noise Method

The thermal-noise method<sup>33</sup> generates heat everywhere in the system by thermal noise, but removes it only in one region by a thermostat. The interaction-truncation noise itself has been used as a heat source and the thermostat as a sink. In one dimension, say  $z$ , the change of temperature  $T$  in response to the curvature of the temperature profile is described by Fourier's law

$$\rho A \left( \frac{\partial T(z,t)}{\partial t} \right) = \lambda \left( \frac{\partial^2 T(z,t)}{\partial z^2} \right) + q, \quad (1-3)$$

where  $\rho$  is a mass density,  $A$  is the cross-sectional area of the system perpendicular to the profile direction  $z$ , the local energy production density is  $q$ , and the thermal conductivity is  $\lambda$ . The value  $q$  accounts for the production of energy by truncation noise or some other mechanism and is taken to be constant and uniform across the system, i.e. independent of  $t$  and  $z$ . In the steady state, when  $t \rightarrow \infty$ , the left side of equation 1-3 is zero, and we have

$$\frac{d^2}{dz^2} T(z) = -\frac{q}{\lambda} \quad (1-4)$$

The solution of this differential equation is a parabolic temperature profile

$$T(z) = B(z - z_{max})^2 + T_{max}, \quad (1-5)$$

where  $B$  is given as  $-q/(2\lambda)$ ,  $z_{max}$  and  $T_{max}$  are the position and the temperature of the maximum of the parabola. In the steady state, the total energy of the system must, on average, be kept constant. Therefore, the average rate of energy produced by the thermal noise must be equal to the energy, which is removed from the system by the thermostat.

$$\left\langle \frac{dE(t)}{dt} \right\rangle = qV = qL_x L_y L_z, \quad (1-6)$$

where  $V$  is the volume, and  $L_x$ ,  $L_y$ , and  $L_z$  are the Cartesian dimensions of the system. For the Berendsen thermostat used here, the average rate of energy removed from the system is given by

$$\left\langle \frac{dE(t)}{dt} \right\rangle = \left\langle \frac{\Delta E}{\Delta t} \right\rangle = \left\langle \frac{\beta^2 - 1}{2\Delta t} \sum_i m_i v_i^2 \right\rangle. \quad (1-7)$$

Here,  $\Delta E$  is the amount of energy removed by rescaling the atomic velocities  $v_i$  of all atoms  $i$  by a factor  $\beta$  in one time step  $\Delta t$ , and the  $m_i$  are the atomic masses. The setup of thermal-noise method is displayed in figure 1-3.

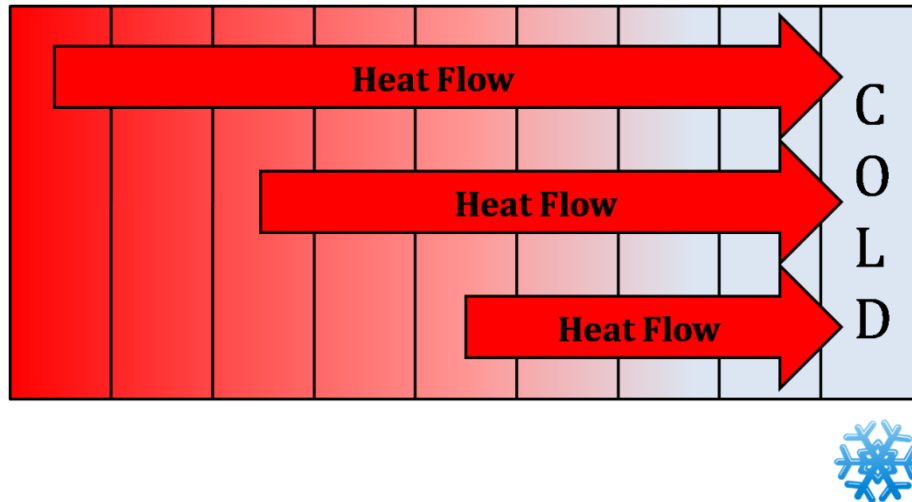


Figure 3-3. Thermal-Noise method.

In order to produce a steady-state nonequilibrium temperature profile, from which to calculate  $\lambda$ , the heating by noise and the cooling by the thermostat must be spatially separated. Therefore, the thermostat operates only on the left side of the system, in the “cold” slab, and the thermal noise is generated throughout the system. When the system reaches the steady state, the parabolic temperature profile can be obtained. From the temperature profile the constants  $B$  and  $T_{max}$  can be obtained. Together with the known average energy removal rate  $\langle \Delta E / \Delta t \rangle$  of the thermostat, the thermal conductivity  $\lambda$  can be calculated

$$\lambda = -\frac{1}{2BV} \left\langle \frac{\Delta E}{\Delta t} \right\rangle. \quad (1-8)$$

The thermal-noise algorithm differs from the NEMD algorithms presented above. It confines only the heat sink to a small, thermostatted subsection of the system, while the heat source is allowed to extend throughout the system. This algorithm shares an advantage with the RNEMD method. At no point, an energy flux needs to be defined or evaluated. Its disadvantage is that the primary quantity to be calculated is a curvature of a parabolic temperature profile, which is numerically less robust to obtain than the slope of a linear profile in the case of the other methods outlined above. The method has however, been shown to produce the same thermal conductivity as RNEMD for a water model.<sup>33</sup>

### 3.1.4. Size Effects

There is a well-known finite size problem in connection with the calculation of transport coefficients. All transport coefficients are a function of the wave vector (or characteristic period). In order to take the macroscopic limit, one could simply use a very big system, but the calculation of the thermal conductivity of 1  $\mu\text{m}$  size, for example, will take years of simulation. On the other hand, one would like to have a system where diffusive thermal transport regime is observed and the thermal conductivity converges. What is, therefore, an

---

optimum size of the simulation box? As we will show below, this question has to be answered for each particular system. There is no guarantee that the box size of  $\sim 7$  nm, which has been found big enough for molecular liquids<sup>11</sup> (chapter 1-2), is suitable for the calculation of the thermal conductivity of polymers. Moreover, the thermal conductivity of single-wall carbon nanotubes diverges with increasing size of the tube and even hundreds of nanometers are not enough to converge it.<sup>37</sup>

### 3.2. Thermal Conductivity of Molecular Liquids

In this chapter, we review several works on the simulation of the thermal conductivities of molecular liquids. The main purpose of the work of Zhang *et al.*<sup>11</sup> has been an identification of influence of the different simulation settings, such as exchange period and method (molecular or atomic) of the RNEMD procedure, size effect, use of thermostat, and influence of the force field. All molecular dynamics simulations have been carried out with YASP package.<sup>42,43</sup> Orthorhombic periodic boundary conditions are implemented in the package. The typical simulation box has been elongated in the  $z$  direction, in which heat flux has been imposed ( $L_x = L_y = L_z/3$ ), in order to avoid size effects. The temperature has been kept constant by Berendsen's thermostat.<sup>44</sup> Temperatures and densities have been chosen at or close to the conditions, where experimental values were available. The nonbonded potential consists of Lennard-Jones terms, and electrostatic interactions for atomic partial charges. The reaction-field method has been used to calculate electrostatic interactions. The intramolecular interaction includes harmonic bond stretching or constraint, harmonic bond angle bending, periodic cosine-type torsional potential, and harmonic dihedral potential. Specific settings of simulation parameters are reported below for the individual systems. For the details of the functional form of potentials, see ref. 42.

The purpose of the benzene simulation has been not only to calculate the thermal conductivity value, but also to find an influence of the velocity exchange period and system size on the thermal conductivity. A benzene system of 645 molecules has been simulated at constant  $NVE$ . Bond constraints, but flexible bond angles and dihedral angles have been used. A linear temperature profile has been reached within 900 ps. The benzene model used is known to be liquid down to 240 K.<sup>45</sup> Thus, there has been no two-phase situation. The thermal conductivity calculations have been performed with three different exchange periods of 150, 300 and 500 fs. They resulted in only a small deviation of the thermal conductivity of 0.193, 0.197 and 0.208  $\text{Wm}^{-1}\text{K}^{-1}$ , respectively. This means that all chosen perturbations are in the linear response regime. The size effect on  $\lambda$  has also been considered. Two systems with a length in the  $z$  direction of  $1/3$  and  $2/3$  of the original  $L_z$  value have been simulated. Only in the case of the shortest system, the thermal conductivity has been found to be 0.27-0.29  $\text{Wm}^{-1}\text{K}^{-1}$ .

---

$^1\text{K}^{-1}$ , i.e. significantly larger than the value of  $0.197 \text{ Wm}^{-1}\text{K}^{-1}$  mentioned above. The thermal conductivity value of the intermediate system ( $\frac{2}{3}L_z$ ) already amounts to  $\sim 0.20 \text{ Wm}^{-1}\text{K}^{-1}$ , which is not very different from the value for the full-size system. It seems that the system size effect can be important for the calculation of the thermal conductivity and it should be evaluated for every system. The calculated thermal conductivity is about 30 % larger than the experimental one<sup>46</sup> ( $0.141 \text{ Wm}^{-1}\text{K}^{-1}$  at 298 K), which may be a consequence of the use of the semiflexible benzene model. Some degrees of freedom in benzene (bond angles involving hydrogens) are stiff enough to be quantum oscillators in their ground states in reality. However, they are treated classically in Newtonian dynamics and thus transfer energy, what they are not able to do in reality. In this way they cause a higher thermal conductivity in the simulation.

Cyclohexane has been chosen, because it can be represented by a force field completely without electrostatic interactions. Therefore, a thermostat can be completely avoided, because there is no artificial heating due to cutoff noise of the Coulomb interactions. Cyclohexane (750 molecules) has been simulated at constant *NVE*. An optimized all-atom force field with bond constraints has been used.<sup>47-49</sup> A thermal conductivity of  $0.235 \text{ Wm}^{-1}\text{K}^{-1}$  has been obtained by the simulations, which is approximately twice as large as the experimental value<sup>46</sup> ( $0.123 \text{ Wm}^{-1}\text{K}^{-1}$  at 298 K). The cyclohexane molecule is more flexible than benzene and it has a larger number of internal degrees of freedom. This is one of the reasons for the larger overestimation of thermal conductivity for cyclohexane than for benzene. The influence of a thermostat has also been investigated for cyclohexane. The Berendsen thermostat with a short coupling time of 0.2 ps has shown very little effect on  $\lambda$  ( $0.234 \text{ Wm}^{-1}\text{K}^{-1}$  in the simulation with thermostat against  $0.235 \text{ Wm}^{-1}\text{K}^{-1}$  without). Besides the model without electrostatic interactions, a second all-atom force field with partial atomic charges ( $q_C = -2q_H = -0.12e$ , reaction-field dielectric constant of 2) has been tested for cyclohexane without a thermostat. This has changed the thermal conductivity to  $0.182 \text{ Wm}^{-1}\text{K}^{-1}$ , i.e. in the direction of the experimental value, indicating that the force field does have an influence on the result of simulation. Also the thermal conductivity of benzene-cyclohexane mixtures of different compositions has been evaluated. Since both liquids have similar thermal conductivities,  $\lambda$  value for different compositions do not differ meaningfully.

The influence of the force field has been further tested using rigid and flexible SPC/E water representations.<sup>50</sup> The influence of molecular versus atomic exchange has also been determined in this simulation. Water (900 molecules, reaction-field correction with a dielectric constant of 72) has been simulated at constant *NVT*. For the rigid SPC/E model with molecular exchange the thermal conductivity amounts to  $0.81 \pm 0.01 \text{ Wm}^{-1}\text{K}^{-1}$ , in a good agreement with a value obtained using thermal-noise method (chapter 1.1.3).<sup>33</sup> However, the simulated value overestimates the experimental thermal conductivity of  $0.607 \text{ Wm}^{-1}\text{K}^{-1}$  at



---

298 K.<sup>46</sup> Details of the long-range interactions do not seem to matter much. The nonbonded interaction cutoff has been changed from 0.98 nm to 0.75 nm, which modified the thermal conductivity value from  $0.810 \pm 0.010 \text{ Wm}^{-1}\text{K}^{-1}$  to  $0.820 \pm 0.010 \text{ Wm}^{-1}\text{K}^{-1}$ . To test the effect of atomic versus molecular exchange, simulations of flexible SPC/E water have been performed, because atomic exchange can be employed only for molecules without constraints. The thermal conductivity of  $0.980 \pm 0.010 \text{ Wm}^{-1}\text{K}^{-1}$  obtained with molecular exchange is only slightly different from the value for the same model with atomic exchange of  $0.950 \pm 0.010 \text{ Wm}^{-1}\text{K}^{-1}$ . Thus, the difference between two exchange algorithms is small. Moreover, the thermal conductivity has been found insensitive to the variations of harmonic force constants. The system size effect has been considered for the water simulation as well as for the benzene system. The size of the simulated system ( $2.05 \text{ nm} \times 2.05 \text{ nm} \times 6.15 \text{ nm}$ ) has been found to be sufficiently large to achieve a converged value of  $\lambda$ .

*n*-Hexane has been studied as an example of a flexible molecule with soft internal degrees of freedom. A modified united-atom Ryckaert-Bellemans model has been used.<sup>51</sup> Two different runs (300 molecules) with constrained and flexible bonds have been performed. For the model with bond constraints, a thermal conductivity of  $0.107 \pm 0.002 \text{ Wm}^{-1}\text{K}^{-1}$  has been obtained. The thermal conductivity of the flexible model amounts to  $0.134 \pm 0.004 \text{ Wm}^{-1}\text{K}^{-1}$ . As for water, the flexible model with a larger number of degrees of freedom has a higher thermal conductivity. However, in contrast to all other systems, the thermal conductivity values of *n*-hexane for rigid and flexible models are within 10 % of the experimental value of  $0.120 \text{ Wm}^{-1}\text{K}^{-1}$ .<sup>46</sup> It seems that this has to do with the use of united-atom model versus all-atom model for the other systems.

The purpose of the next work<sup>23</sup> has been a development of the correct model for methyl-substituted benzenes for the prediction of such thermodynamic properties as liquid density, saturation pressure, and enthalpy of vaporization, as well as transport properties such as self-diffusion, shear viscosity and thermal conductivity. The charged anisotropic united atom (ch-AUA) model for different methyl-substituted benzenes has been developed by Nieto-Draghi *et al.*<sup>23</sup> This model includes electrostatic interactions, which are not required to reproduce thermodynamic properties well, but become crucial for the reproduction and prediction of transport properties such as the shear viscosity and the thermal conductivity. The benzene molecule of this model is represented by 9 sites: a positive partial charge is placed in the center of the ring, two negative charges are placed above and below the plane of the molecule, and six Lennard-Jones centers are placed at offset distance from the carbon centers. Electrostatic interactions have been treated using Ewald summation. The authors have calculated the thermal conductivity of benzene, toluene, *o*-xylene, *m*-xylene and *p*-xylene using the developed ch-AUA model. A modified RNEMD method has been used for the

calculation of the thermal conductivity: the velocity exchange works also for particles with different masses. During this exchange, so-called virtual elastic collision, the particles exchange their momentum. Thus, the total momentum and energy of the system are kept constant. All simulations contained 800 molecules and were performed at 298 K and 0.1 MPa. We have summarized the simulated and experimental values<sup>52</sup> in table 1-1.

Table 3-1. Comparison of calculated thermal conductivities with experimental data.<sup>52</sup>

Molecule	ch-AUA model (Wm <sup>-1</sup> K <sup>-1</sup> )	Experiment (Wm <sup>-1</sup> K <sup>-1</sup> )	Deviation (%)
benzene	0.133 ± 0.002	0.14081	-5.5
toluene	0.131 ± 0.001	0.13051	0.07
<i>o</i> -xylene	0.129 ± 0.002	0.12875	0.2
<i>m</i> -xylene	0.125 ± 0.002	0.12943	-3.1
<i>p</i> -xylene	0.117 ± 0.002	0.12679	-7.7

The use of the ch-AUA model gives a maximum difference of ~8 % from the experimental value. For example, the calculation of the thermal conductivity of benzene using all-atom model by Zhang *et al.*<sup>11</sup> produces a deviation of 40 % from experiment. The ch-AUA model removes some internal degrees of freedom, which participate in the classical MD heat transfer, but do not do it in reality. This example demonstrates again that the choice of the force field, i.e. internal degrees of freedom participating in heat transfer, is very important for the thermal conductivity calculations.

An example of the thermal conductivity calculation for polar liquids such as methanol and ethanol can be found in the work of Guevara-Carrion *et al.*<sup>22</sup> Rigid, nonpolarizable molecular models of united-atom type have been used for the simulation of alcohol molecules. The methanol model has two Lennard-Jones sites, i.e. one for the methyl group and one for the hydroxyl group. Three point charges are placed, i.e. one at each of the Lennard-Jones sites and one at the position of the hydroxyl hydrogen. The ethanol molecule has been modeled using three Lennard-Jones sites, one for the methyl, the methylene and the hydroxyl group. Three point charges are located here on the methylene and hydroxyl Lennard-Jones centers and on the position of hydroxyl hydrogen. The modified RNEMD as it has been described in the previous example has been used for the calculation of the thermal conductivity of methanol and ethanol at different temperatures. In the NEMD simulation, 800 molecules of methanol or ethanol have been placed in the simulation box with  $L_x = L_y = \frac{1}{3} L_z$ . The system has been equilibrated for 1 ns with a following production run of 2 ns. An exchange period of 300 fs has been used. Electrostatic interactions have been treated using the reaction field. Simulated thermal conductivities of pure methanol and ethanol at different temperatures and pressure of 0.1 MPa are summarized in table 1-2.

Table 3-2. Simulated<sup>22</sup> and experimental<sup>46,53</sup> thermal conductivities of methanol and ethanol at different temperatures.

T(K)	Methanol		T(K)	Ethanol	
	Sim(Wm <sup>-1</sup> K <sup>-1</sup> )	Exp(Wm <sup>-1</sup> K <sup>-1</sup> )		Sim(Wm <sup>-1</sup> K <sup>-1</sup> )	Exp(Wm <sup>-1</sup> K <sup>-1</sup> )
220	0.220 ± 0.030	0.223	253.15	0.180 ± 0.010	0.182
260	0.207 ± 0.009	0.212	273.15	0.178 ± 0.009	0.176
300	0.191 ± 0.009	0.201	298.15	0.171 ± 0.009	0.169
320	0.188 ± 0.008	0.194	328.15	0.161 ± 0.008	0.161

The agreement with experimental data is remarkable with an average deviation of 5 % for methanol and 2 % for ethanol. We relate this very good agreement with experimental data to the very convincing united-atom models that have been used for the simulation of methanol and ethanol.

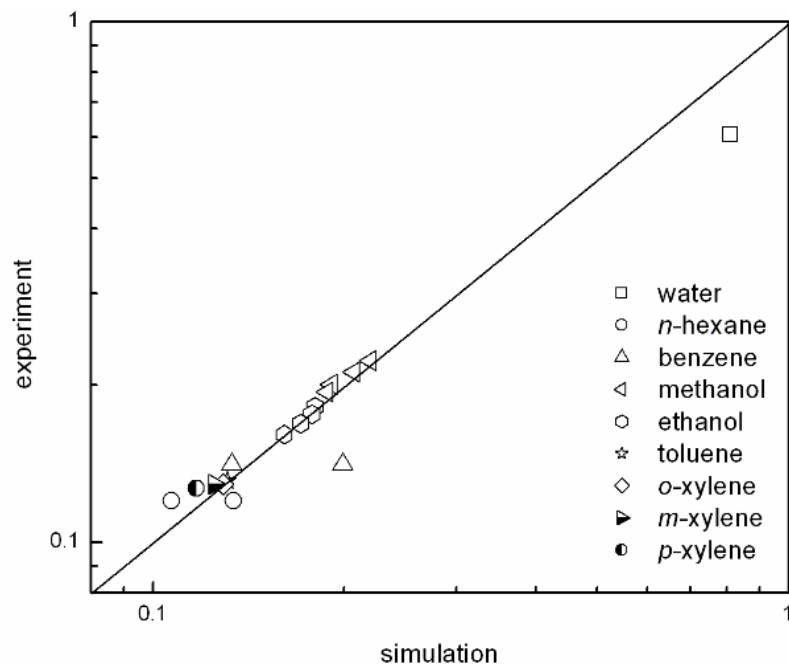


Figure 3-4. Simulated thermal conductivities versus corresponding experimental values for water,<sup>11</sup> *n*-hexane,<sup>11</sup> benzene,<sup>11,23</sup> methanol,<sup>22</sup> ethanol,<sup>22</sup> toluene,<sup>23</sup> *o*-xylene,<sup>23</sup> *m*-xylene,<sup>23</sup> and *p*-xylene.<sup>23</sup>

The thermal conductivities of molecular fluids described above versus their experimental values are compiled in figure 1-4. The agreement is very good for a transport coefficient.<sup>54,55</sup> The reverse nonequilibrium molecular dynamics method seems to be suitable for the calculation of thermal conductivities of molecular liquids. There are several conclusions that can be drawn from the simulations described above:

- The calculated thermal conductivities are insensitive to variation of RNEMD parameters (exchange period, atomic or molecular exchange).

- 
- The calculations show that a system size of several hundred to some thousand molecules and a length of several nanometers are enough to avoid size effects.
  - The thermal conductivities are insensitive to the use of a Berendsen thermostat.
  - With all other parameters at sensible values, the force field has the largest influence on the thermal conductivity.
  - The thermal conductivity increases with the available degrees of freedom. However, they can be reduced by using united-atom models and/or bond constraints. This removes high-frequency motions, which shifts the calculated thermal conductivities in the direction of experimental values.

Hence, we would like to point out that only the use of different force field changes the calculated thermal conductivity significantly. Most often the correct choice of a united-atom model plus constraining the bonds moves the calculated thermal conductivity in the direction of the experimental value. In other words, reducing the number of internal degrees of freedom makes calculation of thermal conductivity more accurate. This is in marked contrast to the calculation of most other fluid properties.

### 3.3. Thermal Conductivity of Polymers and its Anisotropy

In this chapter, we discuss some of the few applications of molecular simulation to the calculation of the thermal conductivity of polymers. Besides the thermal conductivity we also comment on its anisotropy, which is not easy to measure experimentally, but which can be simulated. Moreover, we show that the consideration of the anisotropy can lead to a better understanding of the heat transport in general.

#### 3.3.1. Amorphous Polyamide-6,6

The purpose of the work of Lussetti *et al.*<sup>19,56</sup> has been an extension of the RNEMD method<sup>1</sup> to polymers. The authors focused on the simulation of amorphous polyamide-6,6 using different force field schemes, trying to find which one leads to the best reproduction of the experimental thermal conductivity.

The simulation cell has been elongated in the  $z$  direction, in which the heat flux was imposed ( $L_x = L_y = \frac{1}{2}L_z$ ). Temperatures and densities have been chosen at or close to ambient conditions, where experimental data are most abundant. All simulations have been carried out at constant volume and temperature. Both all-atom and united-atom force fields have been used. The nonbonded potential contained Lennard-Jones terms, with Lorentz-Berthelot mixing rules for unlike interactions, and electrostatic interactions (reaction-field dielectric constant of 5) of the atomic partial charges on the amide groups. The intramolecular force field included harmonic bond stretching or a varying number of constraints, harmonic bond

angle bending, and periodic cosine-type torsional potentials. For details of the functional form, see ref. 42.

Four different force fields have been used in order to investigate the influence of their difference on the thermal conductivity, with special attention to the number of degrees of freedom per chain. The first model was a flexible all-atom model (fl-AA), without any constraints. In the second model, all CH<sub>2</sub> and CH<sub>3</sub> groups have been treated as united atoms, no constraints have been used. This model has been denoted as flexible united-atom model (fl-UA). In the next model, united CH<sub>2</sub> and CH<sub>3</sub> atoms have been used as in the fl-UA one, but all bonds have been constrained except the bonds between amide groups and adjacent CH<sub>2</sub> groups and the central CH<sub>2</sub>-CH<sub>2</sub> bonds of the hexamethylene units. This model has been called partially constrained united-atom model (pc-UA). Finally, in the fully bond-constrained united-atom model (fc-UA) all bonds have been constrained. This last model could only be treated with the dual-thermostat NEMD method,<sup>48</sup> which has been described in chapter 1.1.2. The sample contained 48 chains of 20 repeat units, which corresponds to a molecular weight of 4539 g/mol. Densities of 1.07 g/cm<sup>3</sup> and 1.11 g/cm<sup>3</sup> have been used in the simulations. These values correspond to the extreme points of experimental density interval (1.07 – 1.1 g/cm<sup>3</sup>).

Table 3-3. Experimental<sup>57-59</sup> and simulated thermal conductivities of amorphous polyamide-6,6 at 300 K and 0.1 MPa.

Model	Degrees of freedom per repeat unit	$\lambda(\text{Wm}^{-1}\text{K}^{-1})$
Flexible, all-atom	114	0.45 ± 0.04
Flexible, united-atom	54	0.32 ± 0.02
Partially constrained, united-atom	41	0.29 ± 0.02
Fully constrained, united-atom	36	0.27 ± 0.03
Experiment <sup>57-59</sup>		0.15 – 0.30

The most important result of this work has been the dependence of the calculated thermal conductivity on the force field. The simulated  $\lambda$  value varies from 0.26 to 0.45 Wm<sup>-1</sup>K<sup>-1</sup> (table 1-3). The range of experimental thermal conductivities reflects typical discrepancies between experimental values for different polymer samples.<sup>57-59</sup> A value of 0.24 Wm<sup>-1</sup>K<sup>-1</sup> has been taken as reference.<sup>57</sup> It is typical for simulations to overestimate the thermal conductivity. The fully flexible all-atom model of polyamide-6,6 (fl-AA) with the highest number of degrees of freedom per repeat unit thus gives the highest thermal conductivity. The other extreme point, the most constrained united-atom model with all explicit hydrogens removed (fc-UA), leads to the lowest value, which is closest to the experiment.

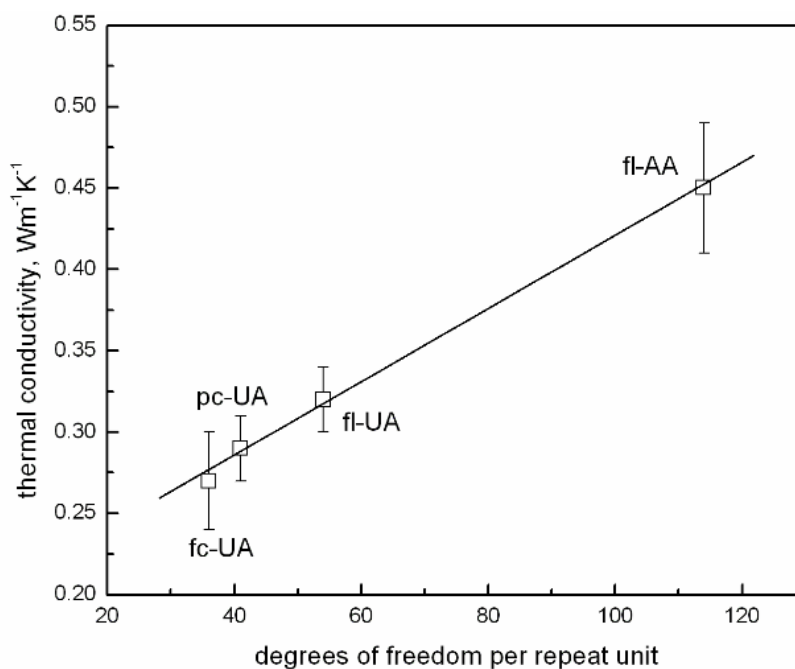


Figure 3-5. The calculated thermal conductivity of polyamide-6,6 as a function of degrees of freedom per repeat unit. The line is a linear fit to the data. Figure has been taken from the work of Lussetti *et al.*<sup>19</sup>

The dependence of the thermal conductivity on the number of degrees of freedom per repeat unit is presented in figure 1-5. It appears to be linear. These results are in agreement with the hypothesis that not all degrees of freedom are thermally excited in reality, but they all participate in the energy transport in classical MD simulations. This concept explains the correlation between the observed thermal conductivity and the force field ansatz, but it is certainly oversimplified. If the assumption that all degrees of freedom contribute equally to the thermal conductivity were true, the line would pass through the origin, which it evidentially does not. The reason is that vibrational modes contribute differently to the thermal conductivity, which will be also shown below for the polystyrene simulations in chapter 1.3.2.

The second important point of this study was the investigation of the thermal conductivity of stretched amorphous polyamide-6,6 with the flexible united-atom model. An amorphous isotropic polyamide-6,6 sample has been stretched in one direction by 27 %. The stretching procedure has been described in detail in the original work.<sup>19</sup> The density of the stretched sample has been adjusted to the one of the isotropic sample (1.07 g/cm<sup>3</sup>). The thermal conductivities parallel to the stretching direction  $\lambda_{\parallel}$  and perpendicular to it  $\lambda_{\perp}$  have been evaluated for the stretched sample. The resulting  $\lambda_{\parallel}$  has been  $0.44 \pm 0.02 \text{ Wm}^{-1}\text{K}^{-1}$ , which is 37 % higher than for the isotropic sample at the same conditions, and the  $\lambda_{\perp}$  has been  $0.28 \pm 0.02 \text{ Wm}^{-1}\text{K}^{-1}$ , which is 12 % lower than for the isotropic sample. The anisotropy of the thermal conductivity  $\lambda_{\parallel}/\lambda_{\perp}$  has been approximately 1.5.

---

Stretching causes polymer chains to orient in the stretching direction. An increased thermal conductivity in the same direction supports the hypothesis that there are two types of heat transport in polymers. The faster is solid-like, through-bond, and progresses along the chain via phonon vibrations. The slower one is liquid-like, through-space, and transfers energy between different chains by collisions.

### 3.3.2. Crystalline Syndiotactic Polystyrene

The thermal conductivity of crystalline syndiotactic polystyrene (sPS) has been investigated by Rossinsky *at al.*<sup>10</sup> The main goals of this work have been an investigation of the dependence of the thermal conductivity on the number of degrees of freedom and an investigation of the anisotropy. Does the thermal conductivity of sPS increase linearly with the number of degrees of freedom as for amorphous polyamide-6,6? This question has been answered in the work. The basic simulation cell contained 12 polystyrene chains of  $\delta$  modification, which is best described as loosely packed, parallel helices. Every chain consisted of 16 monomers. A view of the simulation cell is shown in figure 1-6.

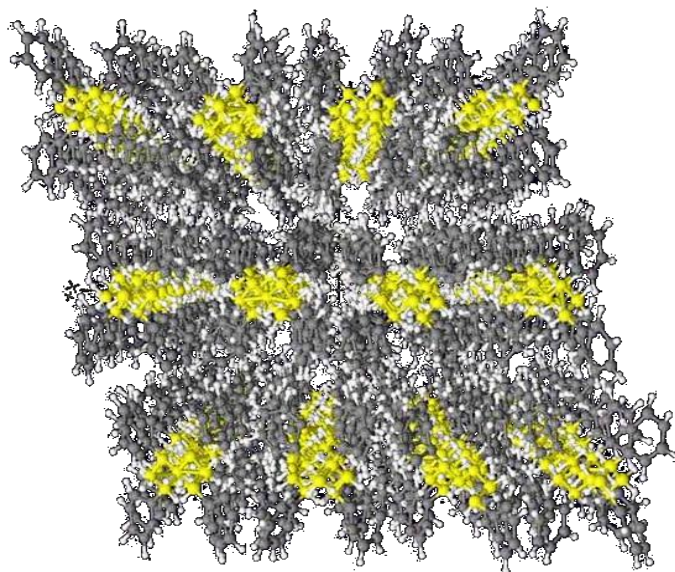


Figure 3-6. The  $\delta$  modification of sPS viewed along the helix axis ( $z$  direction). Backbone atoms are highlighted in yellow.

Periodic boundary conditions have been applied in all directions. The system simulated corresponds to the limit of a perfect polymer crystal. The basic cell has been replicated 3 times in the direction of the heat flow to get the final simulation box. All simulations have been carried out with the YASP package.<sup>42,43</sup> The temperature has been kept constant at 300 K by Berendsen's method<sup>44</sup>. The thermal conductivity has been calculated in the  $x$ ,  $y$  and  $z$  directions, with  $z$  being the helix direction. Momentum exchange between atoms or molecular groups has been performed every 450, 550 and 250 fs for the calculation of thermal

conductivities in  $x$ ,  $y$  and  $z$  directions, respectively. The equilibration run lasted 10 ns, the RNEMD calculations have been run for at least 1 ns.

The experimental thermal conductivity of crystalline sPS does not seem to be available. An experimental measurement for semicrystalline sPS of unknown crystallinity at 300 K has shown a thermal conductivity of  $0.19 \pm 0.03 \text{ Wm}^{-1}\text{K}^{-1}$ .<sup>60</sup> As it has been calculated in the simulations of  $\delta$  form of syndiotactic polystyrene, the average thermal conductivity  $\bar{\lambda} = (\lambda_x + \lambda_y + \lambda_z)/3$  is between 0.20 and 0.30  $\text{Wm}^{-1}\text{K}^{-1}$  depending on the constraint pattern used. The heat transport in the helix direction ( $z$ ) appears to be much larger than in the perpendicular directions (table 1-4). The anisotropy defined as  $2\lambda_z/(\lambda_x + \lambda_y)$  amounts to 2.7 for the  $\delta$  form of sPS. The reason for the perpendicular thermal conductivities showing a (minor) difference is a closer contact between atoms of opposite phenyl rings in the  $y$  direction, which has been observed before by de Rosa *et al.*<sup>61</sup>

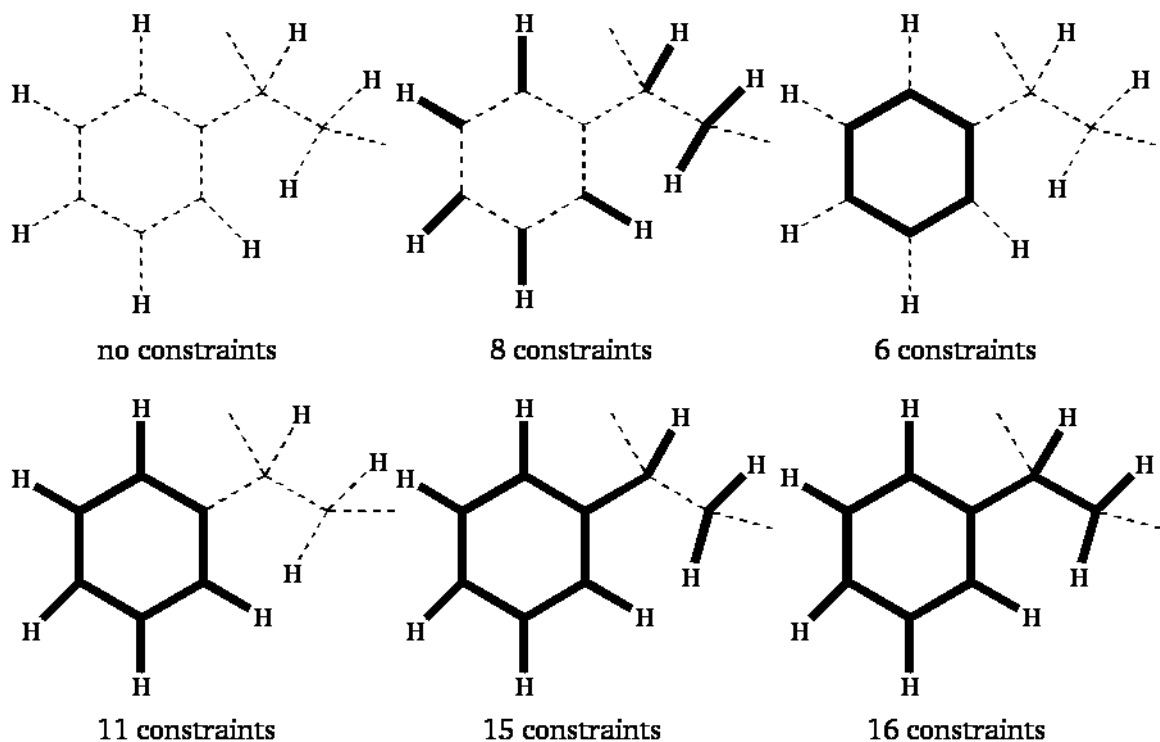


Figure 3-7. Scheme of the different constraint patterns. Constrained bonds are marked by thick solid lines, flexible bonds by thin dashed lines.

Different force field setups have been used for the simulation of crystalline polystyrene<sup>10,45,54,55,62</sup> in order to investigate the influence of the number of degrees of freedom on the calculated thermal conductivity. They differ by bond constraints versus flexible bonds used in the model. The constraint patterns are presented in figure 1-7.



Table 3-4. Components of the thermal conductivity in Cartesian directions ( $\text{Wm}^{-1}\text{K}^{-1}$ ) and average thermal conductivity for the  $\delta$  phase of sPS.

	No constr.	8 constr.	6 constr.	11 constr.	15 constr.	16 constr.
$\lambda_x$	$0.171 \pm 0.005$	$0.162 \pm 0.001$	$0.156 \pm 0.004$	$0.155 \pm 0.005$	$0.172 \pm 0.007$	$0.107 \pm 0.004$
$\lambda_y$	$0.224 \pm 0.004$	$0.198 \pm 0.001$	$0.207 \pm 0.002$	$0.184 \pm 0.004$	$0.200 \pm 0.004$	$0.186 \pm 0.004$
$\lambda_z$	$0.554 \pm 0.012$	$0.475 \pm 0.025$	$0.523 \pm 0.010$	$0.512 \pm 0.010$	$0.510 \pm 0.027$	$0.301 \pm 0.014$
$\bar{\lambda}$	0.316	0.278	0.295	0.284	0.294	0.198

The resulting thermal conductivities are reported in table 1-4. As it has been shown for amorphous polyamide-6,6, number of degrees of freedom does matter for the heat transport. Constraining bonds decreased the number of available degrees of freedom and subsequently the thermal conductivity. Table 1-4 shows that the situation is different for crystalline syndiotactic polystyrene. The variations due to the different constraint patterns are small for all of them except the most constrained model (16 constraints). The typical difference in the thermal conductivity caused by different constraint patterns is about 30 %, for a given thermal conductivity component, while for amorphous polyamide-6,6 it has been about 10 %. It seems that the thermal conductivity of crystalline sPS is robust against variations of number of degrees of freedom in the model. Only for the most constrained model a systematically lower thermal conductivity has been observed. This can probably be explained by the fact that not only the number of degrees of freedom matters, but also their location. The thermal conductivity decreases significantly only when the carbon-carbon backbone bonds are constrained. This is consistent with the notion that fast heat transport occurs via phonons along the polymer backbone. In contrast, the side-chain atoms and groups contribute mainly to the less efficient collisional energy transfer between neighbouring chains, but are dead ends concerning the energy transport along the backbone. Thus, it is not important if they contain constraints or not.

### 3.3.3. Polyethylene

There are not many thermal conductivity calculations for polymers in the literature besides the above mentioned amorphous polyamide-6,6, crystalline and amorphous polystyrene. In this chapter we discuss a thermal conductivity calculation for polyethylene. Polyethylene is the most widely used polymer. It has very simple structure which makes it convenient and cheap for simulations.

In the work of Ni *et al.*<sup>20</sup> the thermal transport in crystalline polyethylene (PE) and at polyethylene-diamond interfaces has been investigated by a nonequilibrium molecular dynamics method. This direct method for the calculation of the thermal conductivity has been developed by Schelling *et al.*<sup>63</sup> and successfully used for the thermal conductivity calculations

---

for silica and diamond. In this method temperature, a thermal gradient is imposed on the system by establishing “hot” and “cold” bath regions. Equal amounts of energy are added and removed at the “heat source” and “heat sink” regions of the system. In order to produce a heat source and a heat sink in the bulk, the velocity rescaling mechanism of Jund *et al.*<sup>64</sup> has been employed. The reactive empirical bond order (REBO) potential<sup>65</sup> has been used to describe crystalline polyethylene. The authors have calculated the thermal conductivity along the polyethylene chains. Several systems have been investigated, where the molecular weight of one PE chain has been varied between  $2.8 \times 10^3$  and  $2.24 \times 10^4$  g/mol. The temperature profile has been averaged over 300000 MD steps with a time step of 0.1 fs. The calculated thermal conductivity has increased monotonically from 11.7 to  $99.6 \text{ Wm}^{-1}\text{K}^{-1}$  as the length of the polymer chain increased. The thermal conductivity value of  $310 \pm 190 \text{ Wm}^{-1}\text{K}^{-1}$  has been obtained by extrapolating the calculated values to infinite molecular weight. This extrapolated value is significantly larger than the value of  $\sim 40 \text{ Wm}^{-1}\text{K}^{-1}$  determined experimentally for ultradrawn single crystal PE mats.<sup>66</sup> The authors attribute this to the impurities and defects, which are always present in experimental crystals, but which can be avoided in simulations. They have simulated one kind of defect, which is often present in experimental samples: C=C double bonds, which are shorter and stiffer than C-C single bonds. It can be expected that the presence of any kind of defect will result in the reduction of the thermal conductivity. However, when the content of polyacetylene units is less than 75 %, it does not change the thermal conductivity of crystal, but when its concentration is higher than 75 %, the thermal conductivity is actually higher than the one of pure PE. The reason is the thermal conductivity of pure polyacetylene ( $\sim 50 \text{ Wm}^{-1}\text{K}^{-1}$ ), which is much larger than that of polyethylene ( $\sim 17 \text{ Wm}^{-1}\text{K}^{-1}$ ). It seems that the shorter and stiffer C=C double bonds in PA increase the efficiency of heat transport. It obviously follows that the decrease in thermal conductivity due to defects in the chain is balanced by the increase due to the higher thermal conductivity in PA units. Thereby, when polyacetylene becomes dominant in the PE-PA random copolymer the thermal conductivity increases. Another type of defect considered in the work of Ni *et al.*<sup>20</sup> is cross-linking. The thermal conductivity of PE with 5 % and 10 % of the C atoms on each chain being cross-linked has been calculated. This has led to the reduction in thermal conductivity of 26.6 % and 44.2 %, respectively. To emphasize, the thermal conductivity of perfectly elongated PE chain found in simulation is very high and exceeds the experimental value about 7 times. The admixture of a defect like cross-linking, which is always present in experiment, decreases the thermal conductivity significantly, but not to the experimental value.

---

### 3.4. Thermal Conductivity and Thermal Rectification in Carbon Nanotubes

Carbon nanotubes have been widely studied during the last few years.<sup>21,67-70</sup> The large interest in this nanosize structure is determined by its remarkable properties such as very high electrical<sup>71</sup> and thermal conductivity.<sup>67</sup> For instance, the longitudinal thermal conductivity of single walled carbon nanotubes (SWNT) has been found to be in the range from several hundred to several thousand  $\text{Wm}^{-1}\text{K}^{-1}$  in different simulations<sup>67,68,70</sup> and experiments<sup>72,73</sup>. Thereby, the value of SWNT's thermal conductivity exceeds the value of such well-known thermal conductor as silver ( $429 \text{Wm}^{-1}\text{K}^{-1}$ ). Nevertheless, it is difficult to synthesize a high-quality and well-ordered nanotube, and it is still challenging to perform perfect thermal conductivity measurements. At this point simulations become useful. Properties, which cannot be properly measured in experiment, can be predicted by simulations. In this chapter we summarize several works, which have been done recently on the thermal conductivity of SWNTs.

The thermal conductivity of SWNTs, and its dependence on temperature, length and diameter has been studied in the recent work of Alaghemandi *et al.*<sup>37</sup> The simulations have been performed using the RNEMD approach described in chapter 1.1.1. The intramolecular force field contains harmonic bond stretching, harmonic bond angle bending and harmonic dihedral angle terms. The nonbonded potential includes Lennard-Jones terms. It has been added to account for C-C interactions of the van der Waals type, where needed. Force constants and details of potential form can be found in the original work.<sup>37</sup>

As it has been reported in the literature before,<sup>21,67</sup> the thermal conductivity of a carbon nanotube depends on the length of the tube. Thermal conductivities of different tubes with chiral indices of (5, 5), (10, 0), (7, 7), (10, 10), (17, 0), (15, 15), and (20, 20), and of lengths between 5 and 350 nm have been calculated in the simulation of Alaghemandi *et al.*<sup>37</sup> The length dependence of the thermal conductivity is shown in figure 1-8.

The thermal conductivity increases with the tube length  $L$ . This is consistent with the length dependence found in other MD studies.<sup>18,21,31,70</sup> It has been demonstrated experimentally that, for tubes of a length below the phonon mean free path ( $\sim 0.5 \mu\text{m}$ ), the thermal conductivity does not converge with tube length to a constant limit. The thermal conductivity in figure 1-8 increases with a power law  $L^\alpha$ . The room temperature constant  $\alpha$  amounts to approximately 0.77 for short ( $L < 25 \text{nm}$ ) and 0.54 for longer ( $100 \text{nm} < L < 350 \text{nm}$ ) SWNTs. A similar dependence has been found in the theoretical work of Wang *et al.*<sup>74</sup> Another message that can be extracted from figure 1-8 is independence of the thermal conductivity from the diameter and chirality of the tube. There is small splitting for short tube lengths, but almost no difference for longer tubes.

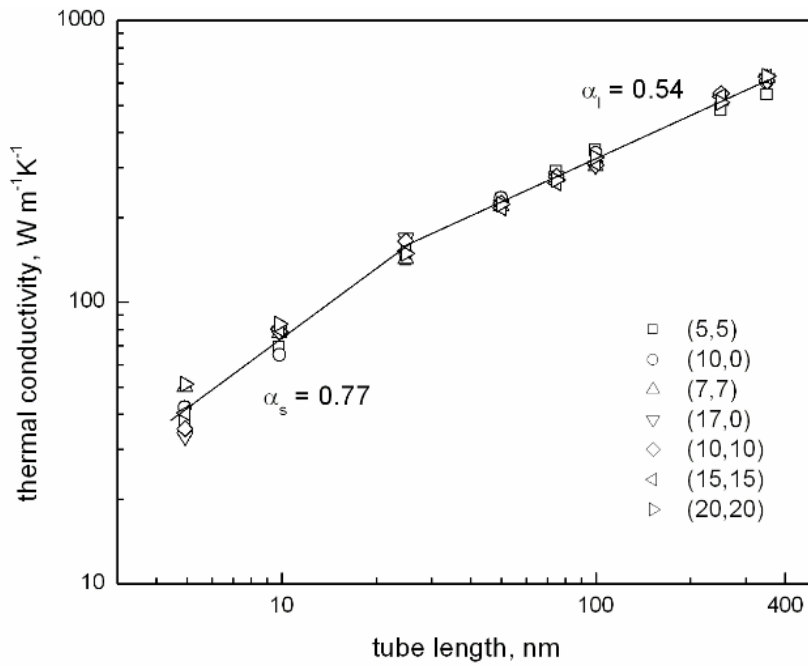


Figure 3-8. Thermal conductivity versus tube length for (5, 5), (10, 0), (7, 7), (10, 10), (17, 0), (15, 15), and (20, 20) SWNTs at 300 K.

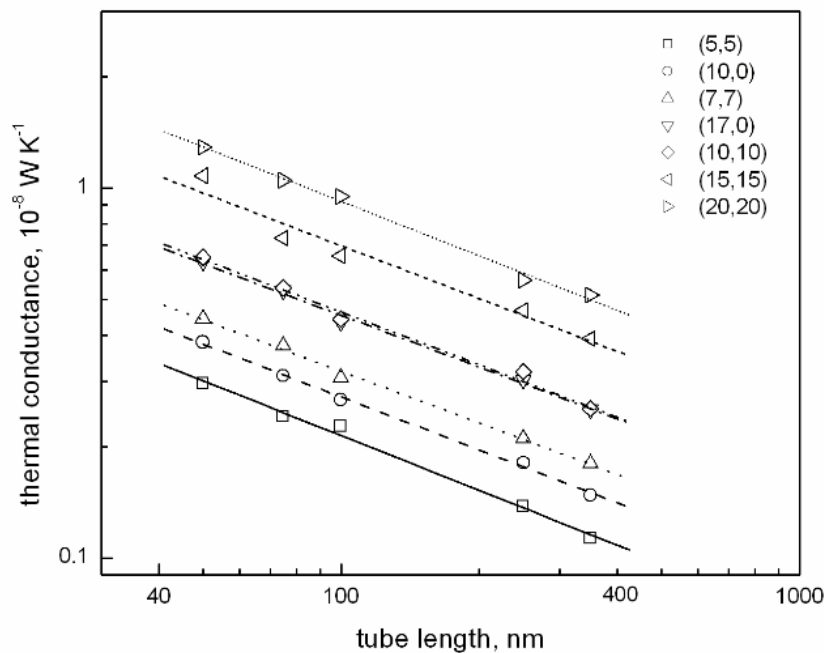


Figure 3-9. Thermal conductance  $\sigma$  for different tubes at 300 K with a tube length between 50 and 350 nm.

One of the ambiguous definitions in the calculation of the thermal conductivity of CNT is that of the cross-sectional area  $A$  for the heat flux. In the work of Alaghemandi *et al.*<sup>37</sup> it has been defined as a ring of the diameter of the SWNT and a thickness of the Van der Waals diameter of 0.34 nm for each carbon atom. Since this choice is arbitrary, it is much more consistent to work with the thermal conductance  $\sigma = \lambda \times A/L$ . The dependence of the thermal conductance on the length of the tube is presented in figure 1-9.

According to the definition of  $\sigma = \lambda \times A/L$  and the power law  $L^\alpha$  dependence of the thermal conductivity, the thermal conductance should obey following power law relation

$$\sigma = \beta L^{-\gamma}, \quad (1-11)$$

where  $\gamma = (1 - \alpha) < 1$ . Since  $\alpha$  is more or less constant ( $\alpha \approx 0.54$ ) for tubes of all diameters, the exponent  $\gamma \approx 0.46$  is universal too. Moreover, the prefactor  $\beta$  has been found to be a linear function of the number of carbon atoms  $n$  in the circumference of the tube, which is given by the sum of the two chiral indices (indicating once more the importance of the number of degrees of freedom available for energy transport). This dependence reads

$$\beta = 2 \times 10^{-9}(n - 1). \quad (1-12)$$

The two equations for  $\sigma$  and  $\beta$  (Eqns. 1-11 and 1-12) provide a rough estimate of the thermal conductance of SWNTs.

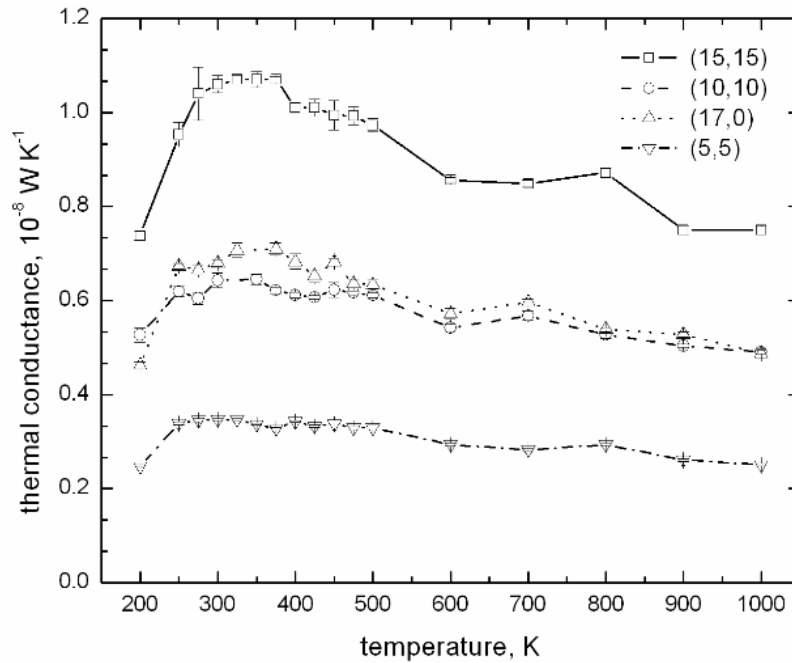


Figure 3-10. Thermal conductance  $\sigma$  versus temperature for different SWNTs of 30 nm length after applying quantum correction.

The thermal conductance for different nanotubes with lengths of 30 nm has been calculated for temperatures between 200 and 1000 K. The thermal conductance obtained by classical MD differs from the experimental results due to the neglect of quantum effects in MD. A so-called quantum correction has been suggested in the recent work of Lukes *et al.*<sup>18</sup> The quantum correction leads to the thermal conductance  $\sigma_q = \frac{dT_{MD}}{dT_q} \sigma$ , where  $T_{MD}$  is the MD temperature and  $T_q$  quantum temperature. The assumption is that the total energy of the system at  $T_{MD}$  is given by twice the mean kinetic energy. And  $T_q$  is a fitting parameter obtained by the equation a total energy to the phonon energy of the system. The thermal conductance as a function of temperature is plotted in figure 1-10.

The quantum corrected thermal conductance increases rapidly to around 250 K followed by a broad maximum and a slow decrease at higher temperatures ( $T > 400$  K). Figure 1-10 demonstrates that the  $\sigma_q$  curves of the (10, 10) and (17, 0) nanotubes are similar. Thus, the thermal conductance of SWNTs with the same length and diameter coincide more or less.

Another topic discussed in the work of Alaghemandi *et al.*<sup>37</sup> is thermal rectification. Rectification describes a process, which is faster in one direction than in the reverse direction. It has been found in experiment that a carbon nanotube externally loaded with heavy molecules exhibits rectification behavior.<sup>38</sup> The heat flow from the high loaded to the low loaded region has been roughly 2 % faster than in the opposite direction.

To model the experimental setup, simulations have been organized in two ways. In the first system, a single-walled carbon nanotube (10, 10) of 60 nm length has been modified in the way that the carbon atomic masses increase linearly from 12 to 300 amu along the tube, see atomic mass profile in figure 1-11. The heavy atoms have been placed either in the cold region (center) or in the hot region (sides). Of course, this setup should be regarded as an idealized model. The second simulated system corresponded more closely to the experiment: The nanotube has been externally loaded with extra atoms either placed on the hot or the cold region of the simulation cell. Details can be found in the original work of Alaghemandi *et al.*<sup>37</sup>

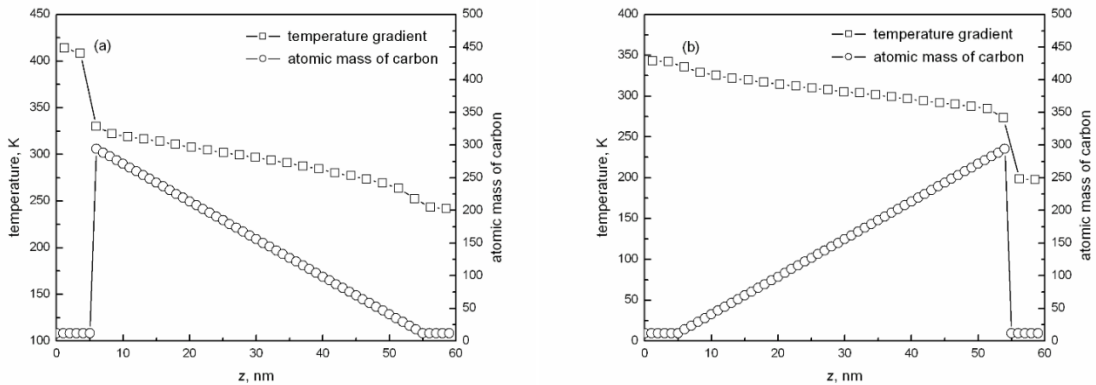


Figure 3-11. Atomic mass and temperature profiles in the (10, 10) single-walled nanotube with a mass gradient at an average temperature of 300 K. (a) Heat flows into the direction of lower atomic masses. (b) Heat flows into the direction of higher atomic masses.

Since the systems are inhomogeneous, the temperature gradient and the thermal conductivity will vary locally. The observed temperature gradient is plotted in figure 1-11. The thermal conductivity has been calculated by dividing the heat flux, which is imposed on the system, by the temperature gradient  $\langle -dT/dz \rangle$  for the range of  $z$  where the temperature gradient is linear. As a result, the thermal conductivity at 300 K is  $25.66 \text{ Wm}^{-1}\text{K}^{-1}$  when heat flows from low mass to high mass and  $23.24 \text{ Wm}^{-1}\text{K}^{-1}$  for the opposite flow.

The thermal rectification is defined as

$$R = \frac{\lambda_{L \rightarrow H} - \lambda_{H \rightarrow L}}{\lambda_{L \rightarrow H}} \times 100, \quad (1-13)$$

where  $\lambda_{L \rightarrow H}$  stands for the thermal conductivity when heat flows from low to high mass; vice versa for  $\lambda_{H \rightarrow L}$ . At 300 K, the calculated  $R$  amounts to 10.4 %. In the second setup with external mass-loading, the thermal conductivity at 300 K is larger in the direction of increasing external loading ( $169.19 \text{ Wm}^{-1}\text{K}^{-1}$ ) than in the reverse direction ( $141.20 \text{ Wm}^{-1}\text{K}^{-1}$ ). This is in line with the results for the first system, but it contradicts recent experiment findings,<sup>38</sup> where one half of the tube has been externally loaded with molecules of heavy mass. In the experimental work, a 2 % higher thermal conductivity has been observed in the direction from high to low loading. In addition, the preferred heat flux from high to low mass atoms has been found in a recent theoretical study of a monoatomic strictly one-dimensional chain.<sup>75</sup> The nature of thermal rectification in such systems has not been understood completely yet.

Recently many works have been done on the determination of the thermal conductivity of carbon nanotubes experimentally<sup>72,73</sup> as well as theoretically.<sup>67,68,70</sup> It has been proven that the thermal conductivity is high and diverges with the length of the tube.<sup>67</sup> The work by Padgett *et al.*<sup>21</sup> studies the influence of chemisorption on the thermal conductivity of CNT. The many-body bond order potential developed by Brenner *et al.*<sup>65</sup> has been used to describe the interatomic forces.

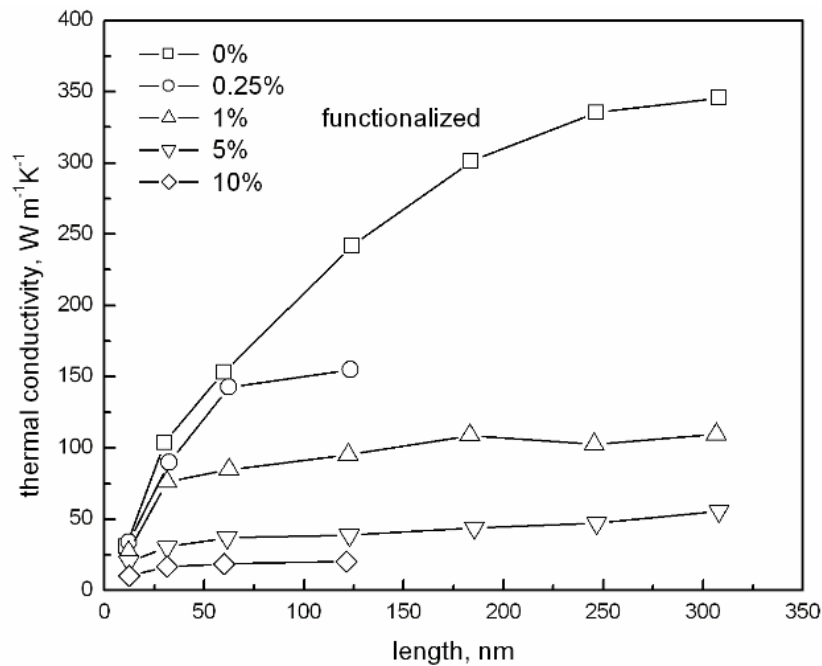


Figure 3-12. Thermal conductivity versus nanotube length for various degrees of functionalization.

The thermal conductivity calculations have been performed using RNEMD described above on pristine CNTs and on CNTs, on which 0.25, 1, 5 or 10 % of the carbon atoms have a phenyl

---

group attached. The atoms carrying the phenyl groups have their hybridization changed from  $sp^2$  to  $sp^3$ . In figure 1-12 the thermal conductivity for various degrees of functionalization has been plotted as a function of nanotube length.

Calculations for the pristine CNT show divergence with the length. For functionalized CNTs, thermal conductivity decreases significantly with enhanced functionalization. Moreover, the thermal conductivity converges faster, when more phenyl groups are attached to the tube.

### 3.5. Force Field Considerations for the Calculation of Thermal Conductivities

Usually, the thermal conductivity is overestimated in classical MD simulations for all types of materials.<sup>11,14,19</sup> Since other simulation parameters have only a small influence on the simulated value, the force field becomes important. The most significant question that arises for the thermal conductivity simulation is: Which force field has to be used to reproduce the thermal conductivity most closely? In reality, the stiff degrees of freedom are quantum oscillators in their vibrational ground state. Their vibrational energy (in wave numbers) is  $1000\text{-}2500\text{ cm}^{-1}$ , whereas  $kT$  at room temperature is  $207\text{ cm}^{-1}$ . These stiff degrees of freedom cannot be excited at room temperature. Neither can they transport energy. In contrast, in classical molecular dynamics simulations, all degrees of freedom can store and transfer energy, as they are all populated according to the equipartition theorem. This hypothesis gives us a possible proactical solution of the problem: freezing or eliminating the atoms with fast stretching and bending vibrations, e.g. C-H bonds. This leaves just those soft degrees of freedom, which do contribute to the heat transport at the room temperature.

A reasonable heuristic choice has emerged from the presented above simulations. If one uses united atoms to avoid the fast hydrogen vibrations plus bond constraints to remove the remaining fast degrees of freedom, the calculated thermal conductivities are in useful agreement with experiment. This choice seems to remove, on average, the right number of degrees of freedom, which would not contribute to heat conduction in reality because of their quantum nature. Similar considerations have been known to apply to the calculation of the heat capacity, too. Thus, we have the curious situation that for these thermal properties a simpler force field often provides a better agreement with experiment – not by coincidence, but for very good physical reasons.

Many studies have been done recently on thermal conductivities. Significant progress has been made for molecular liquids. It has been seen that the choice of simulation parameters affects the thermal conductivity only slightly, within error bars of simulations. Size effects on the thermal conductivity tend to disappear when the simulation box size is about several nm (7-10 nm) in the direction of heat transfer. The force field chosen seems to be the most important parameter when one simulates thermal conductivity of molecular fluids.



---

Completely flexible molecular models lead to the overestimation of the thermal conductivity, while bond-constrained models and united atoms shift the thermal conductivity in the direction of the experimental value. Therefore, the development of new force field models for more molecules seems to be the most important part of thermal conductivity calculations for molecular liquids.

For carbon nanotubes, thermal conductivity calculations perform well. Single-walled carbon nanotubes consist of a single atom type only, which makes their thermal conductivity calculations quite simple. Several methods have been adopted for the calculation of thermal conductivities of CNTs. Different potential types have been used to describe the intramolecular forces in CNT. However, all methods and potential types result in the same range of thermal conductivity values (300 – 6600 Wm<sup>-1</sup>K<sup>-1</sup>), which have also been found in the experimental work.<sup>67,72,73</sup> The only problem in the determination of CNT thermal conductivities is comparability, as this property deviates from Fourier's law and depends strongly on the tube length for nanotubes shorter than 500 nm. The thermal conductivity converges when the length of the tube is comparable with a phonon mean free path, which is about 500 nm. It is still expensive to perform simulations on such long systems on the atomistic scale. Another phenomenon, which concerns thermal transport especially in CNTs, is thermal rectification. It has been observed in experiments<sup>38</sup> that in conically mass-loaded carbon nanotubes heat transfer is faster in the direction from high to low mass than in the opposite direction. Thermal rectification is an effect of low-dimensional solids and has, for example, been discovered in one-dimensional monoatomic chains. Recent simulations of carbon nanotubes reproduce the effect of thermal rectification, but with an opposite sign, heat transport from low to heavy mass being faster than in the reverse direction. There are many speculations about the origin of thermal rectification, but a conclusive explanation is still missing.

There are only few examples of simulations of thermal conductivities of polymers. Their complexity and variety makes the computation expensive. To avoid size-effects, one has to simulate long polymer chains and as a consequence big systems, which leads to a large requirement of simulation time. The next problem is the ambiguous choice of force field parameters. An all-atom flexible model for a polymer can result in a large overestimation of the thermal conductivity, while a united-atom constrained model brings the calculated value into better agreement with experiments. However, some degrees of freedom are more important than others for heat transport, so the thermal conductivity may be sensitive to force field variations to a different extent. This dependence or independence on force field parameters is conditional on the polymer structure and has to be considered for each particular case. We note that more simulations on polymers with different chemical

---

structures, topologies, morphologies and phases are needed to establish the range of applicability of molecular dynamics calculations as a predictive tool for the thermal conductivity of polymer materials. One should keep in mind, however, that during the last years a remarkable progress has been made in the understanding of the anisotropy of the thermal conductivity of oriented and crystalline polymers, as well as of the relative contribution of fast solid-like through-bond heat transport via phonons along the backbone and the slower liquid-like through-space heat transport by collisions between neighboring chains.

---

#### 4. Thermal Conductivity of Atactic Amorphous Polystyrene and its Mixture with Supercritical Carbon Dioxide

---

The thermal conductivity of polymers plays an important role in a number of processing and product applications. Polymers and polymer blends occur in many products and devices. The thermal conductivity ( $\lambda$ ) in polymeric thermal insulators e.g., should be as low as possible. In the encapsulation of electronic devices, however, high  $\lambda$  values are desirable. Moreover, the thermal conductivity is of great importance in the production of polymers. Reliable predictions of the thermal conductivity can lead to improvements in the processing design. As experimental studies over a well-defined pressure ( $p$ ), temperature ( $T$ ) and composition range are missing for a number of polymers, computer simulations have become an important tool for the prediction of thermal conductivities in polymer science.

In the past years it has been demonstrated that polymer sorption and swelling processes in supercritical fluids can have advantages in comparison to processes under non-critical conditions. The increasing research activities in this direction are documented in the literature.<sup>76-78</sup> The adoption of carbon dioxide as a supercritical solvent has been guided strongly by ecological reasons. It has been verified experimentally that it is possible to substitute toxic organic solvents by CO<sub>2</sub> without reducing the yield of the process.<sup>79,80</sup>

Polymer processing with supercritical fluids includes purification, impregnation and fractionation as well as the production of porous foam or powder polymers. Thus it is necessary to investigate the physical properties of polymers swollen in supercritical media. Experimental and simulation techniques have been adopted simultaneously to determine the physical properties of polymers. Despite these activities the behavior of many polymers in supercritical fluids is still not understood completely.

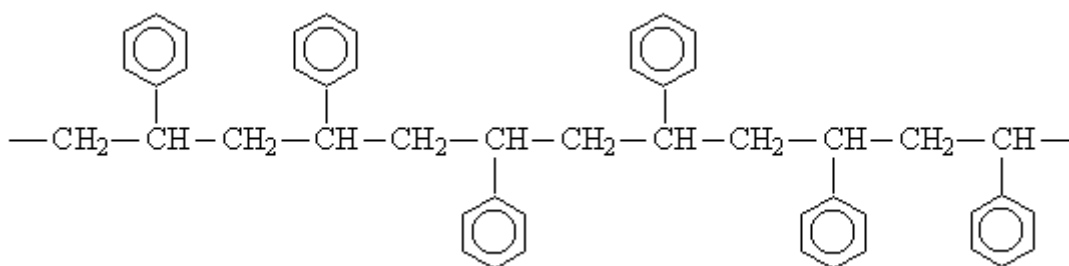


Figure 4-1. Schematic representation of atactic polystyrene which is characterized by a random distribution of the phenyl rings.

In this work we have investigated the thermal conductivity of atactic polystyrene (PS) swollen in supercritical CO<sub>2</sub> by reverse nonequilibrium molecular dynamics (RNEMD) simulations.<sup>1</sup> The schematic structure of atactic PS is shown in figure 2-1. As experimental  $\lambda$  values for the binary systems have not been reported, we have extended our computer simulations to the

---

components PS and CO<sub>2</sub>, for which measured data are available.<sup>2,3</sup> The comparison of calculated and experimental thermal conductivities of the components is a prerequisite to quantify the capability of the present theoretical tools. Our strategy offers a second benefit, i.e. the presentation of an analytical interpolation formula to relate the thermal conductivity of the components PS and CO<sub>2</sub> to the thermal conductivity of the binary mixture. Furthermore, we have considered implications of the quasi-degeneracy in multi-level polymer systems.<sup>81,82</sup> Their large number in the degrees of freedom usually leads to a manifold of configurations of roughly the same energy that, however, may differ in other physical properties. Such a manifold of configurations within a narrow energy range is denoted as “quasi-degenerate”, a descriptor more popular in electronic structure theory; we refer to the detailed discussion in ref. 83. In addition to the finite-size effect this phenomenon might cause error bars in physical quantities that are larger than the error bars due to the statistical nature of the formalism used. In polymers as well as in solid-state systems, e.g., one can have local modifications in the density, in the spatial arrangement of non-bonded neighbor contacts or in the magnetic ordering that are of similar energy. To come to the present problem; we have found that the orientation of the carbon-carbon bonds in the backbone of PS relative to the direction of the temperature gradient is important for the heat transport in the system. See ref. 2, where this behavior has been confirmed in experiments on oriented and unoriented PS samples. Let us summarize: we have analyzed the thermal conductivity of PS-CO<sub>2</sub> mixtures as a function of the temperature, pressure and CO<sub>2</sub> concentration by RNEMD simulations. The computational results of the present approach are explained in sections 2.2-2.4.

#### 4.1. Computational Details

In the present work the RNEMD method, which is described in chapter 1.1.1, has been used for all simulations. All molecular dynamics simulations have been carried out with the YASP package,<sup>42,43</sup> which uses the leapfrog algorithm and orthorhombic periodic boundary conditions. Temperatures and densities have been chosen at conditions, where experimental information for the components is most abundant. The Berendsen method<sup>44</sup> has been employed to perform simulations at constant temperature. The intramolecular force field contains harmonic bond stretching, harmonic angle bending, and periodic cosine-type torsional potentials. The non-bonded potential includes Lennard-Jones terms with Lorentz-Berthelot mixing rules<sup>12</sup> for unlike interactions as well as electrostatic interactions that are mapped by partial atomic charges. The latter were treated using the reaction-field method with a relative permittivity of 2.5. For details of the functional form of the force field, see ref. 55. Non-bonded interactions were evaluated from a Verlet neighbor list, which was updated every 15 timesteps (of 0.001 ps length) using a link-cell method.

---

A flexible full atomistic model has been used for the present simulations. The force constants for PS have been reported previously for a rigid bond model.<sup>55</sup> The constants for the harmonic bond stretching forces (C(aliphatic)-C(aliphatic): 259780 kJ mol<sup>-1</sup> nm<sup>-2</sup>; C(aliphatic)-C(aromatic): 265646 kJ mol<sup>-1</sup> nm<sup>-2</sup>; C(aromatic)-C(aromatic): 393022 kJ mol<sup>-1</sup> nm<sup>-2</sup>; C-H(aliphatic): 200000 kJ mol<sup>-1</sup> nm<sup>-2</sup>; C-H(aromatic): 200000 kJ mol<sup>-1</sup> nm<sup>-2</sup>) have been adopted from other work.<sup>19,84</sup> Potential parameters and atomic charges for a flexible full atomistic model of carbon dioxide have been evaluated by Harris and Yung.<sup>85</sup> These authors have adjusted the parameters to reproduce the vapor-liquid coexistence curve and critical properties of carbon dioxide. These parameters have also been used to obtain transport properties, such as the self-diffusion coefficient of carbon dioxide in a supercritical state. It has been shown that the model of Harris and Yung reproduces the transport properties of CO<sub>2</sub> quite well.<sup>86</sup>

The molecular dynamics simulations have been performed at constant temperature and pressure. For the Berendsen thermostat a coupling time  $\tau_T$  of 0.2 ps and for the barostat a coupling time  $\tau_p$  of 2 ps has been used.  $\tau_T$  and  $\tau_p$  have been sufficient to keep the measured average temperature within 1 K from the target temperature and the measured average pressure within 1 kPa from the target pressure. It has been checked that different choices of  $\tau_T$  and  $\tau_p$  did not change the thermal conductivity. In the RNEMD runs, the simulation box was divided into 20 slabs in the direction of the heat flux. Atom velocities were exchanged every 0.5 ps.<sup>11,19</sup> It has been checked that, at this exchange period, the thermal conductivity converges. A nonequilibrium run typically covered 7 ns, the last 1 ns has been used for the production.

An atactic polystyrene chain of 300 monomers with random tacticity of the phenyl rings has been generated in vacuum. In order to check the length dependence of the thermal conductivity several additional simulations with chain length of 100 and 600 monomers have been performed. Within the error bars of the method the thermal conductivity of all samples is highly identical. Due to the prohibitive computational effort we had to restrict the present simulations to the length of 300 monomers. This setup seems to be suitable to allow for a comparison with experimental polymers. The discussion of scaling relations as a function of the polymer length is not the topic of the present contribution. We refer to an older experimental study.<sup>87</sup> The initial polymer conformations have been obtained via pivot Monte Carlo calculations<sup>88</sup> of a single polymer chain in vacuum with a bond-based interaction cutoff to generate a melt-like structure. The interaction cutoff of 7 bonds has been chosen on the basis of the persistence length of PS. This chain has been inserted into the periodic simulation cell. Molecular dynamics simulations with a soft-core potential have been employed to prevent overlaps and to remove possible entanglements and concatenations. Then it has been

equilibrated for 10 ns by equilibrium MD at constant pressure and temperature. After equilibration we have got a cubic simulation box of PS with a density of 1.042 g/cm<sup>3</sup>.

A single amorphous atactic polystyrene chain of 300 monomers has been used in all simulations. The following systems have been investigated: neat PS, neat CO<sub>2</sub> and mixtures of PS with different concentrations of CO<sub>2</sub> at supercritical conditions. Simulations have been performed in a temperature range between 350 and 500 K, and for pressures between 0.1 MPa and 60 MPa. Both the temperature and pressure range considered have been employed in experimental studies of the components.<sup>76,89</sup> The concentration of carbon dioxide in the mixture has been varied from 10 to 30 mass %. Four different mixtures with a total number of 79, 125, 177 and 304 CO<sub>2</sub> molecules added to a single PS molecule have been simulated. The binary systems generated by this choice contain 10, 15, 20 and 30 mass % of CO<sub>2</sub>.

#### 4.2. Thermal Conductivity of Neat Polystyrene

The thermal conductivity of neat PS has been calculated in order to compare simulation and experimental results. As validation of the model, we tried to match the simulated density ( $\rho$ ) of polystyrene at  $T = 300$  K and  $p = 0.1$  MPa to the experimental one. The density value simulated amounts to 1.042 g/cm<sup>3</sup>. Since the simulations have been carried out using orthorhombic periodic boundary conditions, the density of simulated PS is defined as the mass of a single PS chain divided by the box volume. The experimental density of polystyrene depends both on the structure (syndiotactic or atactic) and on the molecular weight; it varies from 1.032 to 1.069 g/cm<sup>3</sup> at 300 K and 101.3 kPa.<sup>90</sup>

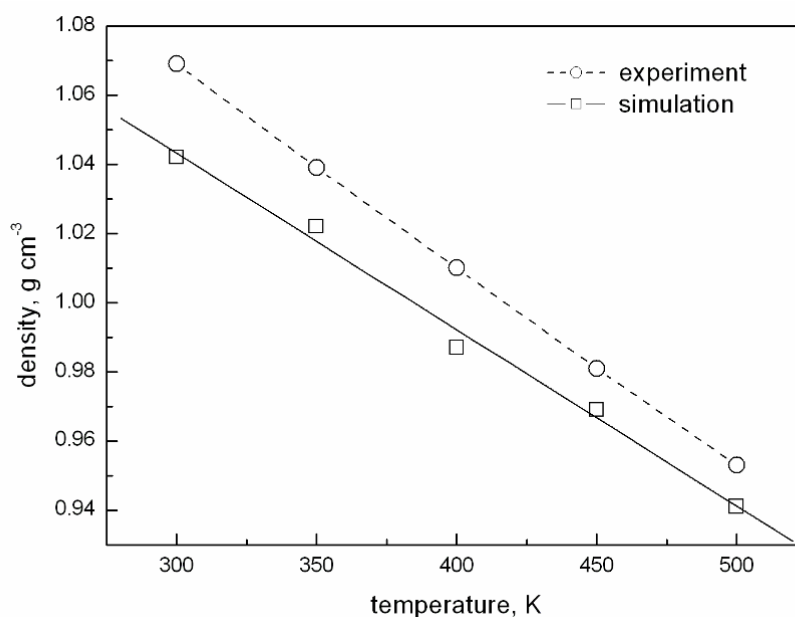


Figure 4-2. Density of neat PS at 0.1 MPa as obtained in experiment<sup>90</sup> and by simulations.

---

The temperature dependence of the simulated and experimental density of neat PS is presented in figure 2-2. As one can see, experiment and simulations agree in so far that the density is reduced linearly with increasing temperature. The calculated densities are however smaller than the measured ones. This might be caused by the fact that the molecular weight of PS in the simulation ( $\sim 3000$  g/mol) is smaller than in experiment (80000 – 400000 g/mol).<sup>91</sup> The calculated thermal conductivity of PS at 300 K and 101.3 kPa amounts to  $(0.187 \pm 0.005)$  Wm<sup>-1</sup>K<sup>-1</sup>, while the experimental one at the same temperature and pressure is 0.156 Wm<sup>-1</sup>K<sup>-1</sup>.<sup>2</sup> We first note that the agreement between simulations and experiment is quite good. The deviation between both numbers is typical for polymer simulations. The uncertainties of all simulations are defined as the standard deviation from the average thermal conductivity in the last ns of the production run. On the basis of the previous simulation studies described in chapter 1 we suggest – in addition to the errors caused by the potential - the following explanation for this difference between the present classical simulation data and experiment. The combination “full atomistic model” and “classical MD simulations” guarantees that all spatial degrees of freedom can store energy. The dynamics of the atoms is not restricted by energy quantization. In a more realistic quantum approach all degrees of freedom would have to be described by nuclear fluctuations in the vibrational ground state or – for soft modes – in excited states. The stiff degrees of freedom, however, cannot be excited thermally as their vibrational energy (in wave number units) is found between 1000 and 2500 cm<sup>-1</sup>, whereas the thermal energy at room temperature amounts to 207 cm<sup>-1</sup>. Hence, these modes are not accessible for the transport of energy in the quantum limit realized experimentally. This distinction between a classical model and experiment may explain the overestimation of  $\lambda$ . An improvement of RNEMD results due to quantum correction has been commented on in the recent simulation study on carbon nanotubes.<sup>37</sup> For the thermal conductivity of polyamide-6,6 it has been reported that the best agreement with experiment occurs for a fully bond-constrained united-atom model.<sup>19</sup> Even under the neglect of error compensations we have found that the flexible atomistic model chosen leads to a sufficient agreement between experiment and simulation. This might indicate that the dominant mechanisms of the thermal transport in polyamide-6,6 and polystyrene differ. In polystyrene the most important heat transfer channel is along the backbone.<sup>10</sup> Heat transfer through phenyl rings (by collisions) is less important. For syndiotactic PS it has been reported that not only the number in the degrees of freedom is important, but also their spatial location.<sup>10</sup>

The next benchmark chosen has been the temperature dependence of the thermal conductivity of neat PS. The simulation and experimental results over a wide temperature range are plotted in figure 2-3. The calculated thermal conductivity grows at lower

temperatures and converges to a constant value between 400 and 450 K. This trend is in line with experimental results showing a constant plateau between 350 and 380 K.<sup>2</sup> In figure 2-3 we see that the simulated  $\lambda$  is again reduced for  $T > 450$  K. Due to the error bars of the simulations this statement should be used only with care.

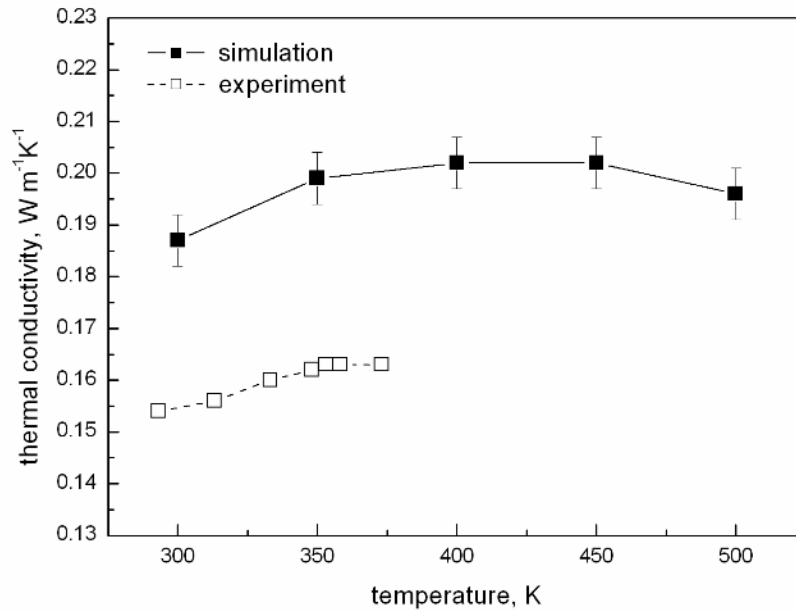


Figure 4-3. Thermal conductivity of polystyrene versus temperature at 0.1 MPa obtained in experiment<sup>2</sup> and by simulations.

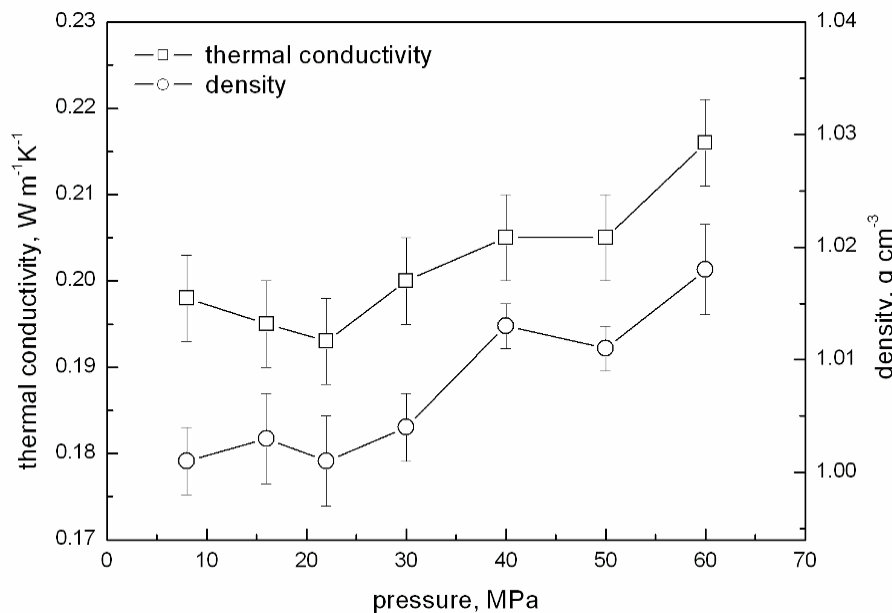


Figure 4-4. Thermal conductivity and density of polystyrene versus pressure at 400 K.

The pressure dependence of the thermal conductivity and density is shown in figure 2-4. As could be expected a priori, density and thermal conductivity are both enhanced with increasing pressure. Experimental information is not available. In a large number of simulations we have found that the thermal conductivity of PS strongly depends on the



number and orientation of C-C bonds in the backbone relative to the direction of the temperature gradient (and the collinear heat flux). In order to demonstrate this effect we have calculated the thermal conductivity of the same polystyrene sample in two perpendicular directions, i.e.  $y$  and  $z$ . Remember, however, that simulation cell as well as the pressure conditions is isotropic. Differences in  $\lambda$  in the two directions are a manifestation of the above mentioned quasi-degeneracy as well as finite-size effects. The present RNEMD simulations into the two perpendicular directions lead to thermal conductivities of  $0.213$  and  $0.179 \text{ Wm}^{-1}\text{K}^{-1}$ . To understand this difference we have calculated the direction cosine of all backbone C-C bonds relative to the direction of the heat transport. In other words we have calculated the orientation of C-C bonds in the backbone. The results are presented in figure 2-5.

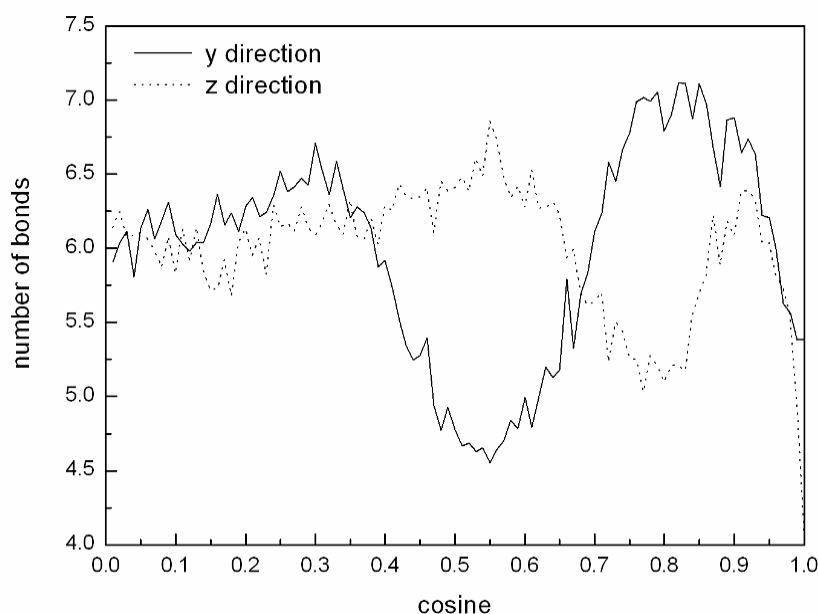


Figure 4-5. Orientation of C-C bonds in the backbone.

As one can see, number of backbone bonds oriented into the  $y$  direction is larger than number of bonds oriented into  $z$  direction. The implications of this difference can be seen in the two  $\lambda$  values, the thermal conductivity is larger in the  $y$  direction and smaller in the  $z$  direction.

It has been found both in experiments and the present simulations that a preferred orientation of the backbone of the polymer in the direction of the temperature gradient may lead to an enhancement in the thermal conductivity.<sup>2,19</sup> It proves that the thermal transport in polymers is faster when it progresses along the chain via phonons than by means of lateral collisions. This topic will be discussed in more detail in connection with RNEMD simulations on stretched and non-stretched PS in chapter 3. Here, we should mention that polymer systems are so-called multi-level systems with a manifold of quasi-degenerate configurations with non-negligible differences in the nature of local non-bonded contacts. This phenomenon as well as the finite-size effect in the polystyrene system leads to the thermal conductivity values

reflecting differences in the local geometric arrangements which are often predetermined by the initial configuration chosen.<sup>81,82</sup> To calculate the error bars of the simulations, eight different initial configurations of PS system have been investigated by simulation runs. The average thermal conductivity at 400 K and at 40 MPa amounts to  $(0.205 \pm 0.012) \text{ Wm}^{-1}\text{K}^{-1}$ . Thus we have to accept an additional error of 6 % in the thermal conductivity caused by the above influence factor, structural difference of microstructures with almost identical energies.

### 4.3. Thermal Conductivity of Neat Carbon Dioxide at Supercritical Conditions

Carbon dioxide has been simulated under supercritical conditions to check the accuracy of the calculated properties in this limit. As mentioned in section 2.2, the force constants required have been determined by Harris and Yung<sup>85</sup> with the aim to calculate supercritical properties of carbon dioxide with high accuracy.

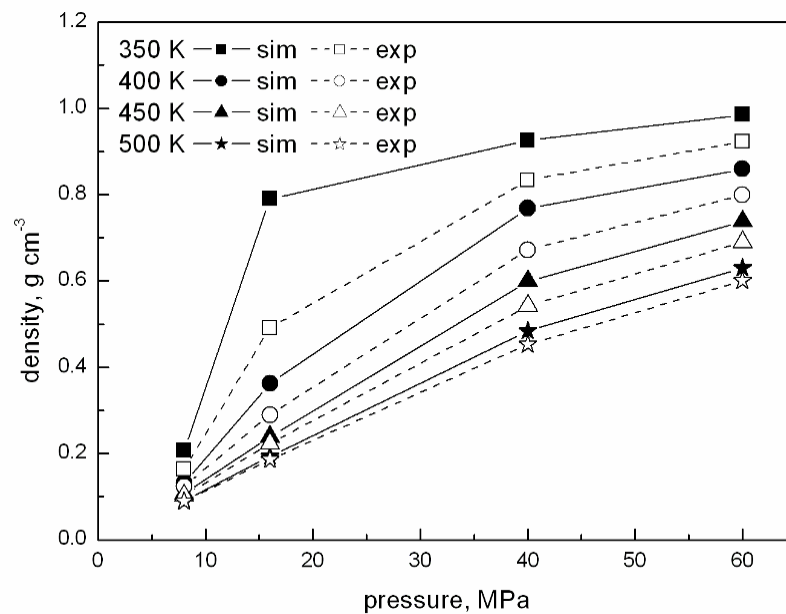


Figure 4-6. Simulated and experimental<sup>92</sup> densities of CO<sub>2</sub> under supercritical conditions. The uncertainties in the simulated densities are smaller than the size of the symbols.

We have calculated the density and the thermal conductivity of CO<sub>2</sub> under supercritical conditions over a wide pressure and temperature range. The simulated and experimentally estimated<sup>92</sup> density of CO<sub>2</sub> versus pressure for different temperatures is plotted in figure 2-6. The density increases with the pressure. In the studied temperature interval between 350 and 500 K the density at a given pressure is reduced with increasing temperature. The comparison with the “experimental” densities derived via an equation of state<sup>92</sup> indicates that the simulated carbon dioxide densities in figure 2-6 at different pressures are typical for supercritical conditions. It is obvious that problems caused by the quasi-degeneracy and finite-size effects as emphasized for PS do not occur for systems with a simple geometric structure such as CO<sub>2</sub>. Before commenting on the thermal conductivity data of CO<sub>2</sub> we want to mention

that the density of CO<sub>2</sub> is smaller than the density of PS. This difference is particularly large for not too high pressures. In order to understand the thermal conductivity values of the binary mixtures we should mention that in classical simulations, density enhancement implies an enhancement in the degrees of freedom per volume element and thus more transport channels for the heat.<sup>19</sup>

The pressure dependence of the thermal conductivity of supercritical CO<sub>2</sub> is displayed in figure 2-7. The error bar in the simulations of CO<sub>2</sub> is much smaller than in the PS case. It is clear that this difference is an outcome of the fact that multi-level problems are restricted to polymers. Correlation with figure 2-6 indicates that the thermal conductivity and density profiles are of similar shape; see above. The same analytical shape has been observed for the measured thermal conductivity of PS.<sup>93</sup> In analogy to the density, the thermal conductivity grows with the pressure and decreases with increasing temperature.

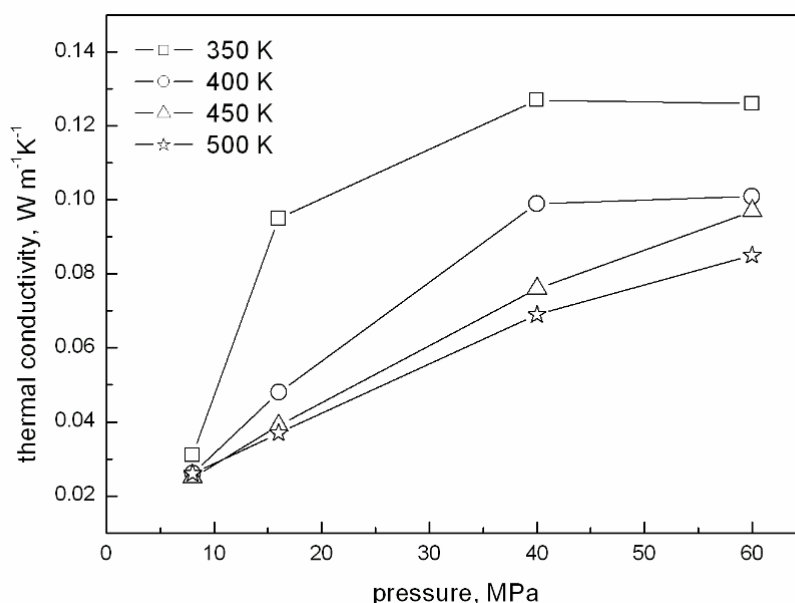


Figure 4-7. Thermal conductivity of CO<sub>2</sub> at supercritical conditions versus pressure at different temperatures. The uncertainties of the simulated thermal conductivity are smaller than the size of the symbols.

The comparison of the simulated data for PS and CO<sub>2</sub>, see figures 2-4 and 2-7, demonstrates that both materials coincide in the qualitative pressure dependence of the thermal conductivity. However, they differ in their temperature dependence. In PS the thermal conductivity increases first with increasing temperature, and then it reaches the plateau before it drops again; please remember the uncertainties in the PS simulations. The thermal conductivity of CO<sub>2</sub> is continuously reduced as a function of temperature. The calculated thermal conductivity of CO<sub>2</sub> under supercritical conditions will be used below to evaluate an empirical thermal conductivity formula for the mixture on the basis of the neat PS and CO<sub>2</sub> data.

#### 4.4. Thermal Conductivity of Binary Mixtures of Polystyrene and Carbon Dioxide

The polystyrene chain has been mixed with different concentrations (10, 15, 20 and 30 mass %) of CO<sub>2</sub>. In figure 2-8 we present the density of the binary mixtures at  $T = 400$  K and  $p = 16$  Mpa as a function of the CO<sub>2</sub> concentration obtained from an equilibrium calculation. The density decreases with an enhanced CO<sub>2</sub> concentration. In consideration of the above discussion of the particle densities of CO<sub>2</sub> and PS this density reduction has been expected. It is a manifestation of the fact that the number of chemical bonds per atom in PS exceeds the average number of bonds in CO<sub>2</sub>.

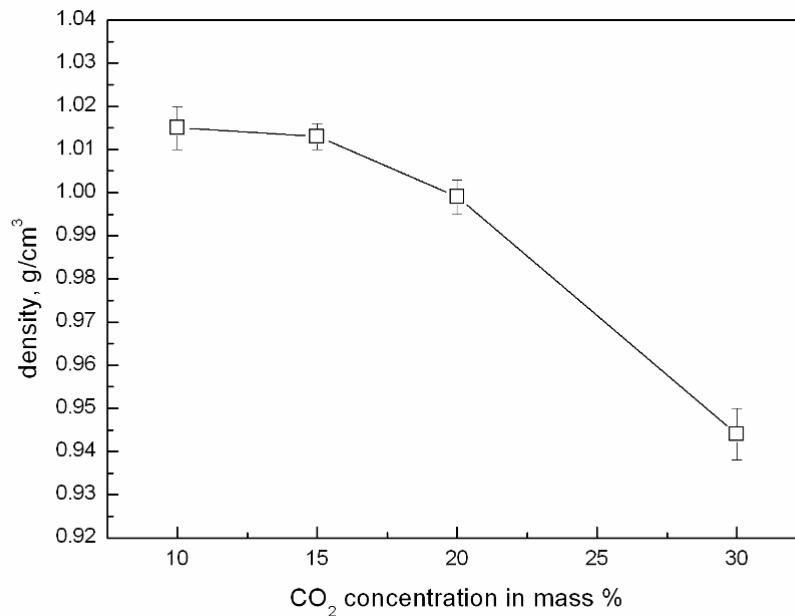


Figure 4-8. Density of the binary mixture versus CO<sub>2</sub> concentration in mass % at 400 K and 16 MPa.

The binary mixtures considered have been equilibrated for 6 ns. After this period RNEMD runs of 7 ns have been performed. The last 1 ns has been used for the calculation of the thermal conductivity of the systems. The thermal conductivity of the binary mixture as a function of the CO<sub>2</sub> concentration is shown in figure 2-9. The observed reduction of the thermal conductivity with increasing CO<sub>2</sub> concentration could be expected a priori on the basis of the thermal conductivity values of neat PS and CO<sub>2</sub>.

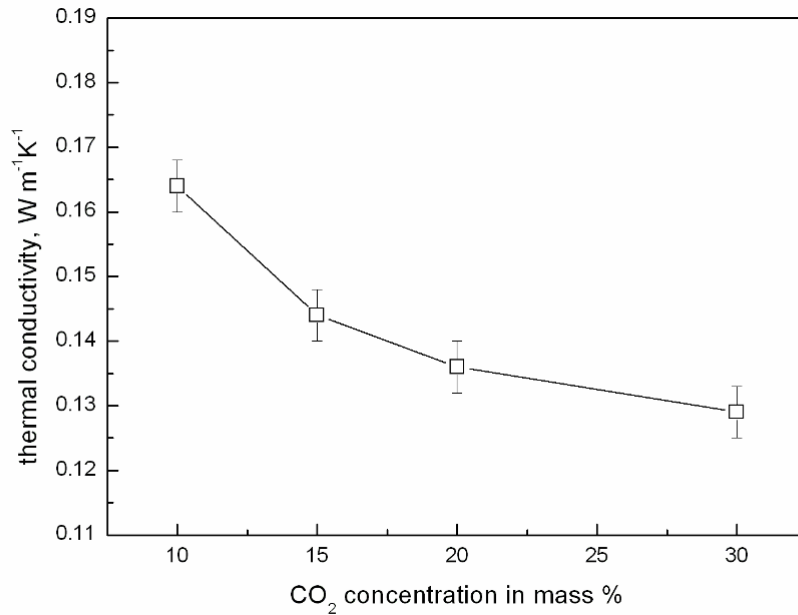


Figure 4-9. Thermal conductivity of the binary mixture versus mass concentration of CO<sub>2</sub> in % at 400 K and 16 MPa.

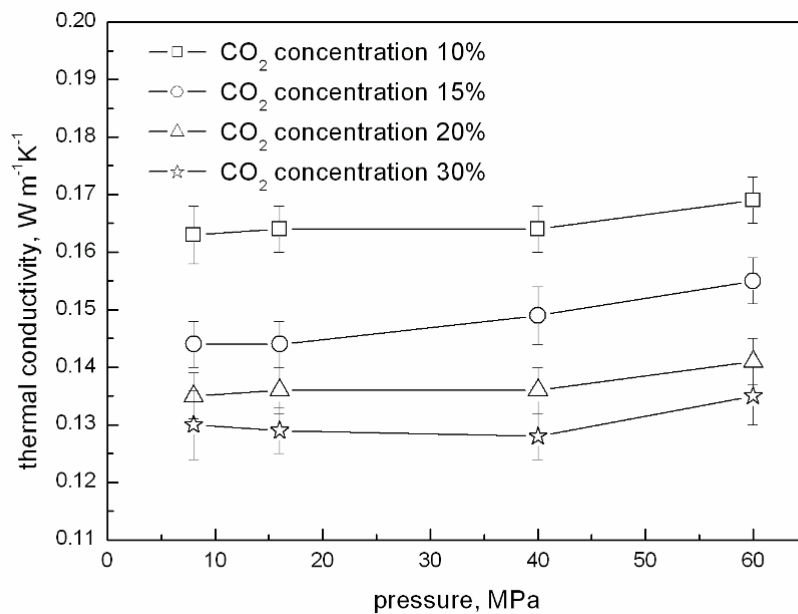


Figure 4-10. Thermal conductivity of binary mixtures versus pressure for different mass concentrations of CO<sub>2</sub> in % at 400 K.

The pressure dependence of the thermal conductivity of the four mixtures is shown in figure 2-10. The  $\lambda$  values of the mixtures slightly increase with increasing pressure and decrease with increasing mass concentration of CO<sub>2</sub>. A similar modification of  $\lambda$  as a function of pressure has been observed for the separate components. The data in the figure clearly emphasize that the density enhancement with increasing pressure makes the heat transfer more efficient. Now let us consider the four curves in figure 2-10 in more detail. Due to the higher compressibility of CO<sub>2</sub> relative to PS we expect that the pressure dependence of the thermal conductivity is enhanced with increasing CO<sub>2</sub> concentration. With exception of the

15 % curve this effect seems to be realized in figure 2-10. We cannot rule out that the shape of the 15 % curve is a result of the error bars of the simulations. For the small CO<sub>2</sub> concentrations considered the above enhancement, however, is rather small.

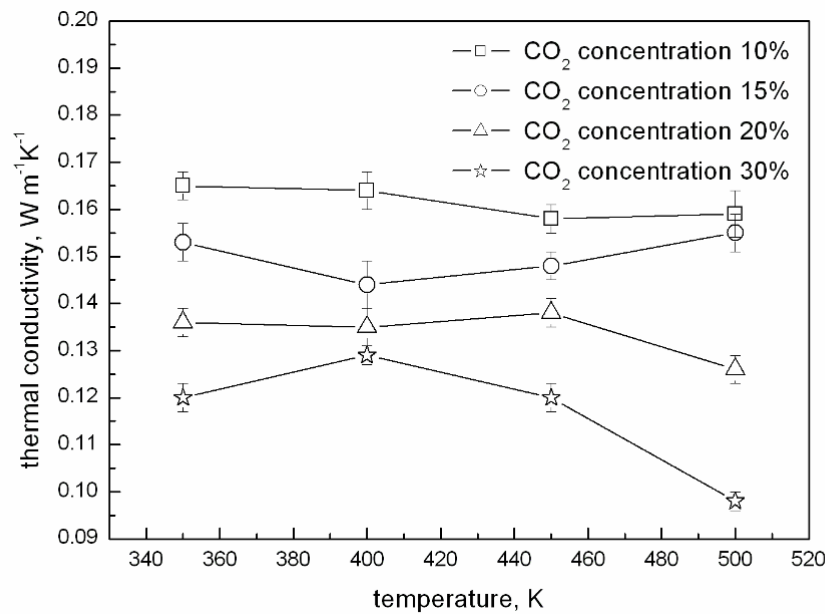


Figure 4-11. Thermal conductivity of binary mixtures versus temperature for different mass concentrations of CO<sub>2</sub> in % at 16 MPa.

In figure 2-11 we display the temperature dependence of the thermal conductivity for the four different binary systems. The  $\lambda$  curves show two expected trends. a) The thermal conductivity is reduced with an increasing amount of CO<sub>2</sub>; again we refer to the above analysis. b) The curve shape of the thermal conductivity at high temperatures (i.e.  $T > 450$  K) of the two mixtures with the lowest CO<sub>2</sub> admixtures differs from the behavior predicted for the materials with the two highest CO<sub>2</sub> concentrations. For the two latter mixtures the thermal conductivity is reduced with increasing temperature while it is enhanced or remains constant for the two samples with small CO<sub>2</sub> admixtures. This switch in the temperature profile reflects differences in the temperature dependence of the thermal conductivity for the two components; see again figures 2-3 and 2-7. For PS we have a temperature window where the thermal conductivity is an increasing function of temperature while the CO<sub>2</sub> thermal conductivity is always reduced with increasing temperature. With an enhanced amount of CO<sub>2</sub> this negative gradient becomes more dominant.

As it has been reported in previous works<sup>10,19</sup> and mentioned above, the number in the degrees of freedom per unit volume is a decisive quantity for the thermal transport. To demonstrate this we have calculated the thermal conductivity of PS as a function of number of degrees of freedom per volume. The results of the calculations are presented in figure 2-12 for a selection of the systems investigated. The thermal conductivity increases with an enhanced

number of degrees of freedom. The line in figure 2-12 results from a linear fit of the simulated data under the boundary condition to cross the origin (0,0). This choice reflects the fact that an energy transport is not possible in the absence of any degrees of freedom.

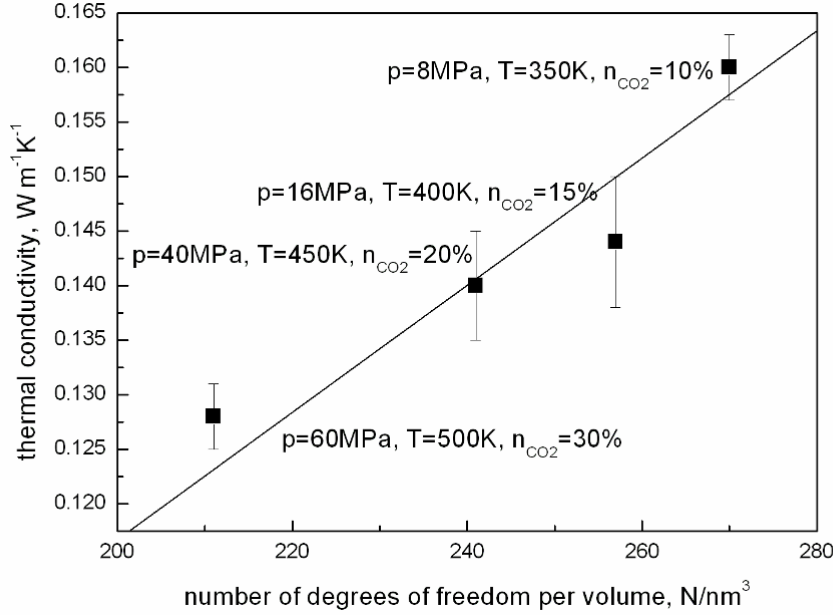


Figure 4-12. Thermal conductivity of binary PS-CO<sub>2</sub> admixture as a function of the degrees of freedom per unit volume encountered in the system.

The rather large scattering in figure 2-12 clearly indicates that the number of the degrees of freedom, i.e. number of atoms, is only one parameter influencing the thermal conductivity. In the present work we have shown that not all degrees of freedom are equivalent. Recall the decisive role of the orientation of the bonds in the polystyrene backbone. Up to now the influence of the temperature on this correlation has not been commented on. The non-identical temperature variation of  $\lambda$  and the density clearly indicates that the correlation between  $\lambda$  and number in the degrees of freedom is strictly valid only under a constant temperature. However, it seems that this temperature effect leads to minor modifications only.

On the basis of the thermal conductivities of the neat PS and CO<sub>2</sub> systems we have obtained an empirical interpolation formula for  $\lambda$  of the mixture as a function of the concentration of CO<sub>2</sub>, pressure and temperature. The data for the two components at different conditions are summarized in table 2-1. The interpolation formula for the thermal conductivity of the binary mixture reads

$$\lambda_{mix}(C_{CO_2}, p, T) = \frac{(1-C_{CO_2})((1-C_{CO_2})\lambda_{PS}(p,T) + C_{CO_2}\lambda_{CO_2}(p,T))}{(0.00904 - 0.00002T)p + (0.6228 + 0.0009T)} \quad (2-1)$$

where  $C_{CO_2}$  is the mass fraction of CO<sub>2</sub> in the mixture,  $T$  the temperature in Kelvin, and  $p$  the pressure in MPa.

Table 4-1. Thermal conductivities of neat PS and neat CO<sub>2</sub> at different temperatures and pressures; experimental values<sup>93</sup> in parenthesis.

$p$ (MPa)	$T$ (K)	$\lambda$ of PS (Wm <sup>-1</sup> K <sup>-1</sup> )	$\lambda$ of CO <sub>2</sub> (Wm <sup>-1</sup> K <sup>-1</sup> )
8	350	0.191	0.031 (0.028)
	400	0.198	0.026 (0.030)
	450	0.201	0.025 (0.033)
	500	0.197	0.026 (0.036)
16	350	0.189	0.095 (0.056)
	400	0.195	0.048 (0.040)
	450	0.201	0.039 (0.039)
40	350	0.198	0.037 (0.040)
	400	0.201	0.127 (0.097)
	450	0.205	0.099 (0.076)
	500	0.210	0.076 (0.064)
60	350	0.206	0.069 (0.059)
	400	0.205	0.126 (0.115)
	450	0.216	0.101 (0.095)
	500	0.216	0.097 (0.081)
	500	0.208	0.085 (0.074)

The starting thermal conductivity value has been estimated as follows: Assume that the thermal conductivity of the mixture is proportional to  $\lambda$  of the neat components weighted by their mass fraction. In order to determine  $\lambda_{mix}$  with sufficient accuracy, we had to consider the influence of pressure and temperature in the denominator of the interpolation formula. Deviations from the simple additivity are taken into account by a multiplicative constant  $f_{na}$  in the numerator. It turned out that  $f_{na}$  can be approximated by  $(1 - C_{CO_2})$ . For  $C_{CO_2} \rightarrow 0$  the interpolation scheme reproduces the correct asymptotic limit  $\lambda_{PS}$  but fails to map the boundary  $C_{CO_2} \rightarrow 1$ . The thermal conductivity of the mixture obtained from this formula differs by less than 10 % from the value calculated for the binary system. A comparison of the thermal conductivity as calculated from this formula and from simulations is presented in figure 2-13. The interpolated and exactly calculated thermal conductivities coincide within the error bars of the simulation.



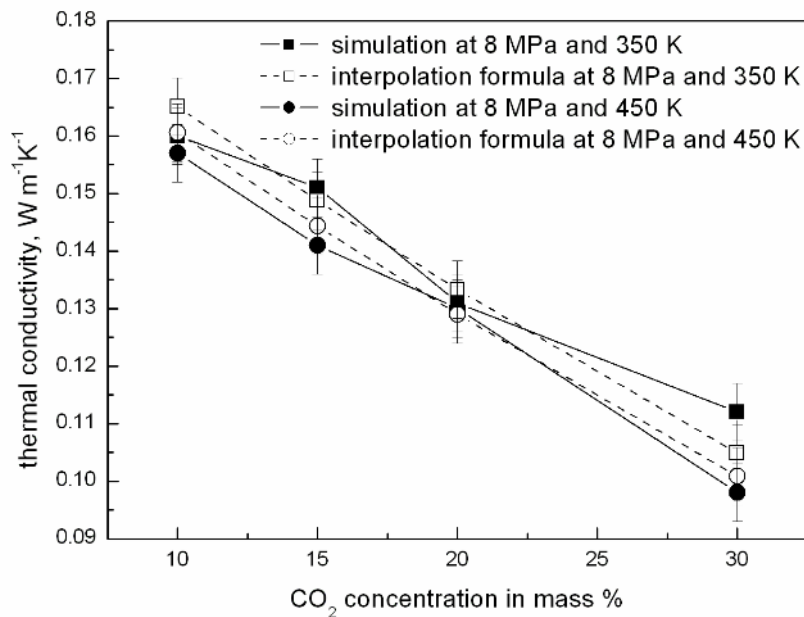


Figure 4-13. Thermal conductivity of the binary mixture as a function of CO<sub>2</sub> mass concentration derived by RNEMD simulations of the binary system and estimated via the interpolation.

Interpolation schemes of the present type might be useful, when the theoretical determination of quantities of a binary system over a large concentration, pressure and temperature range is intended on the basis of a smaller set of simulation or experimental results.

#### 4.5. Summary

The thermal conductivity  $\lambda$  of amorphous atactic polystyrene swollen in supercritical carbon dioxide has been investigated over a wide temperature, pressure and concentration range by nonequilibrium molecular dynamics simulations with a fully atomistic model for the force field. The data for the binary systems have been supplemented by thermal conductivity values derived for the components PS and CO<sub>2</sub>. Neat PS as well as the binary mixtures are so-called multi-level systems characterized by very small energy differences in the presence of larger differences of other physical quantities. Computer simulations of such systems are very time-consuming as it requires a high effort and much experience to reduce the error bars for the quantities studied to an acceptable minimum. The pressure and temperature dependence of the thermal conductivity has been discussed in detail. For the neat components it has been possible to relate the calculated results to experimental data. Density trends for both PS and CO<sub>2</sub> have reproduced the experimental ones correctly. The thermal conductivity of PS differs from experiment by less than 20%. We have shown that the thermal conductivity of PS is much larger than the thermal conductivity of CO<sub>2</sub>. This leads to a reduction of the thermal conductivity of the mixture with an enhanced concentration of CO<sub>2</sub>. It has been possible to present an interpolation formula for the thermal conductivity of the binary samples on the basis of  $\lambda$  values for the two components PS and CO<sub>2</sub>.

---

The present RNEMD simulations have reproduced another recent result, i.e. the correlation between the thermal conductivity and the number of C-C bonds in the polymer backbone in the direction of the temperature gradient, which had been found for amorphous polyamide-6,6.<sup>19</sup> In chapter 3 this topic will be analyzed in more detail for PS samples under uniaxial stress.

---

## 5. Anisotropy of the Thermal Conductivity for Amorphous Polystyrene and its Mixture with Supercritical Carbon Dioxide

---

Many polymers are highly anisotropic. Properties such as elastic moduli,<sup>94,95</sup> viscosity<sup>96</sup> and electrical conductivity<sup>97</sup> have been investigated in detail in these materials. The thermal conductivity is one of the quantities where an anisotropic behavior has been studied, too.<sup>48</sup> It has been observed in polymers with an amorphous structure and in partially oriented samples.<sup>8</sup> Anisotropies in the thermal conductivity have been found both in experimental and simulation studies.<sup>8,19</sup> In the design of modern polymer-based products, the anisotropy in physical properties should be considered carefully, as it brings a new potential to the design of novel materials that can be used in electronics, for example. Accurate theoretical predictions of  $\lambda$  and its anisotropy can lead to improvements in the processing and application design. For instance, the thermal conductivity of insulating materials is a determining factor in their energy efficiency.<sup>98</sup> Thermal conductivities of polymers over a wide temperature and pressure range are not always available. In this case computer simulations of the molecular dynamics (MD) type become an important instrument for the prediction of the thermal conductivity of polymers.<sup>1</sup> The correlation between measured heat capacities and calculated thermal conductivities can be used to derive physically reliable force field parameters in simulation methods. These techniques finally offer the possibility to relate measured  $\lambda$  values to structural units of polymers.

Another focus of recent polymer studies are swelling processes in supercritical fluids. Much work has been done for mixtures of a polymer and CO<sub>2</sub> under supercritical conditions. The large ecological advantage of CO<sub>2</sub> in comparison to organic solvents is its non-toxicity.<sup>76-78</sup> Furthermore, it has been shown experimentally that the substitution of toxic organic solvents by CO<sub>2</sub> under supercritical conditions does not lead to strong reductions in the yield of purification, impregnation, and fractionation as well as in the production of porous foam or powder polymers.<sup>79,80</sup> To optimize these processes, it is necessary to investigate the physical properties of polymers swollen in supercritical media. Experimental and simulation approaches have been used simultaneously to determine these polymer properties.<sup>99,100</sup> The behavior of many polymers in supercritical fluids is still not understood quantitatively. From the point of view of fundamental science the investigation of the thermal conductivity of polymers and swollen polymers can lead to the better understanding of the heat transfer process itself. It has been described theoretically that at least two mechanisms are relevant for the heat transport in polymers, i.e. vibrational effects and collisions.<sup>101,102</sup> To come back to the anisotropy of the thermal conductivity, this quality has been analyzed in several experimental

---

and theoretical studies on polymers, such as amorphous polystyrene (PS) and polyethylene.<sup>2,4,8</sup>

In this chapter we have investigated the anisotropy of the thermal conductivity of stretched atactic polystyrene swollen in supercritical CO<sub>2</sub> by reverse nonequilibrium molecular dynamics (RNEMD) simulations.<sup>1,9-11</sup> The arrangement of stretched PS in the MD simulation box has been displayed in figure 3-1. Atactic polystyrene is characterized by a random distribution of the phenyl rings on both sides of the chain. The carbon-carbon bonds of the backbone in figure 3-1 are marked in red color. As one can see from the  $xz$ -projection in figure 3-1, the simulation cell is elongated along the  $z$  direction, while the  $x$  and  $y$  directions are identical.

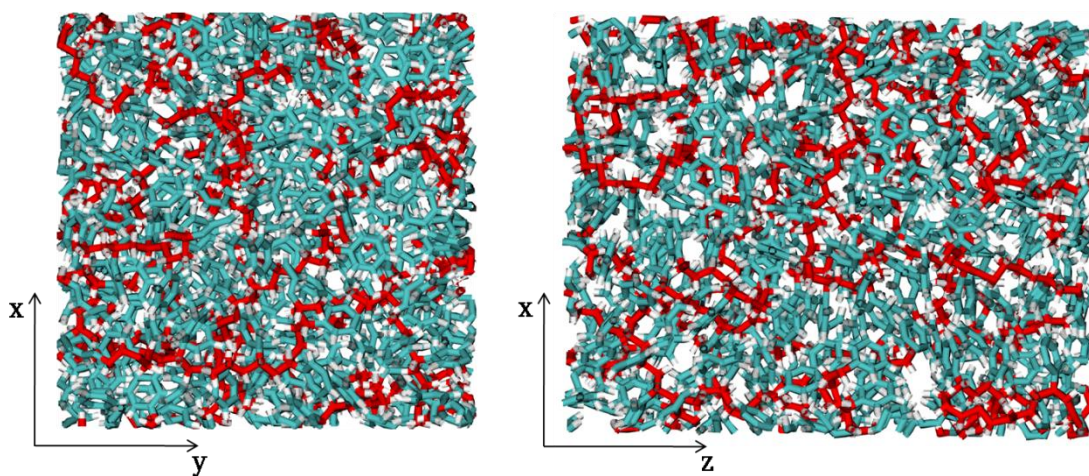


Figure 5-1. Arrangement of stretched polystyrene in the simulation box as projected on the  $xy$  and  $xz$  plane. Stretching occurs in the  $z$  direction. The carbon atoms in the backbone chain have been highlighted in red.

In the previous chapter we have analyzed the implications of finite-size effects and the quasi-degeneracy in multi-level systems.<sup>82</sup> In such polymer systems or solids one can have local changes in the density or in the spatial arrangement of the atoms that are energetically quasi-degenerate but are responsible for anisotropy in physical quantities. In chapter 2 we have detected such finite-size effects via anisotropy of the thermal conductivity of PS although we have employed an isotropic simulation cell. An analysis of these computational results has shown that the thermal conductivity strongly correlates with the orientation and number of the C-C bonds in the backbone of PS. Stretching of the PS sample and the PS-CO<sub>2</sub> mixtures, say into the  $z$  direction, causes an enhanced orientation of these C-C backbone bonds in this preferred direction and, thus, an enhancement of the thermal conductivity relative to this direction. In other words, in the work described in chapter 2 any anisotropy has been an outcome of finite-size effects or quasi-degeneracy. Now it has been generated via the sample preparation in the simulation runs.

The thermal conductivity of neat PS and CO<sub>2</sub> as well as of different binary mixtures has been calculated in chapter 2 and compared with experimental results. The simulation box adopted

---

in these RNEMD simulations has been isotropic. In the present work we have analyzed the anisotropy of the thermal conductivity in stretched polystyrene. Differences in  $\lambda$  between oriented and unoriented PS samples have been described in the literature many years ago<sup>2,4</sup>. The present study, however, has not been restricted to a comparison with these experimental results but covers theoretical calculations as well. In recent MD simulations of our group, the thermal conductivity of polyamide-6,6<sup>19</sup> and of the crystalline  $\delta$  phase of syndiotactic PS<sup>10</sup> has been calculated. In polyamide-6,6 it has been shown that the system degrees of freedom are more or less equivalent, i.e. the thermal conductivity strongly correlates with their number. Crystalline PS, however, is a polymer system, where this equivalence is violated. In analogy to the work described in chapter 2 the decisive influence of the orientation of the C-C *backbone* bonds relative to the direction of the temperature gradient on  $\lambda$  has been pointed out in ref. 19. This comparison with recent theoretical results forms the second main topic of chapter 3. To sum up: In polymers we can find systems where all degrees of freedom have an identical influence on  $\lambda$  and we can also have systems where certain degrees of freedom play a dominant role. This contribution aims to find out which concept applies to amorphous polystyrene.

## 5.1. Computational Details

As the nonequilibrium technique adopted has been described in recent articles of the group, we refer the reader to these references.<sup>1,9,11</sup> The molecular dynamics simulations in the present article have been performed with the YASP package,<sup>42,43</sup> which makes use of the leapfrog algorithm and orthorhombic periodic boundary conditions. The chosen temperatures and pressure ranges refer to conditions close to experiment. The intramolecular force field is defined by harmonic bond stretching, harmonic angle bending, and periodic cosine-type torsional potentials. The non-bonded potential is described via Lennard-Jones terms with Lorentz-Berthelot mixing rules<sup>12</sup> for unlike interactions as well as via electrostatic interactions that are mapped by atomic partial charges. The electrostatic field has been computed by the reaction-field method with a relative permittivity of 2.5. A cutoff of 1.1 nm has been used in all simulations. A detailed description of the force field can be found in ref. 55. The non-bonded interactions were evaluated from a Verlet neighbor list, which was updated every 15 timesteps (of 0.001 ps length) using a link-cell method with a cutoff of 1.2 nm.

The molecular dynamics simulations have been performed at constant (overall) temperature and pressure. A coupling time  $\tau_T$  of 0.2 ps has been used for the Berendsen thermostat,<sup>44</sup> while the coupling time  $\tau_p$  for the Berendsen manostat amounts to 2 ps. Both parameters have been sufficient to keep the calculated average temperature within 1 K of the target temperature and the calculated average pressure within 1 kPa of the target pressure. It has

---

been checked that modifications of  $\tau_T$  and  $\tau_p$  did not change the thermal conductivity. The simulation box in the RNEMD runs has been divided into 20 slabs in the heat flux direction. The velocities of the atoms of identical mass were exchanged every 0.5 ps. We have controlled that the thermal conductivity converges within this exchange period. A nonequilibrium run typically covered 3 ns, the last 1 ns has been used for the production.

One atactic polystyrene chain of 300 monomers and random tacticity has been generated in vacuum. The initial conformations have been obtained via pivot Monte Carlo calculations<sup>88</sup> of a single polymer chain in vacuum with a bond-based interaction cutoff to generate a melt-like structure. Since the persistence length is the length over which correlations in the tangential direction are lost, an interaction cutoff of 7 bonds  $\approx 0.895$  nm (persistence length of PS) has been chosen. This chain has been inserted into the periodic simulation cell of a cubic box. The initial density of PS has been of  $0.908$  g/cm<sup>3</sup>. Soft-core potential simulations have been employed to remove possible overlaps, entanglements and concatenations. Then the system has been equilibrated for 10 ns by equilibrium MD at a constant pressure of 101.3 kPa and a temperature of 300 K. Equilibration yielded a cubic simulation box with a PS density of  $1.042$  g/cm<sup>3</sup>, while experimental values vary in the range from  $1.032$  g/cm<sup>3</sup> to  $1.069$  g/cm<sup>3</sup> at the same conditions.<sup>91</sup>

In the subsequent steps 1) to 5) the simulation box has been stretched. The strategy used has been tested before.<sup>19</sup> 1) Heat the sample over 400 ps at constant volume to 600 K. Use a coupling time of 0.1 ps for the thermostat and a heating rate of 0.5 K/ps. 2) Equilibrate the sample at 600 K for 200 ps at constant volume. 3) Stretch the sample in a *NPT* simulation of 100 ps duration using a temperature coupling time of 0.1 ps. Note that the pressure coupling is anisotropic. The initial target pressure of 100000 kPa refers to the average pressure of step 2). The coupling times for the  $x$ ,  $y$ ,  $z$  directions amount to 150, 150, and 1 ps. The target pressure has been kept constant for the  $x$  and  $y$  directions. For the  $z$  direction it has been reduced by -600 kPa/ps leading to an enlargement in the  $z$  dimension of the box. In our simulations the sample has been stretched up to 10-25 % to simulate changes in the thermal conductivity as a function of the stretching ratio. As practically no contraction was allowed in  $x$  and  $y$  directions, the density of the sample has been lower than the density of the isotropic sample at the end of this step. 4) Cool the sample to 400 K in an *NPT* simulation of 200 ps. The initial bath temperature of 600 K has been lowered with a rate of -0.5 K/ps and the target pressure has been fixed to 60 MPa in all directions. At the end of this step the density of  $1.02$  g/cm<sup>3</sup> is still lower than the density of the isotropic sample. 5) Now perform an isotropic compression of the sample in an *NPT* simulation at 400 K with a target pressure of 60 MPa. This step generates a density of  $1.040$  g/cm<sup>3</sup>. Subsequently the sample has been equilibrated in different *NPT* simulations (at temperatures in the range between 300 and 500 K, pressures

---

of 0.1, 8, 16, 40 and 60 MPa). Now the densities of the stretched samples have achieved the densities of isotropic samples; see section 2.2.

A flexible full atomistic model has been selected for the present MD approach. The force constants for PS have been reported previously for a rigid bond model.<sup>55</sup> The constants for the harmonic bond stretching forces have been adopted from other works.<sup>19,84</sup> Potential parameters and atomic charges for a flexible full atomistic model of carbon dioxide have been developed by Harris and Yung<sup>85</sup> with the aim to reproduce its vapor-liquid coexistence curve and critical properties. These elements have been used also for the determination of transport properties such as the self-diffusion coefficient in a supercritical state. The capability of the Harris-Yung model for transport properties, such as a thermal diffusion coefficient has been discussed in the literature.<sup>86</sup>

The following systems have been investigated: neat PS, neat CO<sub>2</sub> at supercritical conditions and mixtures of PS with different concentrations of CO<sub>2</sub> at supercritical conditions. The simulations have been performed in a temperature range between 350 and 500 K and for pressures between 0.1 and 60 MPa. Both the temperature and pressure range considered have been employed in experimental studies of the mixture.<sup>76,89</sup> They include the investigation of the solubility of PS in supercritical CO<sub>2</sub>, and the miscibility of the two components. Studies of the thermal conductivity, however, are not available. The concentration of carbon dioxide in the mixture spans a range from 10 to 30 mass %. Four different mixtures with a total number of 79, 125, 177 and 304 CO<sub>2</sub> molecules added to a single PS chain have been studied. The binary systems generated contain 10, 15, 20 and 30 mass % of CO<sub>2</sub>.

## 5.2. Anisotropy of the Thermal Conductivity of Neat Polystyrene

One of the purposes of the present work has been an investigation of heat transport mechanisms. Our hypothesis is that the heat transport in polymers through delocalized phonons<sup>101,102</sup> is more efficient than the transport via collisions. This can lead to the situation when the orientation of bonds is of great importance for the heat transfer. Contrary to polymer systems the main heat transport channel in amorphous structures such as CO<sub>2</sub> or benzene is provided by collisions. Our hypothesis will be discussed in detail under consideration of recent findings.

In chapter 2 we have calculated the thermal conductivity of neat isotropic polystyrene and compared our data with experimental results. The measured thermal conductivity of neat PS at 300 K and 101.3 kPa amounts to 0.156 Wm<sup>-1</sup>K<sup>-1</sup>, while the calculated value is of 0.187 Wm<sup>-1</sup>K<sup>-1</sup>. Possible reasons for this difference have been mentioned already in section 2.2. Now we relate the thermal conductivity of stretched polystyrene to  $\lambda$  of the isotropic system. The stretched polystyrene sample is characterized by the stretching ratio  $r_s$ :

$$r_s = \frac{L_{\parallel} - L_{\perp}}{L_{\parallel}} \cdot 100 \quad (3-1)$$

where  $L_{\parallel}$  and  $L_{\perp}$  stand for the length of the simulation box parallel and perpendicular to the stretching direction.

The pressure dependence of the thermal conductivity of the stretched polystyrene sample at 400 K and a stretching ratio of 35 % is presented in figure 3-2. An anisotropy in  $\lambda$  exists at all pressures. The difference between the thermal conductivity parallel  $\lambda_{\parallel}$  and perpendicular  $\lambda_{\perp}$  to the stretching direction, however, decreases with increasing pressure. In the parallel direction the sample behaves as a rather incompressible solid, which is characterized by a weak pressure dependence of the thermal conductivity. The pressure dependence of  $\lambda_{\perp}$  is stronger. Here the limit of an incompressible solid is approached only for pressures larger than 40 MPa. The difference between  $\lambda_{\parallel}$  and  $\lambda_{\perp}$  can be traced back to different densities in the covalent PS backbone bonds in the two directions. The larger number of covalent backbone bonds in the parallel direction makes the solid both less compressible and better conductive, while the non-bonded contacts in the perpendicular direction allow a compression of the solid over a larger pressure range. The same effect has been observed in graphite with its highly anisotropic compressibility;<sup>103</sup> the planar Young modulus of graphite is roughly 30 times higher than in the  $c$ -axis direction.

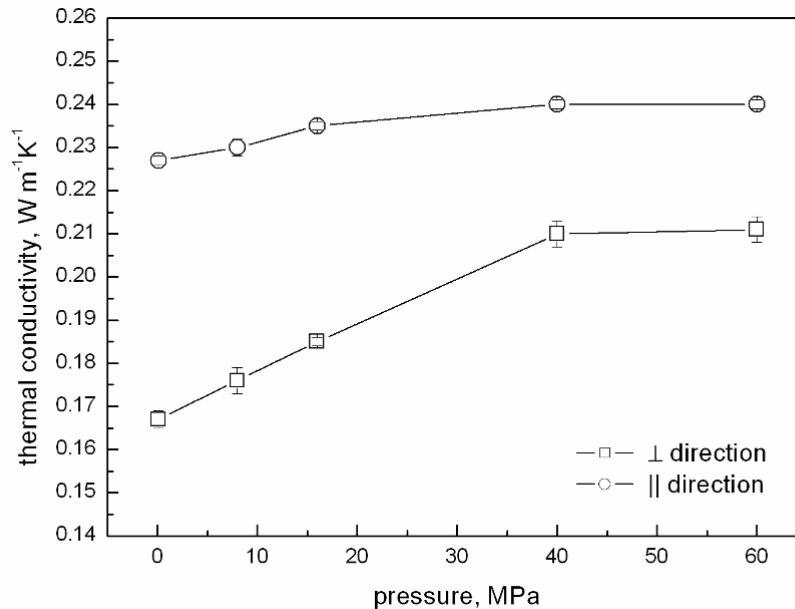


Figure 5-2. Pressure dependence of the thermal conductivity of anisotropic polystyrene at 400 K and a stretching ratio of 35 %.

The temperature dependence of the thermal conductivity of anisotropic polystyrene at 0.1 MPa and a stretching ratio of 21 % is shown in figure 3-3. As already reported in chapter 2, the thermal conductivity of isotropic PS first increases with temperature, it has a plateau in the range between 400 and 450 K, and then it is slightly reduced, see also figure 3-3. From



the figure we deduce the same trend for the anisotropic sample in both directions. The splitting between the two thermal conductivity curves in anisotropic PS does not depend on the temperature.

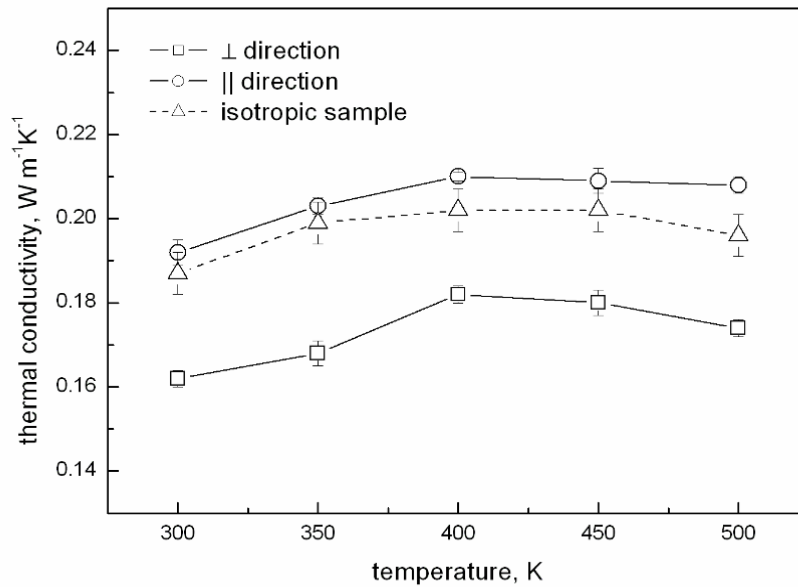


Figure 5-3. Temperature dependence of the thermal conductivity of anisotropic polystyrene at 0.1 MPa and a stretching ratio of 21 %.

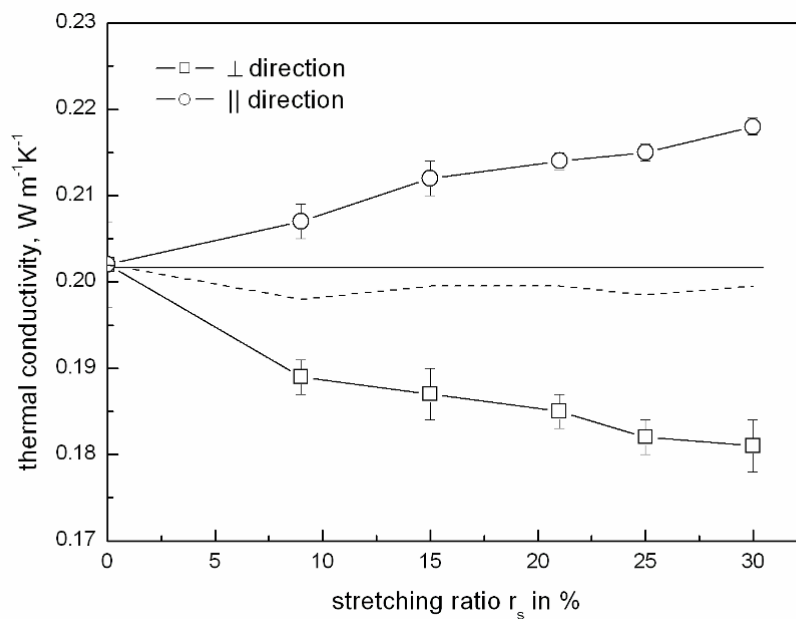


Figure 5-4. Thermal conductivity of anisotropic polystyrene as a function of the stretching ratio  $r_s$  at 0.1 MPa and 400 K. The  $\lambda_{\parallel}$  and  $\lambda_{\perp}$  average has been labeled by a dashed curve. The straight line refers to the thermal conductivity of the isotropic sample.

On the basis of the material in figure 3-2 it can be assumed that the difference between the thermal conductivity in the parallel and perpendicular direction is enhanced with increasing stretching ratio  $r_s$ . A computational verification of this behavior would be an additional support of our hypothesis, i.e. the correlation between the orientation of C-C backbone bonds

and the magnitude of  $\lambda$ . The thermal conductivity of anisotropic samples as a function of  $r_s$  is plotted in figure 3-4; it shows the expected behavior. Also note that the average of the two  $\lambda$  curves is slightly smaller than  $\lambda$  of the isotropic sample. Figure 3-4 visualizes that the conductivity reduction in the stretched sample is constant over a large  $r_s$  range.

In the following let us consider the correlation between the number and orientation of the C-C backbone bonds of PS relative to the direction of the heat transfer and the thermal conductivity in more detail.

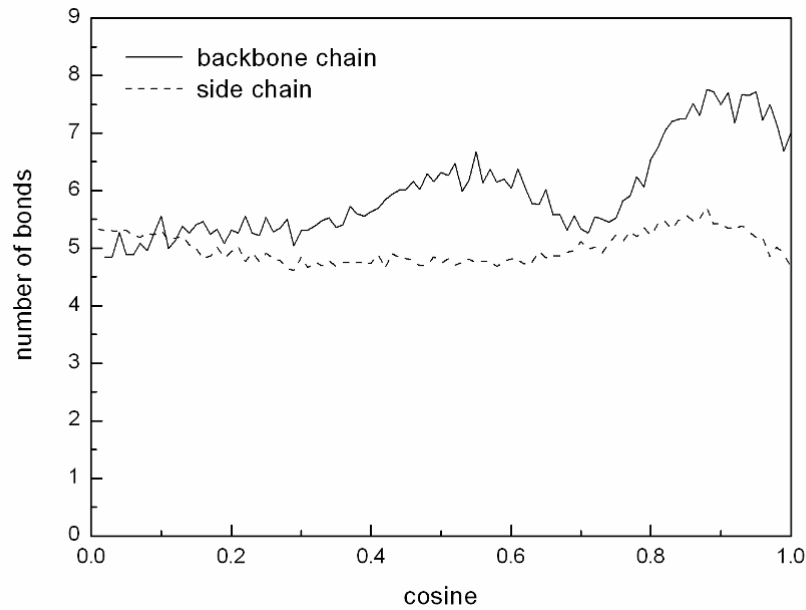


Figure 5-5. Distribution of the direction cosines of the C-C bonds in the PS backbone and side chain in the direction of stretching. The simulations have been carried out at a temperature of 350 K and a pressure of 0.1 MPa.

The distribution function of the direction cosine of these bonds parallel to the direction of the stretching with  $r_s = 15\%$  is shown in figure 3-5. The distribution is calculated from the PS simulation trajectory with a stretching ratio of 15%, a temperature of 350 K and a pressure of 0.1 MPa. It has been averaged over 1000 frames, which corresponds to a simulation time of 1 ns. The negative cosine values in the distribution have been inverted and added to the positive ones. One immediately recognizes that the number of backbone bonds parallel to the stretching direction (cosine  $\approx 1$ ) exceeds the number of bonds in the perpendicular direction (cosine  $\approx 0$ ).

The parallel profile in figure 3-5 exhibits the strongest maximum for a direction cosine of roughly 0.9, indicating that many C-C backbone bonds are oriented almost in the direction of stretching. Since each of the PS backbone carbons lies at the center of a tetrahedron, the angle between the backbone C-C bonds amounts to  $109.5^\circ$ . Thus, the second smaller maximum at about 0.5 follows from this fact. The dashed curve in figure 3-5 represents the distribution of the direction cosine of the C-C bonds in the side chain of the polymer. As one

can see, there is no preferred orientation of the C-C bonds in this PS unit. This fact means that the bond orientation in the side chain does not affect the anisotropy of the thermal conductivity.

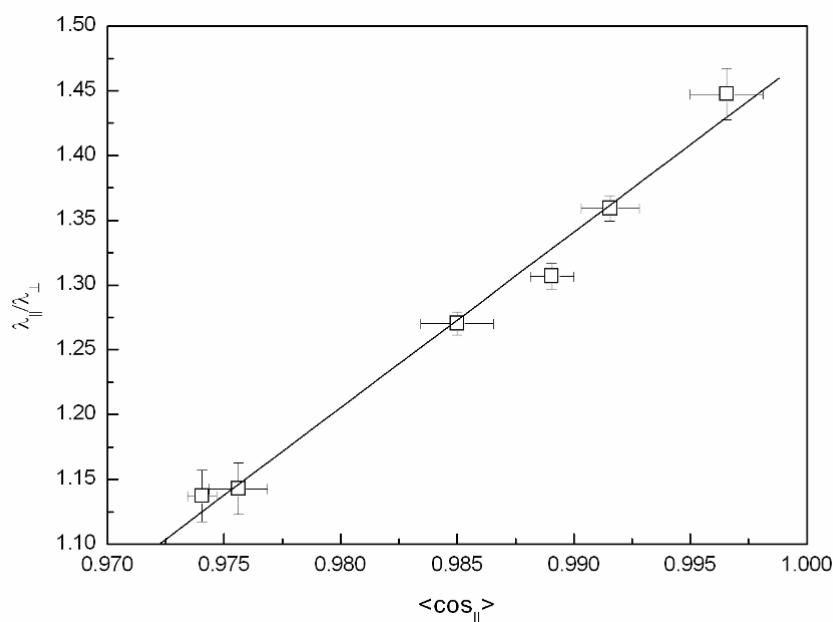


Figure 5-6. Anisotropy of the thermal conductivity  $\lambda_{\parallel}/\lambda_{\perp}$  of PS as a function of the averaged direction cosine of the C-C backbone bonds in the parallel direction  $\langle \cos_{\parallel} \rangle$ . The RNEMD data have been derived for different temperatures and stretching ratios.

With the data of figure 3-5 we have calculated the mean value of the direction cosine of the C-C backbone bonds parallel to the stretching direction. The thermal conductivities perpendicular and parallel to the stretching direction have been calculated as well. The ratio of the thermal conductivities  $\lambda_{\parallel}/\lambda_{\perp}$  versus the weighted averaged direction cosine  $\langle \cos_{\parallel} \rangle$  is presented in figure 3-6. The data have been sampled over a number of temperatures and stretching ratios. The suggested correlation between the thermal conductivity and the orientation of the C-C backbone bonds is easy to identify in the diagram. The enhancement in the anisotropy of PS with increasing stretching is also a message that follows from the calculated data. Stretching causes an enhanced orientation of the bonds in the PS backbone. This ordering is then responsible for higher  $\lambda_{\parallel}$  values. An additional justification of the present correlation can be also deduced from a previous RNEMD simulations of the  $\delta$  phase of syndiotactic PS.<sup>10</sup> Here it has been demonstrated that the phenyl rings of PS are more or less irrelevant for the heat transport. Suppression of these degrees of freedom in a simulation does not affect the calculated  $\lambda$  values. Later we will come back to this point.

### 5.3. Anisotropy of the Thermal Conductivity of Binary Mixtures of Polystyrene and Carbon Dioxide

The pressure dependence of the thermal conductivity of a stretched ( $r_s = 22\%$ ) binary mixture with 10 mass % of  $\text{CO}_2$  is presented in figure 3-7. We have included the data for an isotropic PS- $\text{CO}_2$  mixture (dashed line). Similar to neat PS, the thermal conductivity of the binary mixture is higher in the stretching direction and lower perpendicular to it.

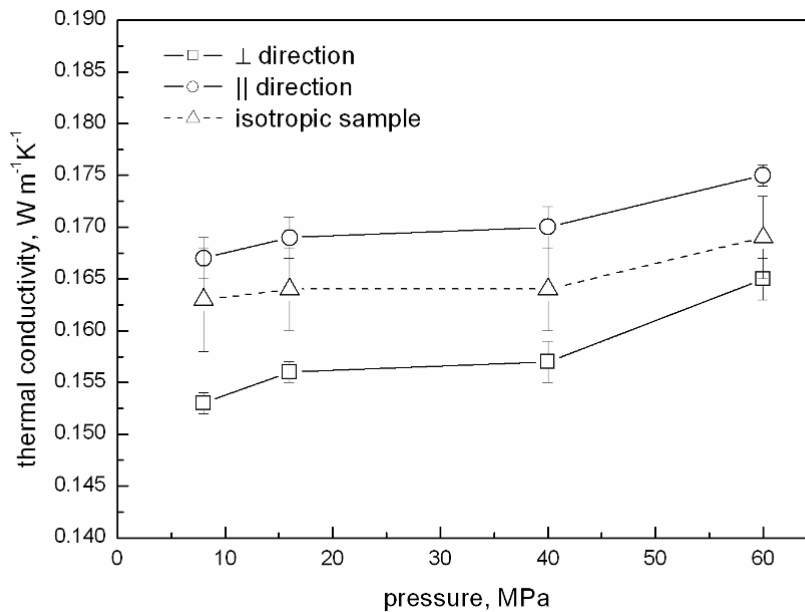


Figure 5-7. Pressure dependence of the thermal conductivity of a binary PS- $\text{CO}_2$  mixture with 10 mass % of  $\text{CO}_2$  and a stretching ratio 22 %. The dashed curve is for the isotropic mixture.

The anisotropy of the thermal conductivity persists at all pressures, but it is slightly reduced at higher pressure. The thermal conductivities in the parallel and perpendicular directions follow the trend of the thermal conductivity in the isotropic sample;  $\lambda$  is enhanced with increasing pressure. The anisotropy of the thermal conductivity in the binary mixture is much smaller ( $\sim 7\%$  difference between  $\lambda_{||}$  and  $\lambda_{\perp}$ ) than in neat PS ( $\sim 20\%$ ). The  $\text{CO}_2$  molecules in the binary mixture introduce additional channels for the heat transfer via collisions<sup>101,102</sup> that do not depend on the anisotropy and thus on the stretching of the polystyrene sample.

The thermal conductivity of binary mixtures as a function of the  $\text{CO}_2$  concentration is shown in figure 3-8. In analogy to figure 3-7 we have added the modification of  $\lambda$  as a function of the  $\text{CO}_2$  concentration in the isotropic sample to the diagram. Both the thermal conductivity components  $\lambda_{\perp}$ ,  $\lambda_{||}$  and the anisotropy  $\lambda_{||}/\lambda_{\perp}$  are reduced with enhanced  $\text{CO}_2$  concentration. This reduction of the anisotropy is simple to explain; see again the discussion in connection with figure 3-7. With enhanced  $\text{CO}_2$  admixtures, the “anisotropic” PS contribution to the thermal conductivity is attenuated while the more or less “isotropic”  $\text{CO}_2$  contribution to  $\lambda$  becomes more important.

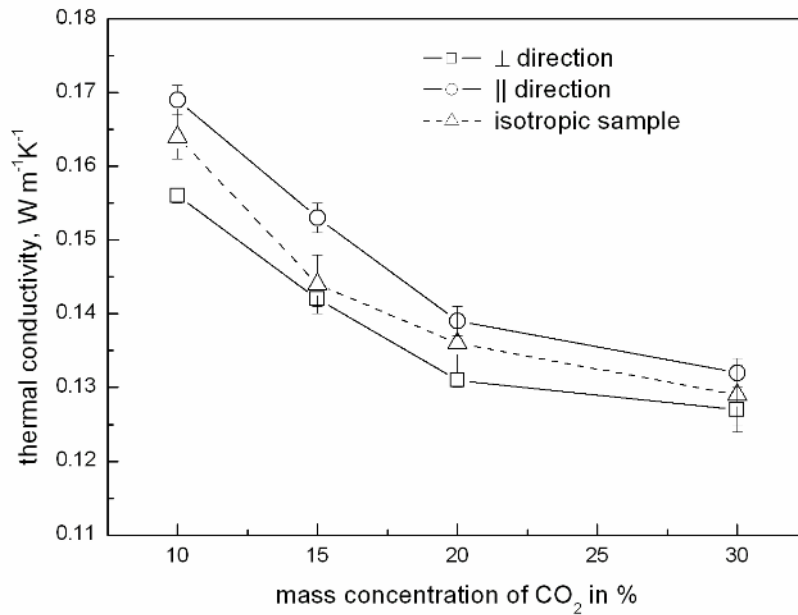


Figure 5-8. Thermal conductivity of binary PS-CO<sub>2</sub> mixtures as a function of the CO<sub>2</sub> mass concentration at 400 K and 16 MPa for a stretching ratio of 23 %. The dashed curve is for the isotropic sample.

In figure 3-9 we have plotted the thermal conductivity of a binary mixture with 10 mass % of CO<sub>2</sub> as a function of the stretching ratio  $r_s$ . The enhancement in the anisotropy of  $\lambda$  with increasing  $r_s$  follows a priori expectations. Nevertheless it is much smaller than in the neat PS sample. This behavior has been expected, too. Contrary to neat PS we see that the average of the two curves coincides roughly with the thermal conductivity of the isotropic polymer. Only for large  $r_s$  numbers the mean value of  $\lambda$  in the binary sample is smaller than  $\lambda$  of neat PS. In consideration of the computational error bars, however, we are left with some uncertainties.

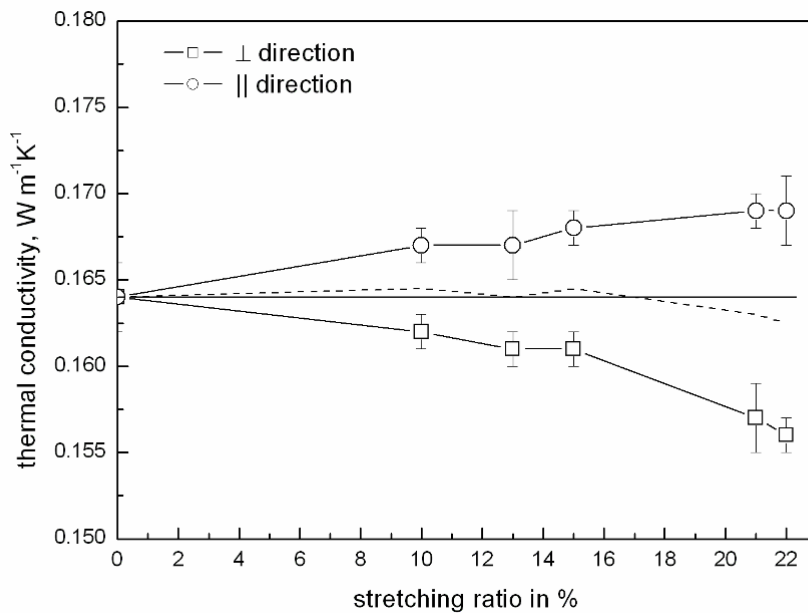


Figure 5-9. Thermal conductivity of a binary mixture with 10 mass % of CO<sub>2</sub> as a function of the stretching ratio at 400 K and 16 MPa. The mean thermal conductivity  $(\lambda_{\parallel} + \lambda_{\perp})/2$  has been symbolized by a dashed curve. The straight line refers to the thermal conductivity of the isotropic sample.

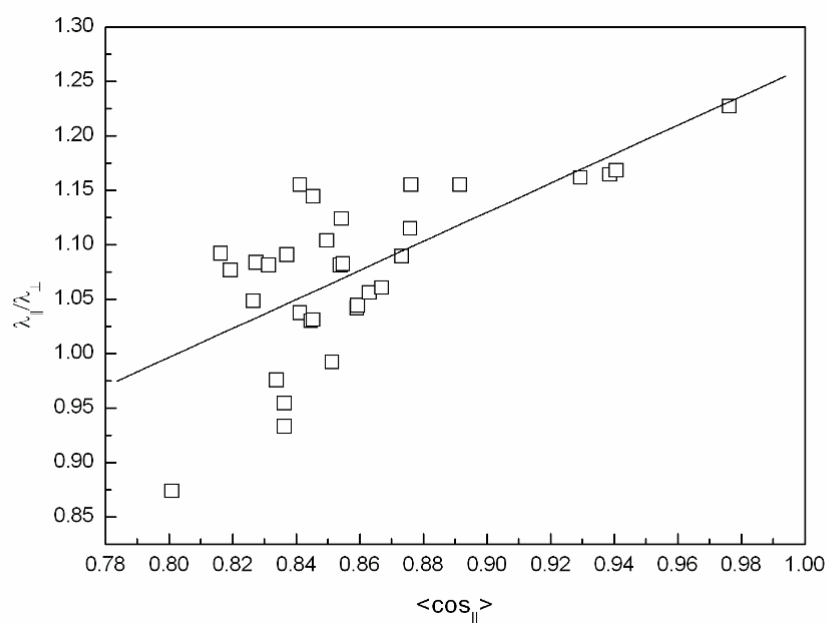


Figure 5-10. Thermal conductivity ratio  $\lambda_{||}/\lambda_{\perp}$  as a function of the average cosine between the C-C bonds of the backbone and the direction of heat transfer  $\langle \cos_{||} \rangle$  for binary mixtures at different pressures, temperatures and concentrations of CO<sub>2</sub>; see the same correlation for neat PS in figure 3-6.

Next let us comment on the correlation between the  $\lambda_{||}/\lambda_{\perp}$  ratio and the average direction cosine  $\langle \cos_{||} \rangle$  for the binary mixtures. For neat PS this dependence has been displayed in figure 3-6. The extension of this diagram to binary systems has been portrayed in figure 3-10. In contrast to neat PS the correlation between the conductivity anisotropy and the average cosine is now less pronounced. Again we notice that an increasing participation of CO<sub>2</sub> in the heat transport causes an attenuation of the “anisotropic” C-C backbone contribution to the overall conductivity. To reemphasize; the heat transfer contributed by CO<sub>2</sub> occurs via collisions, while the PS participation is phonon driven.

#### 5.4. Dependence of the Thermal Conductivity on Number of Degrees of Freedom

Now let us consider the dependence of the thermal conductivity on the number of degrees of freedom of the system per unit volume. In our recent research we have found polymer systems where all vibrational degrees of freedom contribute with the same amount to the thermal conductivity.<sup>19</sup> However there are a number of factors violating this principle; the most important ones are summarized below. Even in classical MD simulations we can have a discrimination between strongly localized and delocalized vibrations.<sup>101,102</sup> The latter contribute more efficiently to the transfer of energy than local modes. It is self-explanatory that such a transition between these two boundaries can be tuned artificially by the force field parameters in a simulation. The importance of the different modes for the thermal conductivity can be quantified by using different patterns of bond constraints and

unconstrained geometrical parameters. A convincing argument for the nonequivalence of the degrees of freedom finally follows from the present computational findings, i.e. the strong correlation between the orientation of the C-C backbone bonds and  $\lambda$  in PS and PS-CO<sub>2</sub> mixtures. In figure 3-11 we have collected calculated thermal conductivities of several materials as a function of the degrees of freedom per unit volume. Changes in the number of degrees of freedom per volume are caused not only by density and concentration variations but also by the use of a force field with different constraints.

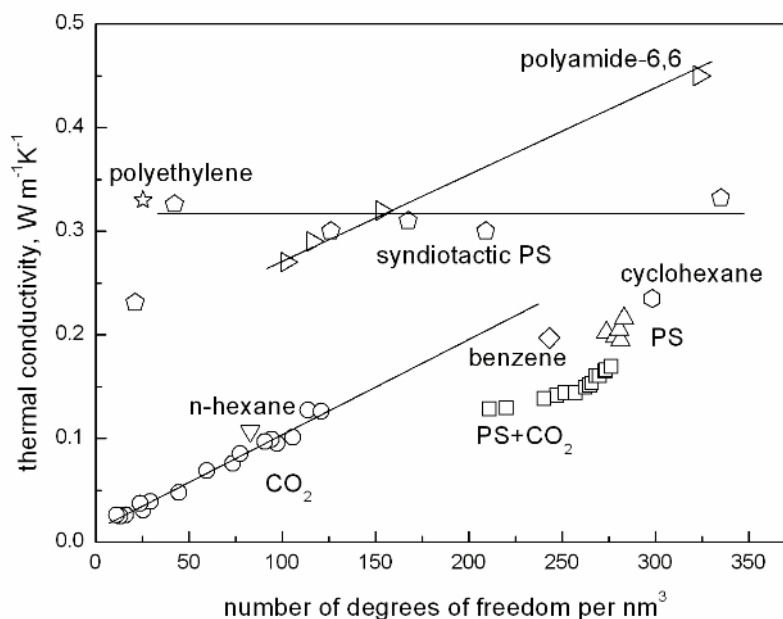


Figure 5-11. Calculated thermal conductivity as a function of the degrees of freedom per volume for amorphous polyethylene,<sup>104</sup> amorphous polyamide-6,6,<sup>19</sup> crystalline syndiotactic polystyrene,<sup>10</sup> liquid benzene<sup>11</sup>, liquid n-hexane<sup>11</sup>, liquid cyclohexane<sup>11</sup>, supercritical CO<sub>2</sub> (present work), amorphous atactic polystyrene (present work), amorphous atactic polystyrene +CO<sub>2</sub> (present work).

The strong correlation between the number in the degrees of freedom and the thermal conductivity of CO<sub>2</sub> follows from a heat conduction provided via collisions.<sup>101,102</sup> The rather localized vibrations in amorphous materials such as CO<sub>2</sub> without covalent bonding network covering the sample dimension make the heat transfer via phonons highly inefficient.<sup>101,102</sup> In PS such an extended network is formed by the C-C backbone bonds. The implications for the thermal conductivity have been mentioned above. To come back to the CO<sub>2</sub> data in figure 3-11; the higher the density, the more degrees of freedom per unit volume are found and the higher is the collision-driven thermal conductivity.

The thermal conductivities of polyethylene, benzene and crystalline syndiotactic polystyrene have been taken from previous simulation studies.<sup>10,11,19,104</sup> The data for amorphous polyethylene are based on a united-atom approach,<sup>104</sup> where one carbon and two hydrogen atoms have been connected to one bead. This step explains the coincidence of a very small number in the degrees of freedom per unit volume and a high thermal conductivity.

---

Responsible for the heat transport in polyethylene are the C-C bonds with their delocalized vibrations, so-called propagons.<sup>102</sup> In analogy to PS they are a prerequisite to have a highly efficient phonon support in the heat transfer. A second instructive example in figure 3-11 is the benzene system, which was modeled using bond constraints throughout. As in CO<sub>2</sub>, the heat transport in this hydrocarbon is caused by collisions of the molecules, not by phonons.<sup>101,102</sup> It seems that the thermal conductivity of benzene, n-hexane and cyclohexane can be estimated approximately when extrapolating the CO<sub>2</sub> data to the number of degrees of freedom encountered in these hydrocarbon systems.

The thermal conductivity data for crystalline syndiotactic polystyrene<sup>10</sup> in figure 3-11 are highly instructive. The RNEMD calculations in ref. 10 have been performed with differences in the degrees of freedom considered, i.e. with 0, 8, 6, 11, 15, or 16 constrained bonds per monomer (for more details see ref. 10). In all simulations, except for the completely constrained monomer, the  $\lambda$  values occur around 0.30 Wm<sup>-1</sup>K<sup>-1</sup>. This, however, means that even a complete suppression of the bond vibrations in the phenyl rings of PS does not influence the thermal conductivity significantly. Only when C-C bonds in the backbone are constrained the thermal conductivity is strongly reduced. In contrast to syndiotactic polystyrene, the thermal conductivity of amorphous polyamide-6,6 depends strongly and linearly on the number of degrees of freedom per unit volume.<sup>19</sup> Therefore, it seems that the degrees of freedom in polyamide-6,6 are equivalent regarding thermal transport while they are not in polystyrene.

To sum up; the calculated conductivities in figure 3-11 indicate quite generally that the collision induced heat transfer is less efficient than the phonon-assisted transfer via long chains with covalent nearest neighbor contacts. From the data in figure 3-11 it also follows that this grading between phonon and collision assisted heat transfer is changed in the absence of delocalized modes.



---

## 6. Conclusions and Outlook

---

In this work we have presented calculations of the thermal conductivity  $\lambda$  of amorphous atactic polystyrene (PS) swollen in supercritical carbon dioxide (CO<sub>2</sub>) over wide temperature, pressure and concentration ranges by reverse nonequilibrium molecular dynamics (RNEMD) simulations with a full atomistic model for the force field. The pressure and temperature dependence of the thermal conductivity has been discussed in detail. For the neat components it has been possible to relate the calculated results to experimental data. The thermal conductivity of PS differs from experiment by less than 20 %. It has been possible to present an interpolation formula for the thermal conductivity of the binary samples on the basis of  $\lambda$  values for the two components PS and CO<sub>2</sub>.

The second part of the work has been the calculation of the thermal conductivity of stretched PS and PS-CO<sub>2</sub> mixtures over wide pressure, temperature and concentration ranges. In neat PS, stretching causes an increase of the thermal conductivity  $\lambda_{||}$  in the stretching direction by up to 20 % with a concomitant decrease of the perpendicular thermal conductivity. In the PS-CO<sub>2</sub> mixtures studied here, the anisotropy of the thermal conductivity is reduced (7 % higher in the stretching direction) due to an enhanced contribution of the CO<sub>2</sub> fluid, which is isotropic. We have found that the orientation of the C-C bonds in the backbone chain relative to the temperature gradient is of great importance. The correlation between the thermal conductivity and the concentration of C-C backbone bonds in the direction of temperature gradient indicate nonequivalence in the degrees of freedom.

Many studies on thermal conductivity have been published recently. However, the simulation methods still need improvements to make the prediction of thermal conductivities more accurate. Fortunately, large progress has been made in recent years for the calculation of the thermal conductivity of molecular liquids, carbon nanotubes and polymers. An influence of simulations parameters, size effects and force field design on the calculated thermal conductivity has been studied in detail. Thereby it has been seen that the influence of the simulation parameters such as the use of thermostats, perturbation period and size of the system on the thermal conductivity is smaller than error bars of the method. Size effects can be avoided by the adoption of simulation cell that is large enough into the direction of the heat transfer. The force field chosen seems to be the most important when one simulates the thermal conductivity. Usage of flexible molecular models can lead to the overestimation of thermal conductivity, while rigid models and using super-atoms (a combination of a group of atoms) shifts the thermal conductivity in the direction of the experimental value.

The RNEMD method, which has been used for the calculations in this work, is capable of giving quite good prediction of the thermal conductivity. Agreement with experiment within

---

5 % for molecular liquids<sup>22</sup> and within 20 % for polymers<sup>14</sup> has been found in different simulations. The correct choice of the force field plays the main role in the prediction. Development and improvement of the force field can significantly improve the prediction capability of the RNEMD method.

For carbon nanotubes, thermal conductivity calculations have been very successful. Several methods have been adopted for the calculation of thermal conductivities of CNTs. All methods and potential types result in the same range of thermal conductivity values (300 – 6600 Wm<sup>-1</sup>K<sup>-1</sup>), which have also been found in the experimental work.<sup>67,72,73</sup> Moreover, the thermal transport in carbon nanotubes has been found to be highly anisotropic, what is in line with findings for crystalline and stretched polymers.<sup>10,20</sup>

Only a few examples of simulations of the thermal conductivity of polymers can be found in the literature. Their complexity and variety makes the computation expensive. However, with increasing computational efficiency of computers more polymers and other complex materials can be simulated with higher accuracy. To avoid size-effects, one has to simulate long polymer chains and as a consequence big systems, which leads to a large requirement of simulation time. The next problem is the ambiguous choice of force field parameters. An all-atom flexible model for a polymer can result in a large overestimation of the thermal conductivity, while a united-atom constrained model brings the calculated value into better agreement with experiments. However, some degrees of freedom are more important than others for heat transport, so the thermal conductivity may be sensitive to force field variations to a different extent. This dependence or independence on force field parameters is conditional on the polymer structure and has to be considered for each particular case. The choice of the force field model is heuristic. We note that more simulations on polymers with different chemical structures, topologies, morphologies and phases are needed to establish the range of applicability of molecular dynamics calculations as a predictive tool for the thermal conductivity of polymer materials. One should keep in mind, however, that during recent years remarkable progress has been made in the understanding of the anisotropy of the thermal conductivity of oriented and crystalline polymers, as well as of the relative contribution of fast solid-like through-bond heat transport via phonons along the backbone and the slower liquid-like through-space heat transport by collisions between neighboring chains.

---

## 7. References

---

- (1) Müller-Plathe, F. *J. Chem. Phys.* **1997**, *106*, 6082-6085.
- (2) Pasquino, A. D.; Pilswort. *Mn J. Polym. Sci. Pol. Lett.* **1964**, *2*, 253-&.
- (3) Gupta, G. P.; Saxena, S. C. *Mol. Phys.* **1970**, *19*, 871-&.
- (4) Washo, B. D.; Hansen, D. *J. Appl. Phys.* **1969**, *40*, 2423-&.
- (5) Morelli, D. T.; Heremans, J.; Sakamoto, M.; Uher, C. *Phys. Rev. Lett.* **1986**, *57*, 869-872.
- (6) Piraux, L.; Kinanyalaoui, M.; Issi, J. P.; Begin, D.; Billaud, D. *Solid State Commun.* **1989**, *70*, 427-429.
- (7) Choy, C. L.; Wong, Y. W.; Yang, G. W.; Kanamoto, T. *J. Polym. Sci. Pol. Phys.* **1999**, *37*, 3359-3367.
- (8) Kurabayashi, K.; Asheghi, M.; Touzelbaev, M.; Goodson, K. E. *J. Microelectromech. S.* **1999**, *8*, 180-191.
- (9) Müller-Plathe, F. *Phys. Rev. E* **1999**, *59*, 4894-4898.
- (10) Rossinsky, E.; Müller-Plathe, F. *J. Chem. Phys.* **2009**, *130*, 134905.
- (11) Zhang, M. M.; Lussetti, E.; de Souza, L. E. S.; Müller-Plathe, F. *J. Phys. Chem. B* **2005**, *109*, 15060-15067.
- (12) Allen, M. P.; Tildesley, D. J. *Computer Simulation of Liquids*; Oxford University Press: New York, 1989.
- (13) Nijmeijer, M. J. P.; Bakker, A. F.; Bruin, C.; Sikkenk, J. H. *J. Chem. Phys.* **1988**, *89*, 3789-3792.
- (14) Algaer, E. A.; Alaghemandi, M.; Böhm, M. C.; Müller-Plathe, F. *J Phys Chem A* **2009**, *113*, 11487-94.
- (15) Hummer, G.; Rasaiah, J. C.; Noworyta, J. P. *Nature* **2001**, *414*, 188-190.
- (16) Huxtable, S. T.; Cahill, D. G.; Shenogin, S.; Xue, L. P.; Ozisik, R.; Barone, P.; Usrey, M.; Strano, M. S.; Siddons, G.; Shim, M.; Keblinski, P. *Nature Materials* **2003**, *2*, 731-734.
- (17) Henry, A.; Chen, G. *Phys. Rev. Lett.* **2008**, *101*, 235502.
- (18) Lukes, J. R.; Zhong, H. L. *J. Heat Transfer* **2007**, *129*, 705-716.
- (19) Lussetti, E.; Terao, T.; Müller-Plathe, F. *J. Phys. Chem. B* **2007**, *111*, 11516-11523.
- (20) Ni, B.; Watanabe, T.; Phillpot, S. R. *J. Phys.: Condens. Matter* **2009**, *21*.
- (21) Padgett, C. W.; Brenner, D. W. *Nano Lett.* **2004**, *4*, 1051-1053.
- (22) Guevara-Carrion, G.; Nieto-Draghi, C.; Vrabec, J.; Hasse, H. *J. Phys. Chem. B* **2008**, *112*, 16664-74.
- (23) Nieto-Draghi, C.; Bonnaud, P.; Ungerer, P. *J. Phys. Chem. C* **2007**, *111*, 15942-15951.
- (24) Richmond, R. J.; Wu, S. T. *NASA Conf. Publ.* **1992**, *2*, 299.
- (25) Choi, H. J.; Austin, R.; Allen, J. K.; McDowell, D. L.; Mistree, F.; Benson, D. J. *J. Comput. Aided Mater. Des.* **2005**, *12*, 57-85.
- (26) McDowell, D. *JOM* **2007**, *59*, 21-25.
- (27) Olson, G. B. *Science* **1997**, *277*, 1237-1242.
- (28) Li, B.; Wang, L.; Casati, G. *Phys. Rev. Lett.* **2004**, *93*, 184301.
- (29) Burrows, P. E.; Gu, G.; Bulovic, V.; Shen, Z.; Forrest, S. R.; Thompson, M. E. *IEEE Trans. Electron Devices* **1997**, *44*, 1188-1203.
- (30) Cha, H. J.; Hedrick, J.; DiPietro, R. A.; Blume, T.; Beyers, R.; Yoon, D. Y. *Appl. Phys. Lett.* **1996**, *68*, 1930-1932.
- (31) Che, J. W.; Cagin, T.; Deng, W. Q.; Goddard, W. A. *J. Chem. Phys.* **2000**, *113*, 6888-6900.
- (32) Evans, D. J. *Phys. Lett. A* **1982**, *91*, 457-460.
- (33) Terao, T.; Müller-Plathe, F. *J. Chem. Phys.* **2005**, *122*.
- (34) Dysthe, D. K.; Fuchs, A. H.; Rousseau, B. *J. Chem. Phys.* **1999**, *110*, 4047-4059.

- (35) Galamba, N.; de Castro, C. A. N.; Ely, J. F. *J. Chem. Phys.* **2007**, *126*, 204511-10.
- (36) Bi, K.; Chen, Y.; Yang, J.; Wang, Y.; Chen, M. *Phys. Lett. A* **2006**, *350*, 150-153.
- (37) Alaghemandi, M.; Algaer, E.; Böhm, M. C.; Müller-Plathe, F. *Nanotechnology* **2009**, *20*, 115704.
- (38) Chang, C. W.; Okawa, D.; Majumdar, A.; Zettl, A. *Science* **2006**, *314*, 1121-1124.
- (39) Yang, N.; Zhang, G.; Li, B. *Appl. Phys. Lett.* **2008**, *93*, 243111.
- (40) Wu, G.; Li, B. W. *Phys. Rev. B* **2007**, *76*.
- (41) Müller-Plathe, F.; Reith, D. *Comput. Theor. Polym. Sci.* **1999**, *9*, 203-209.
- (42) Müller-Plathe, F. *Comput. Phys. Commun.* **1993**, *78*, 77-94.
- (43) Tarmyshov, K. B.; Müller-Plathe, F. *J. Chem. Inf. Model.* **2005**, *45*, 1943-1952.
- (44) Berendsen, H. J. C.; Postma, J. P. M.; Vangunsteren, W. F.; Dinola, A.; Haak, J. R. *J. Chem. Phys.* **1984**, *81*, 3684-3690.
- (45) Witt, R.; Sturz, L.; Dolle, A.; Müller-Plathe, F. *J. Phys. Chem. A* **2000**, *104*, 5716-5725.
- (46) Lide, D. R. *CRC Handbook of Chemistry and Physics*; 82nd ed.; CRC Press: Boca Raton, FL, 2001.
- (47) Milano, G.; Müller-Plathe, F. *J. Phys. Chem. B* **2004**, *108*, 7415-7423.
- (48) Schmitz, H.; Faller, R.; Müller-Plathe, F. *J. Phys. Chem. B* **1999**, *103*, 9731-9737.
- (49) Faller, R.; Schmitz, H.; Biermann, O.; Müller-Plathe, F. *J. Comput. Chem.* **1999**, *20*, 1009-1017.
- (50) Berendsen, H. J. C.; Grigera, J. R.; Straatsma, T. P. *J. Phys. Chem.* **1987**, *91*, 6269-6271.
- (51) van der Spoel, D.; van Buuren, A. R.; Apol, E.; Meulenhoff, P. J.; Thieleman, D. P.; Sijbers, A. L. T. M.; Hess, B.; Feenstra, K. A.; Lindahl, E.; van Drunen, R.; Berendsen, H. J. C. 2005, [www.gromacs.org](http://www.gromacs.org).
- (52) Watanabe, H.; Kato, H. *J. Chem. Eng. Data* **2004**, *49*, 809-825.
- (53) Yaws, C. L. *Chemical Properties Handbook: physical, thermodynamic, environmental, transport, safety, and health related properties for organic and inorganic chemicals*; McGraw-Hill: New York, 1999.
- (54) Müller-Plathe, F. *Chem. Phys. Lett.* **1996**, *252*, 419-424.
- (55) Müller-Plathe, F. *Macromolecules* **1996**, *29*, 4782-4791.
- (56) Terao, T.; Lussetti, E.; Müller-Plathe, F. *Phys. Rev. E* **2007**, *75*, 057701.
- (57) Crawford, R. J. *Plastics Engineering*; Butterworth-Heinemann: Oxford, U.K., 1998.
- (58) dos Santos, W. N.; Gregorio, R. *J. Appl. Polym. Sci.* **2002**, *85*, 1779-1786.
- (59) Isa, I. A. A.; Jodeh, S. W. *Mat. Res. Innovations* **2001**, *4*, 135-143.
- (60) Droval, G.; Feller, J. F.; Salagnac, P.; Glouannec, P. *Polym. Adv. Technol.* **2006**, *17*, 732-745.
- (61) De Rosa, C.; Guerra, G.; Petraccone, V.; Corradini, P. *Polym. J.* **1991**, *23*, 1435-1442.
- (62) Milano, G.; Guerra, G.; Müller-Plathe, F. *Chem. Mater.* **2002**, *14*, 2977-2982.
- (63) Schelling, P. K.; Phillpot, S. R.; Keblinski, P. *Phys. Rev. B* **2002**, *65*, 144306.
- (64) Jund, P.; Jullien, R. *Phys. Rev. B* **1999**, *59*, 13707-13711.
- (65) Brenner, D. W.; Shenderova, O. A.; Harrison, J. A.; Stuart, S. J.; Ni, B.; Sinnott, S. B. *J. Phys.: Condens. Matter* **2002**, *14*, 783-802.
- (66) Choy, C. L.; Wong, Y. W.; Yang, G. W.; Kanamoto, T. *J. Polym. Sci.* **1999**, *37*, 3359-3367.
- (67) Berber, S.; Kwon, Y. K.; Tomanek, D. *Phys. Rev. Lett.* **2000**, *84*, 4613-4616.
- (68) Osman, M. A.; Srivastava, D. *Nanotechnology* **2001**, *12*, 21-24.
- (69) Moreland, J. F.; Freund, J. B.; Chen, G. *Microscale Thermophys. Eng.* **2004**, *8*, 61-69.
- (70) Maruyama, S. *Physica B* **2002**, *323*, 193-195.
- (71) Ebbesen, T. W.; Lezec, H. J.; Hiura, H.; Bennett, J. W.; Ghaemi, H. F.; Thio, T. **1996**, *382*, 54-56.
- (72) Hone, J.; Llaguno, M. C.; Nemes, N. M.; Johnson, A. T.; Fischer, J. E.; Walters, D. A.; Casavant, M. J.; Schmidt, J.; Smalley, R. E. *Appl. Phys. Lett.* **2000**, *77*, 666-668.

- 
- (73) Yi, W.; Lu, L.; Zhang, D. L.; Pan, Z. W.; Xie, S. S. *Phys. Rev. B* **1999**, *59*, R9015-R9018.
- (74) Wang, J. A.; Wang, J. S. *Appl. Phys. Lett.* **2006**, *88*.
- (75) Yang, N.; Li, N.; Wang, L.; Li, B. *Phys. Rev. B* **2007**, *76*.
- (76) Nikitin, L. N.; Gallyamov, M. O.; Vinokur, R. A.; Nikolaev, A. Y.; Said-Galiyev, E. E.; Khokhlov, A. R.; Jespersen, H. T.; Schaumburg, K. J. *Superc. Fluids* **2003**, *27*, 131-131.
- (77) Cooper, A. I. *J. Mater. Chem.* **2000**, *10*, 207-234.
- (78) Chang, S. H.; Park, S. C.; Shim, J. J. *J. Superc. Fluids* **1998**, *13*, 113-119.
- (79) Kendall, J. L.; Canelas, D. A.; Young, J. L.; DeSimone, J. M. *Chem. Rev.* **1999**, *99*, 543-563.
- (80) Watkins, J. J.; McCarthy, T. J. *Macromolecules* **1994**, *27*, 4845-4847.
- (81) Binder, K.; Stauffer, D. *Application of the Monte Carlo method in statistical physics*; Springer Verlag: Berlin, Heidelberg, 1987.
- (82) Böhm, M. C.; Elsässer, C.; Fahnle, M.; Brandt, E. H. *Chem. Phys.* **1989**, *130*, 65-87.
- (83) Böhm, M. C.; Elsässer, C.; Fahnle, M.; Brandt, E. H. *Chem. Phys.* **1989**, *130*, 65-87.
- (84) Valavala, P. K.; Odegard, G. M. *Rev. Adv. Mater. Sci.* **2005**, *9*, 34-44.
- (85) Harris, J. G.; Yung, K. H. *J. Phys. Chem.* **1995**, *99*, 12021-12024.
- (86) Zhang, Z. G.; Duan, Z. H. *J. Chem. Phys.* **2005**, *122*.
- (87) Hansen, D.; Ho, C. C. *J. Polym. Sci. Part A* **1965**, *3*, 659-&.
- (88) Brown, D.; University of Savoie: 2008.
- (89) Wang, W. C. V.; Kramer, E. J.; Sachse, W. H. *J. Polym. Sci. B* **1982**, *20*, 1371-1384.
- (90) Höcker, H.; Blake, G. J.; Flory, P. J. *J. Trans. Faraday Soc.* **1971**, *67*, 2251-&.
- (91) Carwille, L. C. K.; Hoge, H. J. "Thermal conductivity of polystyrene: selected values,," Pioneering Research Division, U.S. Army Natick Laboratories, 1966.
- (92) Span, R.; Wagner, W. *J. Phys. Chem. Ref. Data* **1996**, *25*, 1509-1596.
- (93) Vesovic, V.; Wakeham, W. A.; Olchowy, G. A.; Sengers, J. V.; Watson, J. T. R.; Millat, J. *J. Phys. Chem. Ref. Data* **1990**, *19*, 763-808.
- (94) Zhang, X. M.; Aji, A. *J. Appl. Polym. Sci.* **2003**, *89*, 487-496.
- (95) Gupta, V. B. *Kolloid Z. Z. Polym.* **1973**, *251*, 117-122.
- (96) Boika, B. B.; Insarova, N. I.; Lugina, A. S. *Mekhanika Polymerov* **1965**, *1*, 13-18.
- (97) Arns, C. H.; Knackstedt, M. A.; Roberts, A. P.; Pinczewski, V. W. *Macromolecules* **1999**, *32*, 5964-5966.
- (98) Mar, J. D.; Litovsky, E.; Kleiman, J. *J. Build. Phys.* **2008**, *32*, 9-31.
- (99) Binder, K.; Mognetti, B. M.; Macdowell, L. G.; Oettel, M.; Paul, W.; Virnau, P.; Yelash, L. *Macromolecular Symposia* **2009**, *278*, 1-9.
- (100) Kojima, J.; Takenaka, M.; Nakayama, Y.; Saeki, S. *J. Chem. Eng. Data* **2009**, *54*, 1585-1591.
- (101) Orbach, R. *Philos. Mag. B* **1992**, *65*, 289-301.
- (102) Allen, P. B.; Feldman, J. L.; Fabian, J.; Wooten, F. *Philos. Mag. B* **1999**, *79*, 1715-1731.
- (103) Riter, J. R. *J. Chem. Phys.* **1970**, *52*, 5008-&.
- (104) Hu, M.; Shenogin, S.; Keblinski, P. *Appl. Phys. Lett.* **2007**, *91*.

---

---

## Acknowledgments

---

I would like to thank my supervisor Prof. Dr. Florian Müller-Plathe for the continuous support of my PhD study and research, for his patience, motivation and immense knowledge. His giddiness helped me to finish this work. I would like to thank Prof. Michael Böhm for his help in writing my papers, for his helpful corrections and effective suggestions. Also I would like to thank my colleague and friend Mohammad Alaghemandi for his collaboration. Thanks to all members of the research group of Prof. Dr. Müller-Plathe for giving me friendship, happiness and help. Financial support of this work by the Priority Program 1155 “Molecular Simulation in Chemical Engineering” of the Deutsche Forschungsgemeinschaft is gratefully acknowledged.

---

---

## Curriculum Vitae

---

### Elena Algaer

Bleichstraße 30, 64283 Darmstadt

Date of birth: 09-02-1983

### Education

- *Darmstadt University of Technology, Darmstadt, Germany*  
**Ph.D. in Chemistry** **2007 – 2010**  
Dissertation: "Thermal conductivity of Polymer Materials - Reverse Nonequilibrium Molecular Dynamics Simulation"
- *Novosibirsk State University, Novosibirsk, Russia*  
**M.Sc. Honors in Computational Physics** **2004 – 2006**  
Thesis: "The Event Digitalization Algorithm for the Liquid Xenon Calorimeter of the CMD-3 Detector"
- *Novosibirsk State University, Novosibirsk, Russia*  
**B.Sc. Honors in Physics** **2000 – 2004**  
Thesis: "Computer Simulation of the Liquid Xenon Calorimeter of the CMD-3 Detector"

### School

- Specialized Educational Scientific Center of NSU, Novosibirsk, Russia **1999 – 2000**
- Secondary School of Kasanka, Novosibirsk, Russia **1989 – 1999**

---

## Publications

---

1. “Thermal Conductivity of Amorphous Polystyrene in Supercritical Carbon Dioxide Studied by Reverse Nonequilibrium Molecular Dynamics Simulations”, Algaer, E.A.; Alaghemandi, M.; Böhm, M.C; Müller-Plathe, F. *Journal of Physical Chemistry A*, **2009**, *113*, 11487.
2. “Anisotropy of the Thermal Conductivity of Amorphous Polystyrene in Supercritical Carbon Dioxide Studied by Reverse Nonequilibrium Molecular Dynamics Simulations”, Algaer, E.A.; Alaghemandi, M.; Böhm, M.C; Müller-Plathe, F. *Journal of Physical Chemistry B*, **2009**, *113*, 14596.
3. “Calculation of the Thermal Conductivity of Molecular Liquids, Polymers, and Carbon Nanotubes”, Algaer E.A.; Müller-Plathe, F. *Soft Materials* (submitted).
4. “The Thermal Conductivity and Thermal Rectification of Carbon Nanotubes Studied Using Reverse Nonequilibrium Molecular Dynamics Simulations”, Alaghemandi, M.; Algaer, E.A.; Böhm, M.C.; Müller-Plathe, F. *Nanotechnology*, **2009**, *20*, 115704.
5. “Thermal Rectification in Mass-Graded Nanotubes: A Model Approach in the Framework of Reverse Nonequilibrium Molecular Dynamics Simulations”, Alaghemandi, M.; Leroy, F.; Algaer, E.A.; Böhm, M.C.; Müller-Plathe, F. *Nanotechnology*, **2010**, *21*, 075704.



---

## Eidesstattliche Erklärungen

---

Elena Algaer  
Bleichstraße 30  
64283 Darmstadt

21.01.2010

### Eidesstattliche Erklärung

Ich erkläre hiermit bei Eides statt, dass ich meine Dissertation selbstständig und nur mit den angegebenen Hilfsmitteln angefertigt habe.

Elena Algaer

---

Elena Algaer  
Bleichstraße 30  
64283 Darmstadt

21.01.2010

### Erklärung

Ich erkläre hiermit, noch keinen Promotionsversuch unternommen zu haben.

Elena Algaer